ISTANBUL TECHNICAL UNIVERSITY ★ EURASIA INSTITUTE OF EARTH SCIENCES

STATISTICAL CHALLENGES IN PALEOCLIMATOLOGY: INDEPENDENT COMPONENT ANALYSIS OF LAKE HAZAR AND LAKE VAN DATA, AND A BAYESIAN TEST FOR 4.2 KA BP EVENT

Ph.D. THESIS

Zeki Bora ÖN

Department of Climate and Marine Sciences

Earth System Science Programme

NOVEMBER 2018

ISTANBUL TECHNICAL UNIVERSITY ★ EURASIA INSTITUTE OF EARTH SCIENCES

STATISTICAL CHALLENGES IN PALEOCLIMATOLOGY: INDEPENDENT COMPONENT ANALYSIS OF LAKE HAZAR AND LAKE VAN DATA, AND A BAYESIAN TEST FOR 4.2 KA BP EVENT

Ph.D. THESIS

Zeki Bora ÖN
(601132003)

Department of Climate and Marine Sciences

Earth System Science Programme

Thesis Advisor: Doç. Dr. Mehmet Sinan ÖZEREN

NOVEMBER 2018

İSTANBUL TEKNİK ÜNİVERSİTESİ ★ AVRASYA YER BİLİMLERİ ENSTİTÜSÜ

PALEOİKLİM ÇALIŞMALARINDA İSTATİSTİKSEL UYGULAMALAR: HAZAR VE VAN GÖLÜ VERİLERİNDE BAĞIMSIZ BİLEŞEN ANALİZİ, VE GÖ 4.2 KA OLAYINA BAYESÇİ BİR TEST

DOKTORA TEZİ

Zeki Bora ÖN
(601132003)

İklim ve Deniz Bilimleri Anabilim Dalı

Yer Sistem Bilimi Programı

Tez Danışmanı: Doç. Dr. Mehmet Sinan ÖZEREN

KASIM 2018

Zeki Bora ÖN, a Ph.D. student of ITU Eurasia Institute of Earth Sciences 601132003 successfully defended the thesis entitled "STATISTICAL CHALLENGES IN PALEOCLIMATOLOGY: INDEPENDENT COMPONENT ANALYSIS OF LAKE HAZAR AND LAKE VAN DATA, AND A BAYESIAN TEST FOR 4.2 KA BP EVENT", which he prepared after fulfilling the requirements specified in the associated legislations, before the jury whose signatures are below.

Thesis Advisor :	**Doç. Dr. Mehmet Sinan ÖZEREN** İstanbul Technical University	.....
Jury Members :	**Prof. Dr. Alper Ünal** İstanbul Technical University	.....
	Doç. Dr. Mehmet ILICAK İstanbul Technical University	.....
	Doç. Dr. Nesibe KÖSE İstanbul University-Cerrahpaşa	.....
	Dr. Öğr. Üyesi Ozan Mert GÖKTÜRK Samsun University	.....

Date of Submission : **01 October 2018**
Date of Defense : **19 November 2018**

To my lovely son Aral Efes Ön
and to my best friend Emre Eren,

FOREWORD

I would like to express my best gratitude to my supervisor Sinan Özeren. I have learned a lot from him and I think it would not be possible to write a thesis like this with any other supervisor.

My wife and my colleague Sena Akçer-Ön. Maybe her scientific support can be defined through some stack of words or in manuscript cover letters, but no sentence can describe her emotional support.

Alan Greaves was like a second supervisor, I am truly grateful for his contributions.

Kadir Eriş, Namık Çağatay and Dursun Acar from EMCOL and Günter Landmann shared their own professions and their contributions to this thesis are invaluable.

Nesibe Köse and Alper Ünal were in my thesis progress committee, and their suggestions elevated this thesis to an upper level.

Andaç Hamamcı, Ercan Kuruoğlu and Kerem Uludağ gave inspiring ideas through the research process. Esra Çetin was helpful during the learning process of GMT and plotting the maps in this study.

I also want to thank to all the people who shared their published data through open network sources or through emails.

A foreword without parents must be unacceptable, my mother Fadime Ön and my father Halil Ön; I believe their support through my whole life is something everyone can appreciate.

Lastly, I want to thank to the whole free software and open source communities. Especially, to the Linux OS and Linux Mint community which provided the basis of the whole work. All the research and writing process of this thesis was conducted mainly through R over RStudio, LaTeX over TeXstudio, LibreOffice, Veusz, Engauge Digitizer, Inkscape, SAGA GIS, QGIS and GMT.

November 2018

Zeki Bora ÖN
Geologist

TABLE OF CONTENTS

Page

ABBREVIATIONS

AR : Ahlat Ridge
BP : Before Present
BSTS : Bayesian Structural Time Series
cal : calibrated
dcorr : Distance Correlation
FA : Factor Analysis
FastICA : Fast Independent Component Analysis
ICA : Independent Component Analysis
ICDP : International Continental Scientific Drilling Program
ka : kilo-annum
kyr : kilo-year
LGM : Last Glacial Maximum
µ-XRF : micro-X-ray Fluorescence
MIS : Marine Isotope Stage
MS : Magnetic Susceptibility
NGRIP : North Greenland Ice Core Project
PCA : Principal Component Analysis
PV : PALEOVAN
RCC : Rapid climate change
SGF : Savitzky-Golay filter
TIC : Total Inorganic Carbon
TOC : Total Organic Carbon

SYMBOLS

Uk37	**:** One type of alkennone unsaturarion index
δ^{13}C	**:** Measure of the ratio of stable carbon-13 and carbon-12
δ^{15}N	**:** Measure of the ratio of stable nitrogen-15 and nitrogen-14
δ^{18}O	**:** Measure of the ratio of stable oxygen-18 and oxygen-16
$N()$	**:** Normal distribution
$\Gamma()$	**:** Gamma function

LIST OF TABLES

Page

LIST OF FIGURES

Page

STATISTICAL CHALLENGES IN PALEOCLIMATOLOGY: INDEPENDENT COMPONENT ANALYSIS OF LAKE HAZAR AND LAKE VAN DATA, AND A BAYESIAN TEST FOR 4.2 KA BP EVENT

SUMMARY

There are numerous statistical and numerical methodological problems of paleoclimate studies. In this study, I offer solutions for two problems of paleoclimatology in three different studies.

It is a well known fact that, each geochemical measurement and especially each micro-X-ray fluorescence (μ-XRF) measurement through a sediment core is a reflection of different independent processes, i.e. an indirect indicator of paleoenvironments. That's why most studies present μ-XRF measurements as elemental ratios, in order to eliminate a possible dependence upon a single profile. Some studies use second order statistical methods, such as principal component analysis, to eliminate dependence, however there are systematic problems of second order statistical methods as is used in these studies. In order to overcome this issue, we offer an almost well-defined signal processing technique, independent component analysis of geochemistry data gathered from paleoclimate archives. Accordingly, we propose data based models of paleo-precipitation and paleo-temperature for the studied regions.

In the first study (Chapter 2), a 3.5 m long piston core (Hz11-P03) has been recovered from Lake Hazar and it is used for multiproxy measurements. μ-XRF, magnetic susceptibility (MS) and stable isotope ($\delta^{18}O$ and $\delta^{13}C$) measurements have been carried out for 3 mm, 1 cm and 3 cm resolutions, respectively. A Bayesian age-depth model according to six radiocarbon dates shows that Hz11-P03 represents the last 17.3 ka BP. We apply independent component analysis on Lake Hazar μ-XRF data (namely, Ca, Fe, K, Mn, Sr and Ti counts). By the measure of distance correlation of resulting independent components with the analyzed data and other regional well-defined paleorecords, we select two independent components as proxies of temperature (Hz-ic5) and precipitation (Hz-ic4) of the region. According to the results, the region was wet/cold during 17.3 ka BP and 14.8 ka BP and wet/warm during the Bølling-Allerød period. According to the age model, there is a hiatus at the Younger Dryas period. At the start of the Holocene, temperatures rose gradually and reached the Holocene "normals" around 8 ka BP. During that period, it was wet. Between 8 ka BP and 5 ka BP, it was warm but exceptionally dry. Between 5 ka BP and 3.5 ka BP, it was warm/wet. After 3.5 ka BP within the oscillations there are abrupt cold/dry phases around 3.5 ka BP, 2.8 ka BP and 1.8 ka BP.

In the second study (Chapter 3), ICA method is applied to previously published data from Lake Van, which span the last 250 ka BP. The data used through ICA were element concentrations of Ca, Fe, K, Mn, Si from XRF measurement, TOC and $CaCO_3$ content and B* (color reflectance) of the Ahlat Ridge sediment record. The analysis is based on applying the algorithm several times by changing the initial random unit vector and clustering the possible independent components through average–link agglomeration,

which make it different and innovative than Lake Hazar study. Appropriate components are selected by mutual information method. Accordingly, we claim that Van-IC8 is a proxy for temperature variability for the region, by its similarity with Greenland $\delta^{18}O$ data and (Van-IC7) is a proxy for precipitation variability for the region, by its similarity with B* (Van-IC7) data. The results reveal that, temperature of the region follows the Northern Hemisphere records, i.e. warm during interglacials, cold during stadials with abrupt warming episodes. On the other hand, precipitation record shows that, it was not dry, or at least as much wet as today, during the LGM and at the end of penultimate glacial as previous studies claim.

It was previously proposed that an abrupt climatic change around 4.2 ka BP was the cause of the collapse of the Akkadian Empire. Afterwards, many geological studies arose, which claim to support the climatic deterioration hypothesis. In the third study (Chapter 4), we apply a Bayesian test on the records from Eastern Mediterranean and Arabian Peninsula which claim to show an abrupt climatic change around 4.2 ka BP. To do this, time series are reconstructed using "unaffected" ones in a fully Bayesian framework by the Bayesian structural time series method and then a Bayesian hypothesis test is applied on the results. Our results show that some studies which have previously been cited to support the abrupt 4.2 ka BP event hypothesis hold true, we also show that in a number of other studies, there is no statistically significant abrupt climatic change effect.

PALEOİKLİM ÇALIŞMALARINDA İSTATİSTİKSEL UYGULAMALAR: HAZAR VE VAN GÖLÜ VERİLERİNDE BAĞIMSIZ BİLEŞEN ANALİZİ, VE GÖ 4.2 KA OLAYINA BAYESÇİ BİR TEST

ÖZET

Kuaterner geçmiş iklim çalışmaları, özellikle istatistiksel ve sayısal yöntemler açısından birçok probleme sahiptir. Ben bu tez kapsamında varolan iki paleoiklim problemine üç farklı çalışma ile çözüm önermekteyim.

Kuaterner çalışmalarında, sahadan alınan karot boyunca ölçülen jeokimyasal verilerin, özellikle XRF ölçümleri sonucunda elde edilen element profillerinin, birçok farklı süreç tarafından kontrol edildiği bilinmektedir. Bu sebepten ötürü, verilerdeki farklı süreçlere bağımlılık durumunu bertaraf etmek amacıyla birçok çalışmada bu veriler birbirleriyle normalize edilerek kullanmaktadır. Bazı çalışmalarda ise ikinci dereceden istatistiksel yöntemlere dayalı boyut küçültme teknikleri kullanılmaktadır. Bu yöntemlerden en yaygın kullanılanı temel bileşenler analizidir (PCA). PCA'nın temel amacı varyansı maksimize eden ekseni bulup, diğer eksenleri de bu eksene ve birbirlerine ortogonal ve sıralı bir şekilde varyansı en büyükten küçüğe doğru sıralamaktır. Bu yöntem, eğer maksimal varyansı ifade eden eksene dair bir hipotez varsa veya verideki gürültüden kurtulmak isteniyorsa kullanışlıdır. Kullanırken de yöntemin dayattığı, verilerin normal dağılımlı olması gerekliliği ve/veya veriler arasındaki yüksek lineer korelasyonun sonuçları taraflı vereceği gibi kısıtlamalara dikkat etmek gerekir. İlk iki çalışmada Hazar Gölü ve Van Gölü jeokimya verilerine uyguladığımız bağımsız bileşen analizi (ICA) yöntemini boyut küçültme yöntemlerine alternatif olarak önermekteyiz. Üçüncü çalışmada ise, günümüzden 4.2 ka önce gerçekleştiği iddia edilen ani iklim değişikliğini destekleyen veriler üzerinde Bayesçi test uygulanmıştır. Bu çalışmanın önemi, 2018 yılı içinde Orta/Üst Holosen için stratigrafik sınır olarak kabul edilmiş iklim değişimine dair nicel bir test olmasıdır.

Hazar Gölü, güneydoğu Anadolu'da, deniz seviyesinden 1255 m yüksekte yer alan tektonik bir göldür. Bölge karasal Akdeniz iklim özellikleri göstermektedir. Yıllık yağışın önemli bir bölümü ilkbahar ve kış aylarında gözlemlenmektedir. Hazar Gölü'nden, 2009 yılında 3.8 m uzunluğunda alınan karotta (Hz11-P03) μ-XRF, duraylı izotop (δ^{18}O ve δ^{13}C) ve manyetik duyarlılık ölçümleri yapılmıştır (Chapter 2). Karotta belirlenen altı farklı noktadan radyokarbon ölçümleri alınmıştır. Gözle görülen bir hiatusun da varlığı dikkate alınarak Bayesçi yöntemlerle elde edilen yaş-derinlik modeline göre karot günümüzden önce son 17.3 ka yılı kapsamaktadır. Bölgenin geçmiş iklim parametrelerini ortaya çıkarabilmek adına μ-XRF verileri üzerine (Ca, Fe, K, Mn, Sr ve Ti sayımları) ICA uygulanmıştır (Chapter 2). ICA, PCA sonuçlarından farklı olarak, sıralı sonuçlar vermemektedir. Bu sebepten ötürü, ICA sonuçlarından elde edilen altı bağımsız bileşenden yağış ve sıcaklık eğrilerini elde edebilmek için iyi tanımlı iklim verileri, NGRIP δ^{18}O ve Sofular δ^{13}C, ile bağımsız bileşenler arasındaki uzaklık korelasyonların ölçüsüne bakılmıştır. Uzaklık korelasyonunun lineer korelasyon ölçülerine göre farkı, aykırı değerlerle baş edebilmesi ve lineer olmayan ilişkileri de yakalayabilmesidir. Elde edilen uzaklık korelasyonu sonuçlarına göre,

iki bağımsız bileşenin bölgenin sıcaklığını (Hz-ic5) ve yağışını (Hz-ic4) temsil ettiği düşünülmektedir. Buna göre bölge 17.3 ka BP ve 14.8 ka BP arasında yağışlı ve soğuk, ancak Bølling-Allerød döneminde yağışlı ve sıcaktır. Younger Dryas karotta bir hiatus ile temsil edilmektedir. Bu dönemde göl seviyesinin düştüğü ve bölgenin kurak olması gerektiği söylenebilir. Holosen başında sıcaklıklar kademeli olarak artış göstermiş ve bunun neticesinde yaklaşık 8 ka BP civarında Holosen "normallerine" ulaşmıştır. Ancak, Erken Holosen'de bölge yağışlıdır. 8 ka BP ve 5 ka BP arasında bölge ılık ancak kuraktır. 5 ka BP ve 3.5 ka BP arasında bölge ılık ve yağışlı özellikler göstermektedir. Bundan sonraki dönemde üç tane kısa süreli soğuk ve kurak dönem gözlenmektedir. Bunlar yaklaşık 3.5 ka BP, 2.8 ka BP ve 1.8 ka BP dönemlerine denk gelmektedir. MS ve $\delta^{13}C$ sonuçları yağış sonuçlarını destekler niteliktedir ancak $\delta^{18}O$ sonuçları birden fazla sürece bağlı olduğundan bu çalışmada yorumlanamamıştır.

Van Gölü, Doğu Anadolu'da deniz seviyesinden 1650 m yükseklikte yer alan, dünyanın en büyük sodalı gölüdür. Bölgenin iklimi Hazar Gölü ve çevresine benzemektedir. Karasal Akdeniz iklimi ile karasal iklimin sınırında olduğu iddia edilmiştir. Tektonik bir çöküntü olan havzadan ICDP projesi kapsamında bölgenin geçmiş ortam değişimlerinin araştırılması amacıyla, sondajla çökel istifi çıkarılmıştır. Bu çökellerden elde edilen vekil verilerle halihazırda geçmiş iklim rekonstrüksiyonları yapılmıştır. Bunun yanında, Van Gölü çevresinde gözlemlenen taraçalar ve bunların yaşları gölün seviyesinin Son Buzul Maksimum'da bugüne göre yaklaşık 80 m daha yukarıda olması gerektiğini göstermiştir. Ancak ICDP projesi kapsamında yapılan bazı rekonstrüksiyonlar, gerek oluşturdukları veri tabanlı modellere göre, gerekse de kullanılan bazı dinamik iklim modellerine göre bölgenin bu dönem kurak olması gerektiğini ve su seviyesinin bugüne göre belki de 200 m kadar aşağıda olması gerektiğini öne sürmüşlerdir. Bu ikileme çözüm önermek adına (Chapter 3) Van Gölü, Ahlat Sırtından sondajla alınmış çökel istifi verilerine, bu veriler, XRF'ten elde edilmiş Ca, Fe, K, Mn, Si sayımları, toplam organik karbon ve $CaCO_3$ ölçümleri ve B* (renk yansıması) değerleridir, ICA uyguladık. Bu veriler günümüzden önce 250 ka temsil etmektedirler. Ancak, Hazar Gölü çalışmasından farklı olarak bu çalışmada ICA uygulamadan önce, ölçüm hatasaından kaynaklanabilen, "en aykırı" değerleri veriden temizledik. Bunun ardından, ICA bileşenleri başlangıçta rastgele seçilen birim vektöre göre küçük farklılıklar gösterebildiğinden, başlangıç vektörünü 250 kere değiştirerek kısmen farklı sonuçlar elde ettik. Bu sonuçları birbirlerine olan uzaklıklarına göre kümeleyip olası bağımsız bileşen sayısını tespit ettik. Buna göre, anlamlı sekiz bağımsız bileşen belirledik, ve her bir küme içerisinde toplam benzerliği en yüksek olan bileşen kullanılmak üzere seçildi. Bu sekiz bileşenin karşılıklı bilgi benzerlik ölçüsüyle NGRIP $\delta^{18}O$ ve analize girilen verilerle benzerliklerini kontrol ettikten sonra bu bileşenlerden bir tanesinin (Van-IC8) bölgenin geçmiş sıcaklık değişkenliğine, bir diğerinin ise (Van-IC7) bölgenin geçmiş yağış değişkenliğine karşılık geldiğini iddia etmekteyiz. Elde edilen sonuçlara göre, bölgenin sıcaklığı kuzey yarımküre için sıcaklık eğrisi denebilecek NGRIP $\delta^{18}O$ eğrisine benzemektedir, buzul dönemleri soğuk ve buzularası dönemler ılık geçmektedir. Buzul dönemler içindeki ani ısınma ve kademeli soğuma olayları (Dansgaard/Oeschger döngüleri) sıcaklık eğrisinde gözlemlenmektedir. Yağış eğrisi ise, daha önce ortaya koyulan modellerden farklı nitelikler göstermektedir. Buzullaşmanın maksimum olduğu dönemlerde bölge yağışlıdır. Buzularası dönemlerin başında yağışlı ancak devamlarında ise kurak bir dönem göstermektedir. Yağış eğrisi bölgedeki Son Buzul Maksimum'da oluşmuş taraçalara da cevap vermektedir.

Akad İmparatorluğunun (Yukarı Mezopotamya) günümüzden 4.2 ka önce ani bir iklim değişikliği ile çöktüğü iddia edilmektedir. Bu hipotez ortaya atıldıktan sonra dünyanın farklı yerlerinde bu hipotezi destekleyen deliller gözlemlenmiştir. Yakın zamanda bu olay jeolojik zaman çizelgesinde Orta Holosen ve Geç Holosen için bir sınır olarak kabul edilmiştir. Bu ani iklim değişikliğini temsil ettiğini iddia eden deliller genelde paleoortam vekili olan zaman serileridir. Ancak bu zaman serilerinin varolduğu iddia edilen iklim değişikliğine gösterdikleri tepkiler ve bu tepkilerin geometrileri birbirlerinden oldukça farklıdır. Ani iklim değişikliği hipotezini destekleyen verilerden başka, bu değişikliği desteklemeyen veriler de mevcuttur. Biz bu çalışma kapsamında Doğu Akdeniz'de ve Arap Yarımadası etrafında ani değişimi gösterdiğini iddia eden zaman serilerini, ani iklim değişikliği göstermeyen zaman serileri ile günümüzden önce 4.4 ka yılına kadar sentetik olarak yeniden oluşturup, sentetik veriyi geleceğe ekstrapole ettik (Chapter 4). Verileri sentetik olarak oluştururken Bayesyen Yapısal Zaman Serileri yöntemini kullandık. Günümüzden önce 4.4 ka ve 3.9 ka arasında, sentetik olarak oluşturulmuş zaman serisi ile gerçek zaman serisi arasındaki farka tek taraflı Bayesçi hipotez testi uygulayıp zaman serisindeki etkinin anlamlılığını test ettik. Buna göre, test edilen verilerden hipotezi desteklediğini iddia eden bazı zaman serileri anlamlı bir etki göstermektedir. Bir kısmı ise iddia edilen etkiyi göstermemektedir. Üçüncü grup veri kümesinde ise, etki gözlemlenmesine rağmen etkiden sonra zaman serilerinde seviye kayması gözlemlenmiştir. Bunun sebebi, ya aslında zaman serisi üzerinde düşünüldüğü gibi bir etki yoktur, ya da iddia edilen etki vekil veri üzerinde kalıcı bir etki bırakmıştır.

1. INTRODUCTION

> "All models are wrong; some models are useful."
>
> George E. P. Box [1]

Climate of the earth has never been stable throughout the geological history. Today, climate system keeps its ordinary dynamic tempo regulated through natural factors. However, human race is mainly responsible for today's warming world [1]. While major aim of past climate studies is not to explain future climates, they are useful in terms of understanding the responses of climate system, ecosystems and societies in a dynamically transforming earth.

Unlike abundant direct measurements of meteorology, paleoclimate data are presented through proxies (for an extensive review of proxies, see [2] and references therein). However, proxy data have serious drawbacks. Discussing all problems, except dependence to different climatological/geological processes (see Section 2.2 and Section 3.2), of proxy data is beyond the scope of this study. On the other hand, other than proxy dependence, paleoclimate studies face many other difficulties, such as constructing chronologies, interpretation of proxy data, laboratory measurement errors, spatial interpolating/extrapolating the results etc. In this study, we claim to offer a new method to source separation problem of multiproxy data (Section 1.1) through two case studies.

Through the third study (Section 1.2), I tried to make a contribution to the discussions on the so-called 4.2 ka BP event. In my opinion, some studies in paleoclimatology, sometimes pointlessly, aim to confirm previously hypothesized theories. On the other hand, it is easy to find confirmations [3]. Furthermore, as stated by Karl Popper:

Confirmations should count only if they are the result of *risky predictions*; that is to say, if, unenlightened by the theory in question, we should have expected an event

[1] Statistics for Experimenters, 1978

which was incompatible with the theory — an event which would have refuted the theory [3, p.47].

In this study, we didn't apply a test for the 4.2 ka BP event, on the other hand we applied a Bayesian test on the confirming evidences from eastern Mediterranean and Arabian peninsula.

1.1 Independent Component Analysis of Paleoclimate Data, Lake Hazar and Lake Van Examples

Geochemical measurements are the most extensively used proxies used in Quaternary paleoclimate reconstructions. However, they are affected by several independent factors. It is a standard practice to present the ratios of different geochemical proxies to overcome the dependence of proxy used in a study. On the other hand, there exist dimension reduction statistical techniques, which are occasionally used. Principal component analysis and factor analysis are the most widely used techniques (cf. [4,5]). However, capabilities of these techniques which depend on second order statistics, and misuse of them may lead to wrong interpretations and consequently to wrong models which even contrast with geological field observations (see Chapter 2 and Chapter 3).

Through these chapters, we offer a newer dimension reduction method for paleoclimate studies, independent component analysis (ICA), which is a blind source separation technique and has been widely used for problems of telecommunications theory, signal/image processing and geosciences. Through this study, ICA is used to extract paleo-precipitation and paleo-temperature time series from geochemistry of Lake Hazar [6] and Lake Van [7] sediments, by assuming these climate variables are at least quasi-independent through long periods.

1.2 Test for the 4.2 ka BP Event, Using Bayesian Structural Time Series

The so-called 4.2 ka BP event was first hypothesized by [8]. While there are numerous confirming evidences of the theory, there are also many falsifying ones. In this study, we apply Bayesian Structural Time Series method [9], in order the reconstruct the "confirming" time series through not confirming ones and then apply hypothesis test for the period of interest. Accordingly, we claim that not all the confirming evidences

support the theory of an abrupt climate change around 4.2 ka BP, i.e. the impact related to the 4.2 ka BP event is not statisticaly significant [10].

2. CLIMATE PROXIES FOR THE LAST 17.3 KA FROM LAKE HAZAR (EASTERN ANATOLIA), EXTRACTED BY INDEPENDENT COMPONENT ANALYSIS OF μ-XRF DATA[1]

2.1 Abstract

The elemental composition of lake sediment cores is often the result of several independent processes. In this study we attempt to extract statistically independent climate related signals from μ-XRF multi element data of a core drilled from Lake Hazar in Eastern Anatolia, using the independent component analysis (ICA) method. In addition, we analysed ostracod shells for oxygen and carbon isotopes. The ICA method has advantages over traditional dimension reduction methods, such as principal component analysis or factor analysis, because it is based on maximal statistical independence rather than uncorrelatedness, where independence is a stronger property.

The Hz11-P03 core, which represents the last 17.3 ka, was recovered from Lake Hazar which, at times, formed the headwaters of the Tigris. Applying the ICA method, we selected two out of six independent components by measuring distance correlation similarity. We propose that one of the selected components can be read as a proxy for temperature and the other for precipitation in this region.

Our results indicate that the region was relatively cold and wet during the late glacial, between 17.3 ka BP and 14.8 ka BP, and wet and warm during Bølling-Allerød. The lake level dropped below today's level during the Younger Dryas stadial (12.49 ka BP and 11.76 ka BP), forming a marked hiatus in the core's stratigraphic record. During the beginning of the Holocene, while precipitation values were high, the temperature gradually increased until 8 ka BP. Between 8 ka BP and 5 ka BP, the region was warm but extremely dry. After 5 ka BP, around 3.5 ka BP temperatures suddenly fell, and three abrupt dry phases are observed around 3.5 ka BP, 2.8 ka BP and 1.8 ka BP.

[1]This chapter is based on the paper: Ön, Z.B., Akçer-Ön, S., Özeren, M.S., Eriş, K.K., Greaves, A.M. and Çağatay, M.N. (2018). Climate proxies for the last 17.3 ka from Lake Hazar (Eastern Anatolia), extracted by independent component analysis of μ-XRF data, *Quaternary International*, 486, 17-28.

2.2 Introduction

Geochemical proxies are the most widely used indicators of Quaternary paleoclimates. In particular, the geochemical "archives" contained in lacustrine sediments provide long and high-resolution proxies of terrestrial records. However, such geochemical proxies, especially those gathered from the lakes, can only be indirect indicators of past climates [11] and may be influenced, to different degrees, by several independent factors. In order to overcome this indirectness, multi-proxy methods are widely used. However, it may be complicated and misleading to interpret multi-proxy data qualitatively in order to form a single composite impression about the past dynamics that govern those proxies. Part of this shortcoming is due to the fact that, commonly used data reduction techniques, such as principal component analysis (PCA) and factor analysis (FA), are not capable of imposing certain probabilistic constraints on the problem exposed by the multi-proxy data. The orthogonal transformation of PCA and FA point out the directions of maximal variance. However, maximal variance may not be the researcher's main aim, unless it is aimed to find for the orthogonal directions ordered in maximal changes through the data. On the other hand, the resultant sediment geochemistry can be assumed to be a linear combination of statistically independent processes. In this study, instead of the widely used data reduction methods which depend on uncorelatedness (here by uncorrelatedness of two random variables, as defined in probability theory, two random variables are uncorrelated, if their covariance is equal to zero) of the resulting vectors, we apply the method of independent component analysis (ICA) with the aim of extracting the statistical independent/quasi-independent processes of the past climate causing the variability in the proxy data sets.

Micro-X-ray fluorescence (μ-XRF) of elemental profiles can be used as proxies for different processes in lakes with differing environmental settings (cf. [12]). The statistical dependence of μ-XRF elemental profiles of a core is widely recognized by the research community. For example, instead of elemental profiles, it is a standard practice to use elemental ratio profiles to normalize the effects of some process-related factors and possible systematic errors (cf. [13]). The elemental profiles of lake cores are the results of physical/statistical independent or quasi-independent processes and parameters, such as precipitation, organic production, temperature, water level and redox conditions in the lake or in its drainage basin.

In previous studies, PCA and FA are the most widely used statistical transformation methods applied to extract the underlying components of proxy data. PCA and FA give useful results if the observed time series are normally distributed and are linear mixtures of the source series [14]. However, even modern climate variables rarely obey Gaussian distribution [15,16], and shifts, trends and abrupt events increase the degree of past climate variables' non-Gaussianity and non-linearity. It is unreasonable to expect the data to be in the form of linear mixtures when one considers the highly dynamic environments from which they are sampled. The FA method does not actually extract components, rather it explains the governing factors of the system and the constituents of each factor, in the second order statistical sense. The components extracted by PCA are uncorrelated and the method tries to find the components that explain the maximal variance. Since the extracted components with maximum variances are not separated sources, instead they are mixtures of the true signals [17], the objective of PCA is questionable in the sense of source separation. This low-order nature is due to the fact that the backbone of both FA and PCA methodologies are the variance-covariance matrices.

ICA is a more robust statistical transformation method, developed for signal separation, and provides an alternative to PCA [18]. ICA's fundamental assumption is that the source time series are statistically independent for each point in time [19] and aims to identify a rotation matrix that in practice maximizes the independence of each source component. The main difference between the aims of PCA/FA and ICA is that the former aims to find uncorrelated components, whereas the latter aims to extract independent ones. Since, independency of random variables implies uncorrelatedness, the assumption of being independent is more powerful than being uncorrelated.

ICA has proven its explanatory power in different subjects (see reviews of [20] and [21]), such as feature extraction, signal processing, image processing, telecommunications, financial time series, etc. There are also, some examples in climate research which use ICA as an exploratory tool. By using ICA, [14] claim to reveal the geographical variability of El Niño Southern Oscillation and its links with Atlantic Ocean. [22], [23] and [24] extracted teleconnection patterns from sea level pressure field via ICA. [25] and [26] offer ICA as a preprocessing method in order to reduce dimensions through the downscaling process of general circulation model outputs. However, ICA has never

been applied to paleoclimate time series. Several different approaches to ICA exist, such as those based on the infomax or maximum likelihood methods (for an extended review see [27]). We use the FastICA algorithm [19], because it is a rapid and computationally straightforward method.

In this study, by applying FastICA, we attempt to extract precipitation and temperature related components from the μ-XRF data of a 3.5 m long piston core (Hz11-P03) recovered from Lake Hazar [28,29]. Hz11-P03 spans the last 17.3 *cal* ka, allowing us to understand past climate variability for the region throughout the last glacial-interglacial transition and the Holocene. Lake Hazar lies in the Eastern Anatolia region, feeds the headwaters of the major rivers of the Mesopotamia. Therefore, this study aims to give not only the climate variability of Lake Hazar and its catchment basin, also aims to give insight to the water variability in the so-called cradle of civilization.

There are some past climate studies in the region, such as geochemical and paleoecological data from Lake Nar and Eski Acıgöl [30–35]. There are also longer terrestrial records from Lake Van, which span the last 600 ka BP (see, [36]). However, none of the aforementioned studies use statistical decomposition methods, except [37], which use PCA of Lake Van geochemistry data to reveal hydroclimate variability in Eastern Mediterranean for the last 360 ka BP.

2.3 Regional Setting

Lake Hazar is located in south-eastern Anatolia at an altitude of 1255 m (Figure 2.1). It is a 25 km long, 7 km wide intra-montane sedimentary basin with a surface area of 78.5 km^2 and a volume of 7.5×10^9 km^3. The maximum depth of the lake is 220 m. Lake Hazar is a tectonic lake, located in an active pull-apart basin along the East Anatolian Fault Zone [38, 39]. Eastern Anatolia is the main water source for the major Mesopotamian rivers, Tigris and Euphrates. Lake Hazar lies on the upstream of a tributary of the Tigris river, which was previously an outlet of the lake [40, 41]. Tectonic uplift of the south-eastern part of the lake and excessive use of for agricultural purposes has broken the connection between the lake and the Tigris. Today, it is a terminal lake and fed only by numerous small ephemeral streams.

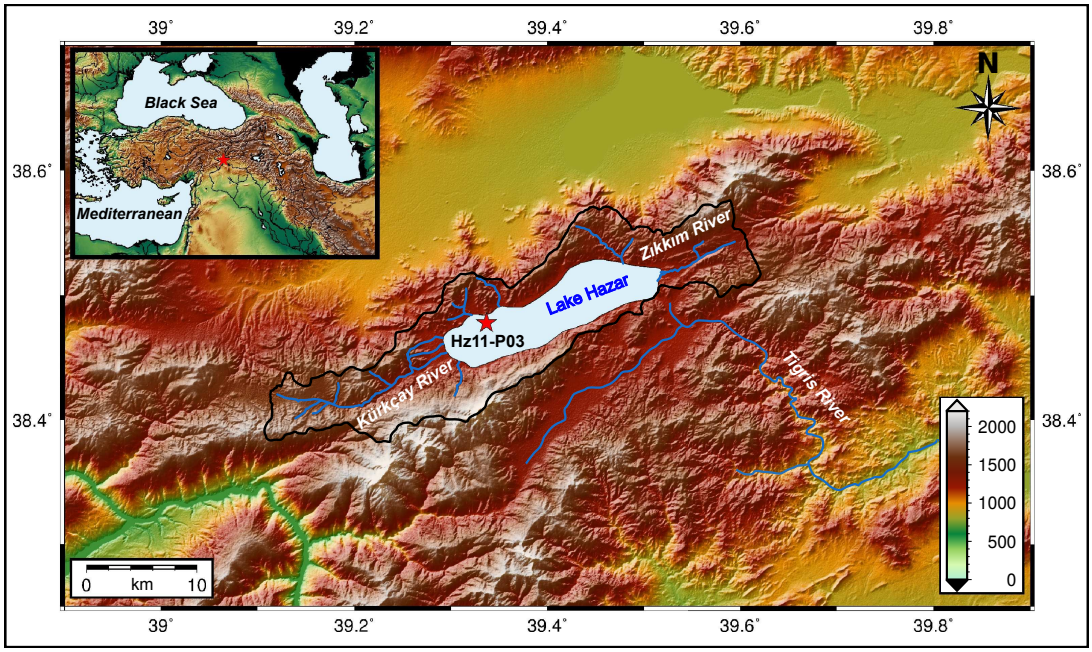

Figure 2.1 : Location map showing the drainage basin of Lake Hazar. The star indicates the location of the Hz11-P03 piston core. This map was prepared using the free mapping tool GMT, version 5.2.2 [42] and the catchment area and rivers were plotted using the free GIS tool SAGA, version 2.1.4 [43].

The main water and sediment sources for the lake are the Kürkçayı and Zıkkım rivers which flow into the south-west and north-east of the lake, respectively. Maximum discharge occurs during the spring season as a result of snow melt and rainfall. The lake's catchment area is mostly covered by magmatic, metamorphic and ophiolitic rocks of the Mesozoic and Paleozoic Eras. The main bedrock along the southern cost of the lake, its most rugged area, also consists of Middle Eocene calcareous rocks and Late Jurassic magmatic rocks.

Lake Hazar is a monomictic, oligotrophic and alkaline lake (pH=9.1 ± 0.2) with high carbonate and bicarbonate concentrations. Complete mixing takes place during the autumn and early winter and incomplete mixing in the spring season. The lake is stratified between June and September, and the surface water temperature changes from 5 °C to 29 °C in the pelagic zone throughout the year [44].

The climate of Eastern Anatolia has long been considered as being a transition between continental and Mediterranean climates and is described as a Continental Mediterranean climate [45] which is distinguished by excess precipitation in spring, rather than in winter [46]. Precipitation in the Mediterranean basin in winter is mainly affected

by the position and power of the subtropical anticyclone settled over the Azores. Weaker high pressure over the Azores is one of the main causes of wetter winters [47]. However, Eastern Mediterranean precipitation is also fed by moisture from the western Mediterranean [48] and the Siberian high pressure system has an effect on winter precipitation and tempereatures [49]. The northward movement of the subtropical high pressure system in the summer leaves the region almost with no precipitation at all. Furthermore, the thermal low, a result of the south Asian summer monsoon, that settles over the Persian Gulf carries dry air in from the Asian interior [50].

The lake area has an annual mean precipitation of 610.1 mm for the time period 1974-2004, according to the closest meteorology station to the study area which is at Sivrice in Elazığ. This precipitation falls mainly between November and May, accounting for more than 87% of the total precipitation.

2.4 Materials and Methods

2.4.1 Core Hz11-P03

The 3.8 m long core, Hz11-P03, was recovered in 2009 from north-west of Lake Hazar, at a depth of 54 m (Figure 2.1). The physical, sedimentological and geochemical methods applied to understand the properties of this core through various analyses are described in detail by [29].

2.4.2 µ-XRF core scanner analysis

The split half core was non-destructively analyzed at 1 mm resolution, using an ITRAX XRF core scanner equipped with a Mo X-ray source set to 60 kV, 0.3 mA and an exposure time of 30 seconds at the EMCOL Core Analysis Laboratory at İstanbul Technical University. Up to 25 elements are semi-quantitatively analysed and concentrations were recorded as counts per second (cps).

2.4.3 Magnetic susceptibility measurements

Magnetic susceptibility (MS) measurements were performed in İTÜ-EMCOL laboratories via Geotek Multi-Sensor Core Logger at 1 cm resolution.

2.4.4 δ^{18}O and δ^{13}C analysis

The split half core was sampled at 30 mm intervals for stable oxygen and carbon analysis from ostracod shells. The samples were freeze-dried and sieved through 63 µm mesh under filtered tap water. Ostracod species were identified under a stereo microscope and the most continuous and abundant species, *Candona neglecta* [51], were selected for the δ^{18}O and δ^{13}C analysis. For each section 20 adult carapace samples were analysed at the University of Arizona stable isotope and geochemistry laboratories, in the USA.

δ^{18}O and δ^{13}C of carbonates were measured using an automated carbonate preparation device (KIEL-III) coupled to a gas-ratio mass spectrometer (Finnigan MAT 252). Powdered samples were reacted with dehydrated phosphoric acid under vacuum at 70°C. The isotope ratio measurement is calibrated based on repeated measurements of NBS-19 and NBS-18 and precision within 1σ error is ± 0.10‰ for δ^{18}O and ± 0.08‰ for δ^{13}C.

2.4.5 Chronology

Accelerator Mass Spectrometry (AMS) radiocarbon dating analyses were carried out at the Woods Hole NOSAMS. Six radiocarbon dates for Hz11-P03 have been documented by [29] (Table 2.1). [29] showed the existence of a hiatus by lithological description and seismic stratigraphy at a depth of 270 cm in the core. The radiocarbon dates were calibrated using IntCal [52] and the age model was constructed using the Bacon (Bayesian accumulation) package [53] in the freeware statistical software package, R [54].

Unlike "traditional" simple linear age-depth interpolation models, Bacon aims to produce more realistic age models, by applying bivariate monotone Markov process between predefined increments between dated intervals. According to [53]. The qualitative difference between the Bacon and other sophisticated age-depth models, such

as OxCal [55] or BChron [56], is that, the results from Bacon are more "environmentally inspired" models.

Table 2.1 : Radiocarbon dates obtained from Hz11-P03. Error intervals, within 95% confidence range, and weighted mean ages are the results of Bacon.

Lab ID	Depth (cm)	Material	^{14}C BP	95% confidence interval (cal BP)	Weighted mean age (cal BP)
OS-106010	59	Mollusc	2240 ∓ 45	$2012 - 2345$	2209
OS-97568	133	Wood	3560 ∓ 45	$3717 - 4327$	3939
OS-106006	208	Mollusc	7800 ∓ 70	$8317 - 8926$	8578
OS-106002	244	Mollusc	9240 ∓ 70	$10201 - 10690$	10416
OS-96328	285	Mollusc	11400 ∓ 50	$12931 - 13437$	13212
OS-96329	348	Mollusc	14600 ∓ 80	$17208 - 18027$	17682

The Bacon package needs two basic pieces of prior information. The first one is the mean accumulation rate and accumulation shape (a parameter which gives the shape of the accumulation rate probability density function- a gamma distribution). Mean accumulation rate value is suggested by Bacon, prior to the calculations. For Hz11-P03, the package estimated a 50 a /cm mean accumulation rate. The rate is reasonable for Hz11-P03, since the length of the core is 350 cm and the IntCal13 age result at 348 cm is 17.78 ∓ 0.215 *cal* ka BP. The accumulation shape parameter is left to default of Bacon (that is 1.5), a figure that was arrived at by analysing 152 Holocene lake deposits [57]. The second piece of prior information required is the section thickness. The code runs over the predefined sections according to the length, which in our case is 5 cm, and makes the linear interpolations over sections. Since section thickness parameter should be changed if a smoother curve is needed, we implemented the default parameter for it. Beside these two parameters, it is possible to change the memory strength/memory mean and hiatus depth/hiatus shape. Memory parameters, which construct the character of the sedimentation in the age model, are defined as a beta distribution in Bacon. As stated by [53], changes in memory parameters do not significantly alter the age model and by changing the parameters we tried to fit the posterior distribution to prior distribution. On the other hand, it is important to note that there is a hiatus at a depth of 270 cm in Hz11-P03. The default hiatus interval length of Bacon is 1000 years, and according to the model this length may change. Since, according to the ages below and above the hiatus, it is somewhere between the uncalibrated ages, 14.6 ka and 11.4 ka ^{14}C BP, we assigned the hiatus to the Younger Dryas (YD) period, formally accepted to be during

between 12.85 ka BP and 11.65 *cal* ka BP [58]. We therefore applied the default value, which is 1000 years, for the duration of the hiatus.

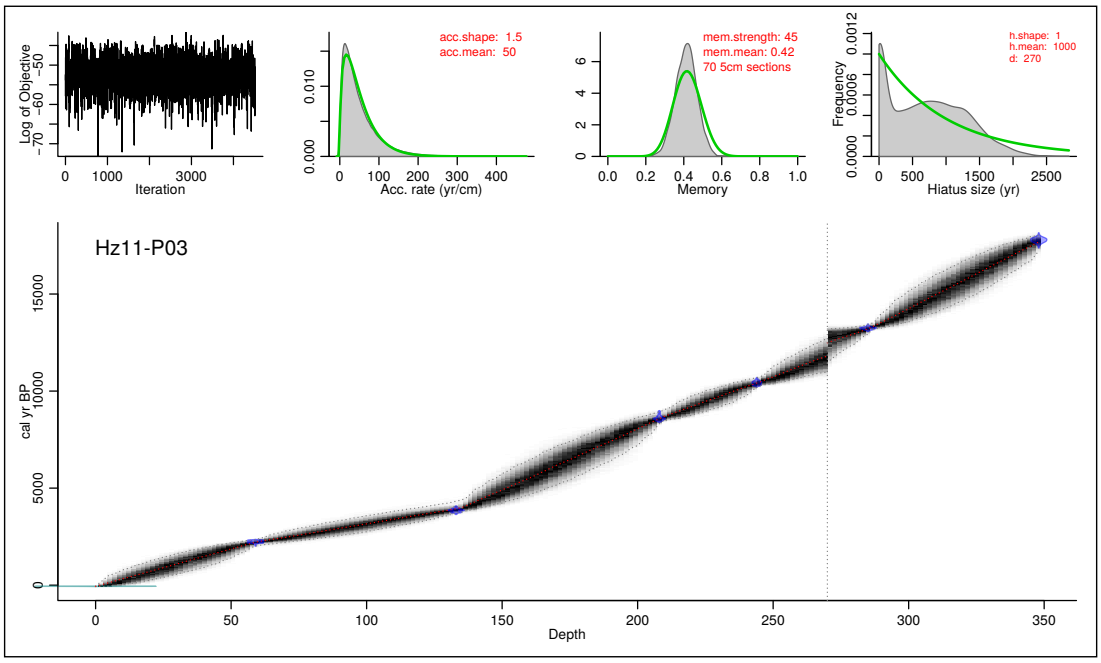

Figure 2.2 : Age model of Hz11-P03, constructed using the Bacon statistical package. The dashed line at 270 cm shows the hiatus location.

2.4.6 Statistical analyses

2.4.6.1 Filtering the data

High resolution µ-XRF data may involve analytical and instrumental noise [13] but a low-pass filter would minimize these errors. Therefore, in order to minimize noise, we applied a first order Savitzky-Golay filter (SGF) to the Hz11-P03 core µ-XRF data with age control points [59]. The SGF fits a polynomial to the data with the desired window length and selects the corresponding point on the polynomial curve and replaces the data point with the selected one. For evenly spaced data a first order SGF is nothing more than a simple moving average. However, for irregularly spaced data, which is more usually encountered in paleoclimate time series, a first order SGF is able to give suitable weights to each point by linear regression in the desired window. In order to fit the data to the age model, after applying the SGF to a five point window length, we resampled the data at one in every five consecutive data points (Figure 2.3). After all the above processes, we applied FastICA algorithm by using a commercial software

(MATLAB 8.2, The MathWorks Inc., Natick, MA, 2013), for which the code is freely available online.

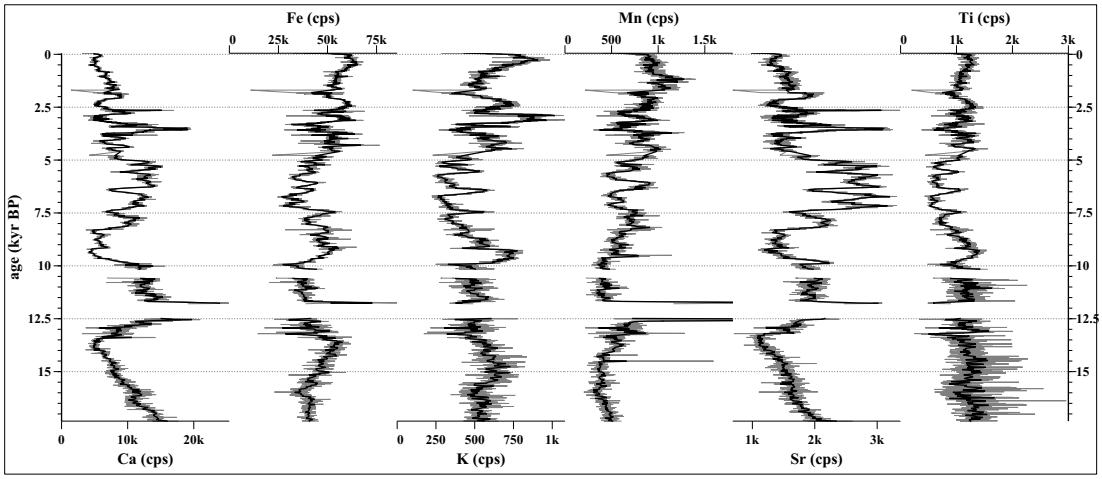

Figure 2.3 : The μ-XRF data in gray and on top of each profile the filtered data in black as described in Section 2.4.6.1 are plotted.

2.4.6.2 Independent component analysis

The ICA model

Assume that, $\mathbf{X} = [\mathbf{x_1}, \mathbf{x_2}, ..., \mathbf{x_n}]$ is a $d \times n$ dimensional observed data matrix and $\mathbf{S} = [\mathbf{s_1}, \mathbf{s_2}, ..., \mathbf{s_n}]$ is the p-dimensional source random variable, with non-Gaussian and independent entries. If the independent components are mixed by an unknown linear transformation $\mathbf{A}_{d \times p}$ by

$$\mathbf{X} = \mathbf{AS}, \tag{2.1}$$

then the model in equation (2.1) is called the ICA model [19]. To solve the ICA model, the mixing matrix, $\mathbf{A}$, must be known. After estimating the matrix $\mathbf{A}$, $\mathbf{S}$, the source, can be found by

$$\mathbf{S} = \mathbf{WX}, \tag{2.2}$$

where $\mathbf{W}$ is the inverse of $\mathbf{A}$.

Preprocessing

Before applying ICA, the data should be centred and then whitened. Whitening is a process of finding standardized principal components, i.e. principal components with unit variances. This process clears the second-order statistical information of the data. The whitening process of the mixing matrix allows ICA to rotate the axes of

the whitened mixed components to the space of independent components, which is essential to liberate the data from the dependency of the covariances [60].

Table 2.2 : Distance correlation coefficients of Hz11-P03 independent components of μ-XRF data with NGRIP δ^{18}O, Sofular δ^{13}C and μ-XRF data.

dcorr	Hz-ic1	Hz-ic2	Hz-ic3	Hz-ic4	Hz-ic5	Hz-ic6
NGRIP-δ^{18}O	0.16	0.17	0.17	0.38	0.47	0.43
Sof-δ^{13}C	0.13	0.15	0.15	0.26	0.43	0.27
Ca	0.21	0.51	0.14	0.38	0.48	0.53
Fe	0.17	0.23	0.20	0.54	0.57	0.54
K	0.16	0.24	0.23	0.58	0.18	0.77
Mn	0.57	0.28	0.22	0.22	0.62	0.44
Sr	0.18	0.45	0.16	0.77	0.29	0.29
Ti	0.12	0.34	0.52	0.76	0.19	0.23

The FastICA algorithm

Independent Component Analysis is a method to separate non-Gaussian signals by imposing the probabilistic constraint of minimizing mutual information. It achieves the separation by making use of "Kullback-Leibler divergence", a measure of difference between two probability distributions of separate signals that become mixed through a variety of processes. As such, unlike the PCA, ICA's starting point is statistical independence which automatically imposes the separability condition on the joint probability distributions of the mixed signals. There are various ways in which ICA can be implemented. In order to extract independent components, [19] offer two different methods. These are *a*) the deflation method and *b*) the symmetric method. The former method estimates independent components one-by-one, whereas the latter estimates all the components together. [61] recommend the deflation method, if the number of independent components is limited. Therefore, the deflation method was preferable for two reasons: firstly to follow the recommendation of [61] and secondly, because the distance correlation results of the reference data with the selected independent components (see Section 2.4.6.2) extracted by the deflation method are higher than the components extracted by the symmetric method.

The algorithm of the deflation method is described as follows. To estimate only one independent component, [62] offers the following algorithm.

i. A non-quadratic contrast function *G* should be chosen. The contrast function is used to estimate the negentropy (for detailed explanations, see [63]), which is a measure

of the Gaussianity of a random variable. Negentropy J of a random variable $\mathbf{y}$ is given by

$$J(\mathbf{y}) = H(\mathbf{y}_{gauss}) - H(\mathbf{y}), \tag{2.3}$$

where $\mathbf{y}_{gauss}$ is the Gaussian random variable with the same covariance matrix of $\mathbf{y}$ and H is the measure of Shannon's entropy, which is:

$$H(\mathbf{y}) = \sum_i p(y_i) \log p(y_i). \tag{2.4}$$

Note that, negentropy of a random variable is zero if and only if it is Gaussian. Maximizing the negentropy of a random variable means to minimize its Gaussian properties and also, maximizing the negentropy of random variables, which have zero mean and unit variance, means minimizing the mutual information, which is a natural measure of independence [19].

The contrast function G should be non-quadratic and for this study we used

$$G(u) = \log(\cosh(u)), \tag{2.5}$$

which is offered by [62] for general purposes.

ii. A random weight vector $\mathbf{w}$ should be chosen in order to initialize the procedure.

iii. By applying Kuhn-Tucker conditions to maximize the negentropy, [19] present the following equation:

$$\mathbf{w}^+ = E[\mathbf{x}g(\mathbf{w}^\mathbf{T}\mathbf{x})] - E[g'(\mathbf{w}^\mathbf{T}\mathbf{x})]\mathbf{w}, \tag{2.6}$$

where g is the first derivative of the contrast function G, and

$$\mathbf{w} = \mathbf{w}^+ / \left\|\mathbf{w}^+\right\|. \tag{2.7}$$

This procedure is then operated iteratively until the convergence to maximal non-Gaussianity is established. Here, the convergence means that, during the iteration the resulting vector $\mathbf{w}$ should almost point in the same direction as the previous one through the iteration process. They call this method the fixed-point algorithm.

To estimate the remaining components, running the algorithm by assumed component number times by different initial random vectors alone is not enough, because these can converge to the same maxima. To prevent this, decorrelation of the components (which

means orthogonalization in the whitened space) is sufficient [62]. After estimating the first p component vectors, i.e. $\mathbf{w}_1 ... \mathbf{w}_p$, the deflation scheme proposed to find the remaining components is

$$\mathbf{w}_{p+1} = \mathbf{w}_{p+1} - \sum_{j=1}^{p} (\mathbf{w}_{p+1}^{\mathrm{T}} \mathbf{w}_j) \mathbf{w}_j \tag{2.8}$$

and then normalizing $\mathbf{w}_{p+1}$ by dividing to its vector length.

Discussion of the advantages of the FastICA algorithm beyond the other independent component algorithms is beyond the scope of this article but they are discussed in detail by [19].

If the number of the variables is more than the sample size, or the variables have strong time dependencies (i.e. the time series are exactly periodic), then ICA algorithm may produce components with exaggerated spikes or bumps [64], this situation is known as "overlearning". In our case, there are 6 variables each with 634 data points and the elemental profiles are not time dependent, which can be tested by spectral analysis or just by looking at the data (see Figure 2.4).

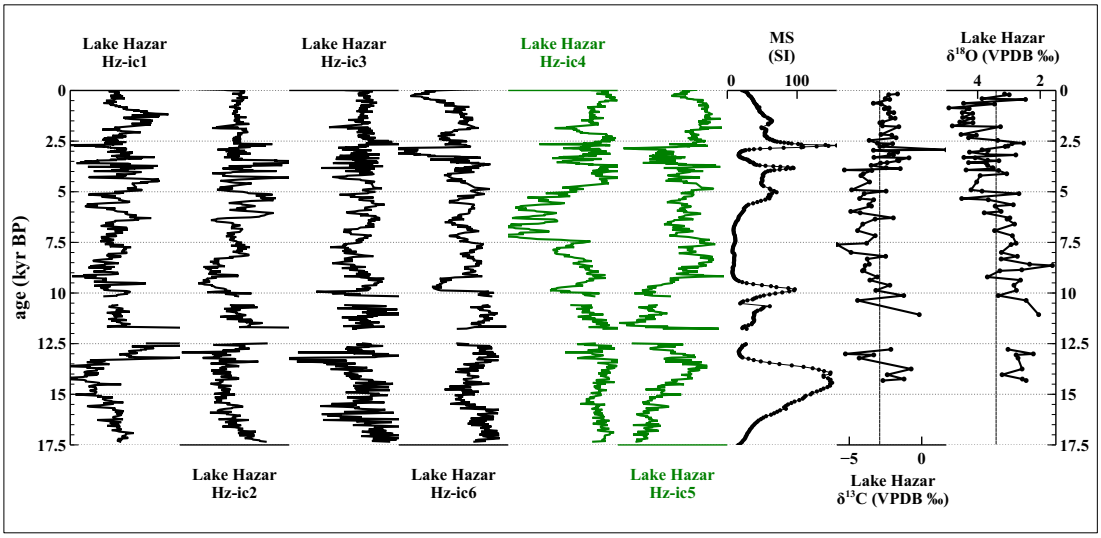

Figure 2.4 : Components after the FastICA, MS and stable isotope data. The vertical lines at the isotope plots show the average of isotope data. Green colored plots are the selected independent components.

Selecting the appropriate components

The resulting vectors of ICA, unlike PCA, are neither given in order nor are their energies known [19]. Therefore, to select the appropriate components, we applied the distance correlation [65] as the similarity measure between the independent components

and past climate records, which for this study are δ^{18}O for NGRIP (North Greenland Ice Sheet Project) [66] and δ^{13}C for Sofular Cave [67]. Polar ice core δ^{18}O data carry information about temperature [68]. Furthermore, NGRIP is the latest drilled ice core and amongst the other ice cores, NGRIP δ^{18}O data is the most sensitive to Holocene climate changes [69]. The Sofular Cave stable isotope sequences provide high resolution records for the Eastern Mediterranean region, with a more than adequate age model. We will therefore use these datasets as the reference data hereafter.

The empirical distance correlation for ordered pair data, $(\mathbf{x}, \mathbf{y})$ with n elements, is defined as follows:

$$R(\mathbf{x},\mathbf{y}) = \begin{cases} \sqrt{\frac{\nu^2(\mathbf{x},\mathbf{y})}{\sqrt{\nu^2(\mathbf{x})\nu^2(\mathbf{y})}}} & \text{,if } \nu^2(\mathbf{x})\nu^2(\mathbf{y}) > 0; \\ 0 & \text{,if } \nu^2(X)\nu^2(Y) = 0, \end{cases} \tag{2.9}$$

where

$$\nu^2(\mathbf{x},\mathbf{y}) = \frac{1}{n^2}\sum_{k,l=1}^{n} A_{kl}B_{kl}, \tag{2.10}$$

and

$$\nu^2(\mathbf{x}) = \frac{1}{n^2}\sum_{k,l=1}^{n} A_{kl}^2. \tag{2.11}$$

A_{kl} and B_{kl} are defined as

$$A_{kl} = a_{kl} - \bar{a}_{k.} - \bar{a}_{.l} + \bar{a}_{..} \tag{2.12}$$

and

$$B_{kl} = b_{kl} - \bar{b}_{k.} - \bar{b}_{.l} + \bar{b}_{..}, \tag{2.13}$$

where $a_{kl} = \|X_k - X_l\|$, $b_{kl} = \|Y_k - Y_l\|$ and $k, l = 1, ..., n$. The subscript "." denotes that the mean is computed for the whole index.

The distance correlation is equal to 0 if and only if the random variables are independent and $0 \leq R(\mathbf{x},\mathbf{y}) \leq 1$. The distance correlation's superiority comes from its power to catch non-linearities, strength on outliers, revealing independencies and computational simplicity. However, its statistical power over rival methods is an on-going topic of discussion [70–73].

Distance correlation, as inputs, needs data vectors each having the same number of elements. Therefore we linearly interpolated the NGRIP δ^{18}O record, with 20 years of resolution [74], and the Sofular Cave δ^{13}C record to Hz11-P03 age model

and computed the distance correlation coefficients to identify any climate-related components (Table 2.2).

2.5 Results and Discussions

According to the age model, Hz11-P03 covers the last 17.3 *cal* ka BP with a hiatus of 700 years between 12.49 ka BP and 11.76 *cal* ka BP (Figure 2.2). The age of the hiatus, according to the dates calculated by using Bacon, fit almost within the YD cold event. This estimate of the hiatus fits with the hypothesis proposed by [29] of a 73 m drop in the level of Lake Hazar during the YD period.

The idea of decomposing mixed data by means of statistical independence has some superiority over orthogonal decomposing with respect to maximal variance [75, 76]. However, there are some drawbacks. The first one is the assumption of non-Gaussianity of the source signal. The non-Gaussianity of modern climate variables [15, 16] makes this assumption plausible. Secondly, the order of the resultant independent components and their signs are unknown. While the assumptions of ICA come from a stronger assertion than the second order statistical techniques, it is not easy to select and give meanings to the results. Therefore, in this study, the candidate components are selected through a similarity measure, which is the distance correlation. Components that are highly correlated with the well dated, high resolution records are taken as basis and the correlation results with the μ-XRF data are discussed. However, especially climatologically well established periods, such as the Bølling-Allerød, make it easy to select the desired components with the correct sign. Here, the use of reference data is not to create a circularity, rather it is used to have a basis on selecting the appropriate components.

The other drawback of the method lies in the nature of the μ-XRF data. It is clear that ICA cannot find any result which does not exist within the data. The values of local extremes in the data may not only depend on natural factors, but also on the precision of the ITRAX core scanner. For example, a period with higher amount of coarse grained sediment input may distract the μ-XRF results [77]. So, while evaluating the magnitude of ICA of μ-XRF data results, it should be kept in mind that the results may be temporally local. It would be better to evaluate a period with events before and after.

A question may arise about the data analyzed. One may want to apply the method on elemental ratios which is widely used in geochemical proxy data interpretations. We also applied FastICA on the Fe, K, Ti, Ca/Ti, Sr/Ca and Mn/Fe dataset, however the results of both analyses are convincingly similar.

2.5.1 Interpretation of the independent components

The μ-XRF Ca, Fe, K, Mn, Sr and Ti concentrations that are extensively used in paleolimnology studies [12], constitute around 95% of the total measured content of the μ-XRF data of the Hz11-P03 core. We therefore applied FastICA to the profiles of these six elements and the resulting components were compared with the reference data and the μ-XRF data via distance correlation.

The distance correlation coefficients between the independent components and the reference NGRIP δ^{18}O and Sofular δ^{13}C data show that the fifth independent component (Hz-ic5) has the highest correlation (Table 2.2). Moreover, the correlation coefficients of independent components with the μ-XRF data imply that Hz-ic5 is also related to Ca, Fe and Mn (Table 2.2) Ca may precipitate as calcium carbonate in lakes via a number of different processes (cf. [78, 79]). Solubility of carbonate minerals is dependent on temperature and salinity. Their precipitation may be related to the organic productivity and evaporation processes, which indirectly related to temperature, evaporation/precipitation and the availability of light. Fe and Mn can be used as a measure of detrital input but both also contain information about reducing conditions in lakes (for extensive summaries see [80] and [12]). The redox reactions are mainly determined by organic matter production and water column stratification, which in turn is mostly affected by light and temperature [81], and which is commonly coupled with Ca precipitation.

NGRIP δ^{18}O reflects the temperature changes in Northern Hemisphere high latitudes [68] and according to [67], the changes in temperature are reflected in the δ^{13}C record from Sofular Cave stalagmites. Therefore, the correlation of Hz-ic5 with the reference data sets and Ca, Fe and Mn could be argued to reflect temperature changes in the lake and its catchment region (Figure 2.5).

While the sixth component (Hz-ic6) has the second highest correlation with the reference data, we could not attach any meaning to it. However, the high correlation

values of the fourth component (Hz-ic4) with Ti, Sr and also with the reference data (Table 2.2), give an indication about a relationship between Hz-ic4 and precipitation. It correlates closely with Ti, Sr, K and Fe (Table 2.2). Ti, K and Fe provide information about detrital input that is mainly dependent on precipitation. Sr is used as a proxy for evaporative processes in lakes [80]. Thus, we can interpret Hz-ic4 as a proxy for precipitation/evaporation (Figure 2.5).

Summarizing our results, we conclude that Hz-ic4 and Hz-ic5 are proxies of precipitation/evaporation and temperature, respectively. However, it should be noted that they have no absolute units, only reflecting relative changes through time, and are referred as "temperature" and "precipitation" for the rest of this paper.

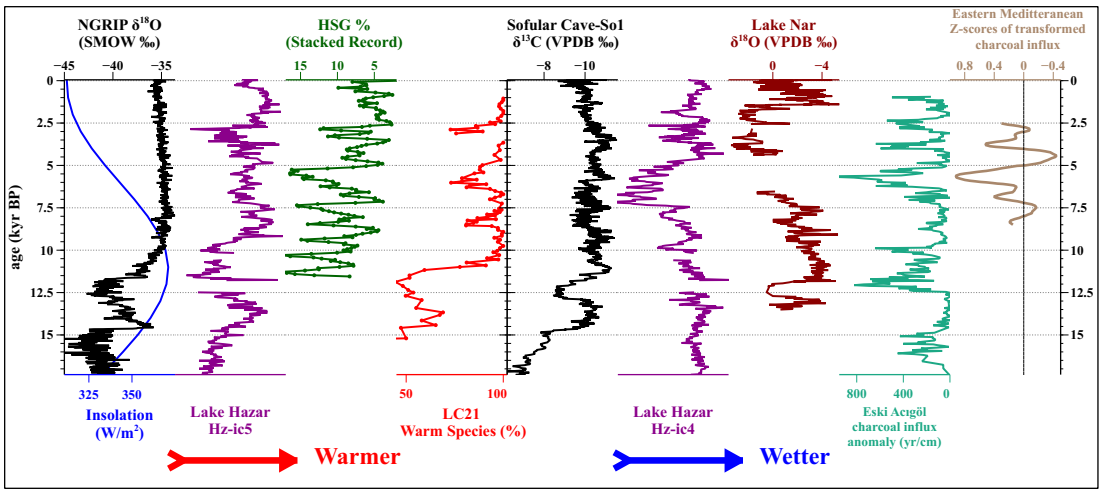

Figure 2.5 : Comparison of the results of this study with other studies. From left to right, NGRIP δ^{18}O [74] and difference between summer solstice and winter solstice insolation for 37°N [82], Hz-ic5, North Atlantic hematite stained grains percent [83], percent of the LC21 core warm species [84], Sofular Cave δ^{13}C [67], Hz-ic4, Lake Nar δ^{18}O, as explained in the original study, %3 shifted Eski Acıgöl charcoal influx anomaly [34], average transformed charcoal influx for Eastern Mediterranean lakes [85].

2.5.2 Temperature and precipitation records

The results from Lake Hazar reveal that before 14.6 *cal* ka BP the temperatures of the region were lower than the following warm period. On the other hand, the precipitation was at almost the same level as the subsequent Bølling-Allerød warm period. Temperatures in the region rise with the start of the Bølling-Allerød and the precipitation record shows a slight increase with this warming. At the end of

Bølling-Allerød, the lake level evidently dropped to 73 m below its modern level [29] producing an 700 yr hiatus during the YD period.

After the start of the Holocene, temperatures evidently rose gradually and achieve the warm conditions of the Holocene within 2 millennia. After 9.5 *cal* ka BP, Hz11-P03 temperature record follows the North Atlantic stacked ocean record [83] within the error range of Hz11-P03 age model. The most striking of all the oscillations is the one around 3.5 *cal* ka BP, which corresponds to the second Bond cycle [83]. This cold period (Table 2.2) lasted until 2.6 *cal* ka BP.

The precipitation record for the Holocene is somewhat different to the temperature record. The start of the Holocene was as wet as the Bølling-Allerød interstadial and but a gradual decrease in precipitation occurred up to 9.5 *cal* ka BP. From 9.5 *cal* ka BP, until 8 *cal* ka BP, the region experienced a wet period. After 8 *cal* ka BP, and lasting for almost 3 ka, a harsh dry period with internal oscillations can be observed. This arid phase is also evident in MS and δ^{13}C records of Hz11-P03. After 5 *cal* ka BP a wet phase occurred following almost directly on from the oscillations in the temperature record, with marked dry phases taking place during 3.5 *cal* ka BP, 2.8 *cal* ka BP and 1.8 *cal* ka BP (Figure 2.5).

2.5.3 Comparison with other regional records

2.5.3.1 Pre-Holocene

Pollen [86, 87], lake level [88, 89] and glacier [90, 91] studies from around the Eastern Mediterranean indicate that the region was cold, but humid after the Last Glacial Maximum (LGM) until the Bølling-Allerød interstadial. In this context, the Lake Hazar results, which indicate, relatively cold and humid conditions before the Bølling-Allerød, correlate well with these other regional records. There exist two main hypotheses about the cause of these cold but wet conditions in the Eastern Mediterranean between the LGM and the Bølling-Allerød. The first is that cool and cloudy summers, that decrease evaporation, are the reason for semi-arid vegetation and high lake levels in this interval [92]. The second hypothesis is that the cause was the southward migration of the jet streams, and resultant moisture-rich westerly winds during LGM [86, 93]. Such a migration would cause wetter conditions in the Eastern Mediterranean. The

precipitation result from Lake Hazar for the 17.3 ka BP and 14.8 *cal* ka BP interval, support the migration of the westerlies hypothesis, although we cannot entirely reject the cool and cloudy summer hypothesis. Probably, both mechanisms were in effect in the Eastern Mediterranean before the Bølling-Allerød.

There are studies in the Eastern Mediterranean which offer a dry period during the Heinrich-1 event [94, 95]. However, our Hz11-P03 data and ICA results do not offer an arid phase for $\sim$ 17 *cal* ka BP.

Following this, Bølling-Allerød period was warm and wet by comparison, as one would expect based on current models and data. As previously documented by [29], the decrease in lake level and resulting hiatus within the core between 12.49 ka BP and 11.76 *cal* ka BP shows that, for the last 17.3 *cal* ka, the region experienced its most extreme dry period during the YD. Also, the low temperature values at the end of the Bølling-Allerød period and at the start of the Holocene indicate that the YD period is likely to have been as cold as expected.

2.5.3.2 Holocene

From the end of the YD period until 9.5 *cal* ka BP, the temperature of the region shows an increasing trend, as seen in the NGRIP δ^{18}O record in the same period. The oscillations in temperature resemble those seen in the North Atlantic stacked HSG record [83]. However, the precipitation record behaves somewhat differently to that for temperature. For the early Holocene, the Lake Nar δ^{18}O record [35] and Hz11-P03 precipitation record closely resemble each other with a wet period up until 9.5 *cal* ka BP, and a decreasing precipitation trend to 8.2 *cal* ka BP. The wet conditions with a drying trend were also documented in previous Eastern Mediterranean studies [30, 93, 96]. During the early Holocene, summer insolation was at its maximum, whereas winter insolation was at its minimum (Figure 2.5). This increasing seasonality may have resulted in the Mediterranean Sea being warmer during cold winters and consequently, as [97] have proposed, it was wetter at the start of the Holocene.

After 8 *cal* ka BP, while the temperature oscillations follow the North Atlantic climatic oscillations [83], precipitation records show a period of great aridity until 5 *cal* ka BP. During this period, North Africa was wetter [98] and evidence for a drought in the Eastern Mediterranean is indicated by charcoal data [34, 85]. During this interval, as

the Northern Hemisphere was receiving more insolation than today, the Intertropical Convergence Zone lay in a more northerly position [99, 100]. As a result of this, the subtropical high pressure belt, which today lies over the southern Mediterranean, particularly affected the north-east Mediterranean and created arid conditions in the region.

Between 5.5 ka BP and 5 *cal* ka BP the precipitation record reveals that the region gradually became wetter, finally reaching modern conditions. However, the abrupt decline in both precipitation and temperature around 3.5 ka BP, 2.8 ka BP and 1.8 *cal* ka BP, which were also documented in the seismic records [29], may have been the result of a coincidence of the strengthening of the Siberian high pressure system during winters [79, 84], and the gradual decrease in solar irradiance, especially around 2.8 *cal* ka BP [101], in accordance with changes in the North Atlantic [83].

For the Holocene, the most striking result is that the spikes in precipitation and temperature records appear to closely follow the North Atlantic Bond events, whereas the trends do not. If the cause of the Bond events is indeed solar forcing, as claimed by [83], then we can also state that the climate oscillations in the region were also greatly influenced by solar forcing. On the other hand, if the cause were related to circulation changes in the North Atlantic [102], then it is noteworthy to add that there appears to be a direct relationship between the temperature of the region and North Atlantic. Additionally, we can state that precipitation oscillations are related to the North Atlantic, but that precipitation appears to be a function of a much more complex system.

The regional context of Lake Hazar is such that not only do the results of the current study have implications for understanding the Holocene climate and environment of eastern Anatolia but also for that of Mesopotamia. This is because, when at its maximum, the waters that flow out from Lake Hazar empty into one of the two great Mesopotamian rivers, the Tigris. Together with the Euphrates, it is rainfall and meltwater from the high mountains of northern Mesopotamia and eastern Anatolia that feed the Tigris and formed the economic basis of that region's ancient civilizations, which relied on river-fed irrigation systems from these two rivers as they flowed through an otherwise dry landscape.

A number of scholars have hypothesized that several incidents of societal collapse in Mesopotamia that are observable in the archaeological record may have been caused by the type of abrupt environmental change that we see in the data from Lake Hazar. Although much more research on the question of the temporal coincidence between climate and changes in human settlement is required, it is interesting to make some preliminary observations on how our scientifically observed climate data may relate to these archaeological phenomena.

For example, an observed archaeological phenomenon for which a climatic cause has been posited is the so-called 4.2 ka BP event [8, 103]. However, here the ICA of the Hz11-P03 core indicates that there is no evidence for any abrupt climatic change at this point in time. We therefore suggest that further studies should be conducted to confirm or deny the existence of abrupt climate change in the Anatolia/Mesopotamia region at this time, but based on our evidence we suggest that an archaeological explanation is more likely to account for this observed cultural phenomenon than a climatic one.

2.6 Conclusions

In this paper, we present a new method to extract paleoclimate signals from μ-XRF data using independent component analysis (ICA) and the stable isotope data from Lake Hazar.

ICA proves to be more suited to the extraction of paleo-climate signals than the traditional second order statistical methods (such as PCA and FA), if it is known that the underlying signals are the results of statistically independent/quasi-independent processes. ICA's aim is to find directions in space that satisfy maximum independence rather than to find directions with maximal variance. In this study, the aim is to offer a method for geochemical time series, which are thought to be representatives of past climates. However, it should be noted that, particularly, the process of component selection from the results of ICA (see section 2.4.6.2) needs to be improved for future studies.

The μ-XRF data from the Hz11-P03 sediment core from Lake Hazar shows six different elemental profiles, which constitute around 95% of the total count, which were subjected to ICA, and accordingly six independent components were gathered. We selected two

of the six independent components from the Lake Hazar μ-XRF data, based on their distance correlations against NGRIP and Sofular Cave isotope data. Our paleoclimatic and paleoenvironmental interpretations of these two components suggest that they are related to precipitation/evaporation and temperature. Based mainly on the profiles of these two independent components, we conclude the following:

1. The interval between 17.3 ka BP and 14.8 *cal* ka BP was cold but as wet as the following the Bølling-Allerød period, a conclusion which is also supported by previous studies around the Eastern Mediterranean. This was, most probably, the result of the southward migration of the Northern Hemisphere jet streams which were restrained from moving northwards by the anti-cyclonic atmospheric system settled over the high latitude LGM ice sheets.

2. The Bølling-Allerød warm interval, which is dated to between 14.8 ka BP and 12.85 *cal* ka BP, was warm and wet.

3. During the Younger Dryas cold event, the level of Lake Hazar fell by 73 m, causing a hiatus in Hz11-P03 during 12.49 ka BP and 11.76 *cal* ka BP.

4. At the start of the Holocene temperatures rose gradually, and reached "Holocene normals" at around 8 *cal* ka BP. This period after the YD was unexpectedly wet because of seasonality due to orbital parameters.

5. Between 8 ka BP and 5 *cal* ka BP, the region's temperature record follows the North Atlantic oscillations. However, its precipitation record shows that it experienced its most arid period during the Holocene. This was the result of the settling of the Subtropical High Pressure system over the north-eastern Mediterranean which blocked humid air streams from the Atlantic. In accordance with the changes in insolation, this dry period gradually came to an end around 5 *cal* ka BP.

6. After 5 *cal* ka BP, and up until 3.5 *cal* ka BP the climate again fluctuated around the "Holocene normal". However, around 3.5 *cal* ka BP, temperatures fell abruptly and sudden cold arid phases occurred around 3.5 ka BP, 2.8 ka BP and 1.8 *cal* ka BP. The cause of this abrupt cooling and drying phase can be the strengthening of the Siberian high and in accordance with the changes in insolation and North Atlantic system.

7. There is no evidence for the putative 4.2 ka climate event in Lake Hazar which has been postulated on the basis of archaeological evidence.

3. TEMPERATURE AND PRECIPITATION VARIABILITY IN EASTERN ANATOLIA: RESULTS FROM INDEPENDENT COMPONENT ANALYSIS OF LAKE VAN SEDIMENT DATA SPANNING THE LAST 250 KYR BP[1]

3.1 Abstract

In this study, we present the results of independent component analysis (ICA) of previously published Lake Van data covering the last 250 kyr BP, to shed light on the precipitation and temperature regime in eastern Anatolia. The data processed were the element intensities of Ca, Fe, K, Mn, and Si analyzed by XRF core scanner; concentrations of TOC and $CaCO_3$ content; and B* (color reflectance) from the Ahlat Ridge sediment record. Our analysis is based on application of ICA on the data by changing the initial random unit vector several times and clustering possible independent components through average-link agglomeration. As components extracted by ICA do not have a hierarchy, mutual information, which is a measure of information content between two random variables, is used as a measure of similarity by which to select candidate components. As a result, we argue, the independent component (Van-IC8), which shows the highest similarity to the Greenland $\delta^{18}O$ record and visually similar to other regional temperature indicating data can be read as a proxy for temperature variability. We also assert that, the independent component (Van-IC7) which has the highest similarity to B* and visually similar to other regional precipitation proxies, and with the lake level reconstruction from another sediment profile from Lake Van is a proxy of precipitation variability across the region. Our results show that the region's temperature approximately maps onto global records, i.e. warm during interglacials and cold during stadials. However, the precipitation proxy reveals that the region was not dry, or at least as wet as it is today, during the end of the MIS 6 and the

[1]This chapter is based on the paper: Ön, Z.B. and Özeren, M.S. Temperature and precipitation variability in eastern Anatolia: Results from independent component analysis of Lake Van sediment data spanning the last 250 kyr BP, *submitted to Quaternary International*.

LGM. The MIS 5e/c and Holocene were characterized by a wet period followed by dry intervals and Dansgaard/Oeschger events are characterized as being warm and wet.

3.2 Introduction

Proxy measurements are indirect indicators of past environments and many studies use multi-proxy approaches to overcome the shortcomings of single proxy data. One reason for studying proxy data is to produce a simplified model of past environments. In this study, we use Independent Component Analysis (ICA) as a parameter extraction tool by which to analyze published sediment data from Lake Van [37, 104, 105]. The results of our analyses can be argued to reflect temperature and precipitation variability across eastern Anatolia. While previous models based on almost the same data were not able to capture lake level changes, where it was claimed as these changes were shaped by precipitation/evaporation balance [106]. We claim that the models presented in this study have the ability to explain these geomorphological features seen around the lake.

In 2010, the PALEOVAN (hereafter PV) drilling campaign in Lake Van was conducted as an ICDP project. In order to study past climatic and environmental changes, a 220 m long composite profile was taken (see Figure 4.1 for the location). Subsequeent laboratory analyses constitute the longest and most complete paleolimnic archive in Anatolia. This dataset has been used in several studies with the aim to understand various aspects of the paleolimnic state (see the special issue: [36]). The PV results show the presence of several glacial/interglacial cycles within the Lake Van sediment data (see for example [104, 107, 108]) and reveal that Lake Van is a unique natural laboratory for paleoclimate studies.

Previous studies, which are not related to PV, only provided *continuous* proxy data for the last 20 kyr BP at most [110–112]. Field studies conducted by [113], [110], [111] and [106] revealed the presence of several terraces at different topographic heights around Lake Van with terraces that stand between 20 m and 80 m higher than the present-day lake level and which have been dated to between 26 and 20 kyr BP - the Last Glacial Maximum (LGM) - and which have been interpreted as evidences of a wet LGM in the region [106, 110]. However, results from previous studies and new data from the PV suggest different interpretations. Some recent analyses using PV data show that the period was drier than the present and that lake level was 200 m below

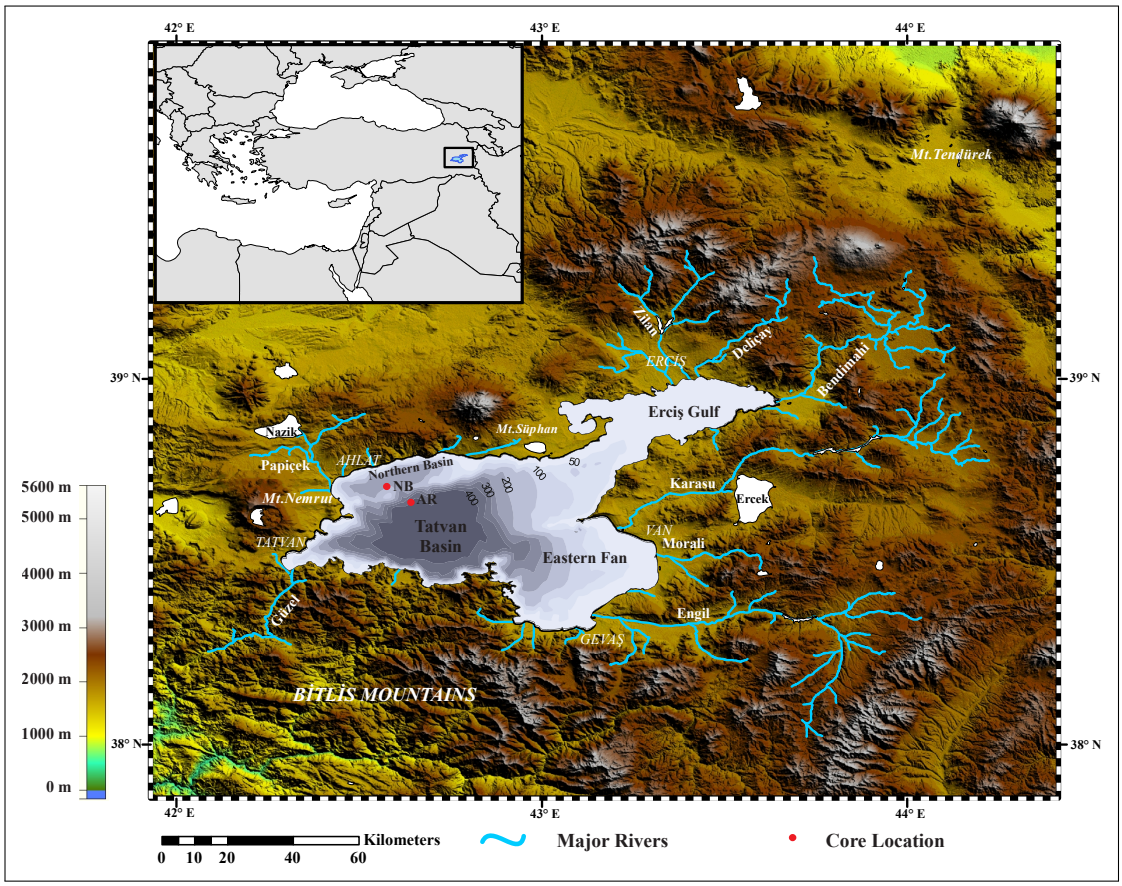

Figure 3.1 : Location map of Lake Van (modified from [109]). Red dots indicate the location of the Ahlat Ridge (AR) and Northern Basin (NB) composite profiles retrieved by the PV project. Major mountains and the locations of meteorological stations mentioned in the text are indicated.

its current level during the LGM [37, 114]. The claim by [37], that the region was dry during the LGM, is mainly based on principal component analysis (PCA) of AR data, but through this study, we discuss the reasons why PCA was inappropriately applied by [37] and offer a new proxy-based model for climate variables of eastern Anatolia using ICA.

ICA is a state of the art signal extraction tool with its roots in information theory [19]. ICA's main algebraic difference from data reduction techniques based on second order statistics, such as principal component analysis (PCA), is that, rather than maximal decorrelation, ICA rotates the axes in directions that maximize statistical independence. More specifically, PCA aims to find orthogonal components, ordered according to the variance that they explain and removes linear correlations between data. ICA is, by definition, a signal *separation* method and has the ability to remove higher order dependence. In the field of paleoclimate multiproxy studies, it is reasonable to pursue

a principal component analysis approach if one is almost confident that data variability is governed by a known agent, or to eliminate noise in the data and then conduct aimed analyses. It is also possible to combine the two former ideas to remove the shared variance based on solid assumptions via genuinely designed tests (see [115]). When using PCA as a signal separation method one should avoid applying it to highly correlated vectors, otherwise the leading principal components would resemble only those correlated vectors. Furthermore, Gaussianity of the stochastic variables is a strict constraint of PCA and since it depends on variance-covariance matrix and outliers should be removed through statistical means before analysis. An ICA approach might be considered superior to PCA for the problem under consideration because individual independent components, in theory at least, correspond directly to observable quantities, such as precipitation or temperature. It is designed to extract independent processes from mixed signals. For this reason, ICA has recently been applied in a paleoclimate study of Lake Hazar [6] in which paleoenvironmental chemistry proxies were assumed to be mixtures of different independent processes and were accordingly used as a basis by which to extract paleo-precipitation and paleo-temperature variability. ICA has also been applied as a signal separation tool on other subjects such as chemistry-based "multiproxy" datasets, similar to paleoclimate data, from different disciplines such as medicine [116] or applied geochemistry [117, 118]. It has also been applied in geographical sciences such as hydrology [76, 119] and climate science [14, 24]. ICA works on two major assumptions that are constraints on the results. These are non-Gaussianity and statistical independence of aimed components. For the purpose of this study, it is assumed that precipitation and temperature are non-Gaussian random variables (for an extensive discussion, see [15]) that are assumed to be quasi-independent, at least for the studied long term interval, with the characteristics of climate variables changing dynamically through non-linear interactions.

In this study, ICA is applied on element intensities (Ca, Fe, Mn, K, Si) from XRF-core-scanning analysis [104], total organic carbon (TOC) and carbonate content ($CaCO_3$) [105] and sediment reflectance color data in blue-yellow chromaticity (B*) [37]. Two of the extracted components are interpreted as proxies of temperature and precipitation variability in the region based on their statistical similarity to Greenland $\delta^{18}O$ data, operating through the assumed dynamic atmospheric relation between the

North Atlantic and the eastern Mediterranean [120]. Results are also supported by other regional and global paleo-data. The temperature record roughly follows the variability observed in Greenland NGRIP $\delta^{18}O$ data, such as the fact that glacials are relatively cold, interglacials are relatively warm, and abrupt warming events of MIS 3 are observable. The precipitation record also reflects abrupt warming events observed in Greenland records, i.e. the region is shown to be relatively wet during Dansgaard/Oeschger events. However, the end of the MIS 6 and LGM appear to be wet, unlike in the PCA results of [37], which used Si, Ca, Ti, TOC and B* data. Our results for precipitation closely follow lake level reconstruction of [79] and support the high-stand lake level during the LGM, as the observed terraces also appear to confirm.

3.3 Regional Setting

Lake Van fills a tectonically active depression at eastern Anatolia and is surrounded by a number of semi-active volcanoes to the north and east [121]. The Bitlis Mountains, which are a part of the southeastern Taurides, separate the basin from the lowlands of the Arabian plate and mark the transition between Mediterranean and continental climate zones [122, 123]. This manifests itself in the region's flora, with the region being on the boundary between forest and steppe-type biomes [124]. According to available meteorological data, average precipitation around the lake is variable with annual average precipitation amounts (data collected and organized by [125]) as follows: i) 380 mm/yr at the east of the lake (Van meteorological station), ii) 580 mm/yr at the southeast (Gevaş station), iii) 800 mm/yr at the southwest (Tatvan station), iv) 560 mm/yr at the west (Ahlat station), v) 440 mm/yr at the north (Erciş station).

The current eastern Mediterranean winter precipitation regime is mainly under the influence of the Atlantic Ocean, with cyclones that originate over the Mediterranean Sea and Asiatic dry high pressure systems. Which one of those factors is the most important in shaping the precipitation regime of the eastern Mediterranean, and of Anatolia in particular, is still a subject of debate. However, the general consensus favors [126] the so-called North Atlantic Oscillation, which is a pressure gradient regime, for the winter months. On the other hand, dry and cold air systems originating in Asia may be fed by temperate Black Sea surface waters to cause precipitation over Black Sea coasts in winter [127, 128]. During summer, the factors dominating the

region's climate are the subtropical high pressure system and the low pressure trough settling over Persian Gulf due to the Indian monsoon. Even though the mean summer surface pressure is lower than the mean winter surface pressure over the Aegean and Mediterranean coasts and the winds that flow over the sea are moisture laden, summers are almost dry in western Anatolia [50]. However, the Black Sea coasts of Anatolia are, again, an exception, receiving precipitation by the monsoonal low circulation saturated with warm Black Sea waters. Therefore, the precipitation regime of the Anatolian peninsula as a whole is far from straightforward to describe, lacking a single pressure system as it does.

In the present day, the lake stands approximately 1650 m above sea level and has a surface area of 3570 km^2. Water salinity is $\sim 21.4‰$ and water pH is ~ 9.8 [129]. During the winter, Mediterranean humid air loses moisture as precipitation over the colder orographic southern boundaries of Anatolia and therefore cannot feed the region. Furthermore, the geographical proximity of eastern Anatolia to cold/dry anti-cyclones from the Asian interior results in a relatively drier regional climate during the winter. Therefore, unlike the dominant winter precipitation in Mediterranean coastal zones, precipitation in eastern Anatolia is mainly recorded in spring and at the end of fall (Figure B.1). Winter precipitation is mainly snow and summer in the region is almost completely dry. Seasonality indices of monthly precipitation data show that the region is on the border of Continental Mediterranean and Continental Eastern Anatolian climates types [122]. The seasonality of climate parameters controls the sedimentation process and varve formation in the lake. Increased runoff during spring and fall provides dissolved calcium ions, detritus, and organic material which manifest as light layers in sediment profiles. Stratification of the lake waters in summer increase organic productivity in the lake, and it also contributes to the formation of light layers. In winter surface waters cool and runoff decreases; consequently stratification ceases and suspended organic matter precipitates, forming the dark layers of sediment profile as a result [130, 131].

3.4 Materials and Methods

3.4.1 Lake Van Ahlat Ridge sediment record and the chronology

The 220 m long Ahlat Ridge (AR) composite profile was drilled at a depth of 360 m below the present lake level with the primary aim of understanding the climatic evolution of the region [36].

The AR record has been subjected to XRF elemental scanning using an Avaatech core scanner by [104] for every 2 cm over a 1 cm^2 area with a slit size of 12 mm. The results are collated by 10 s sampling time and with 10 kV and 0.2 mA generator settings. Also, the color profile of the sediment in L*A*B* color space was photographed at 0.03 mm resolution [37]. $CaCO_3$ and TOC measurements were established for every 2.5 cm through the record [105].

While the age model of the uppermost part of the AR record was constructed by ^{14}C datings and correlation to previously gathered robust varve chronology [132], the chronology of the remainder of the record was established by tuning the proxy data to:

i) NGRIP $\delta^{18}O$ GICC05 and GICC05modeltext timescale [66,133–135] for the interval between 0 and 116 kyr BP and,

ii) speleothem based and EDC3 based synthetic Greenland record [136] for the interval between 116 and 400 kyr BP and 400 and 650 kyr BP, respectively.

This age model was then cross-referenced with several other dating methods, including $^{40}Ar/^{39}Ar$ datings, tephrostratigraphy, magnetostratigraphy and ^{10}Be measurements. The model was then improved by using the AICC2012 timescale [137] for the interval between 90 and 125 kyr BP and by adding more tie points [37]. Whereas the difference between the old and improved age models is negligible for the period younger than 100 kyr BP, before 100 kyr BP there exist intervals with significant age differences, reaching almost 10 kyr (for all the details and construction process of the chronology, see [138], [105] and [37]). The complete record represents the last 600 kyr. In this study, we use only the last 250 kyr section of the data due to the discontinuities below this point.

The resolution of the published XRF data by [104] and [37] and B*, TOC, $CaCO_3$ data are different and therefore we linearly interpolated the data to the one with fewer data points, which corresponds to the data presented in [104]. Before interpolation, we applied a first order Savitzky-Golay filter [59] with a 5 window length to $CaCO_3$, TOC, Ca, K, Si and with a 53 window length to B*. After the smoothing process, every 1 in 5 elements in the former dataset and every 1 in 53 elements in B* were selected to bring the data to approximately the same number of rows as Fe and Mn. Afterwards, filtered and resampled data were linearly interpolated to the age model's (developed by [37]) of Fe and Mn from [104] (Figure 3.2).

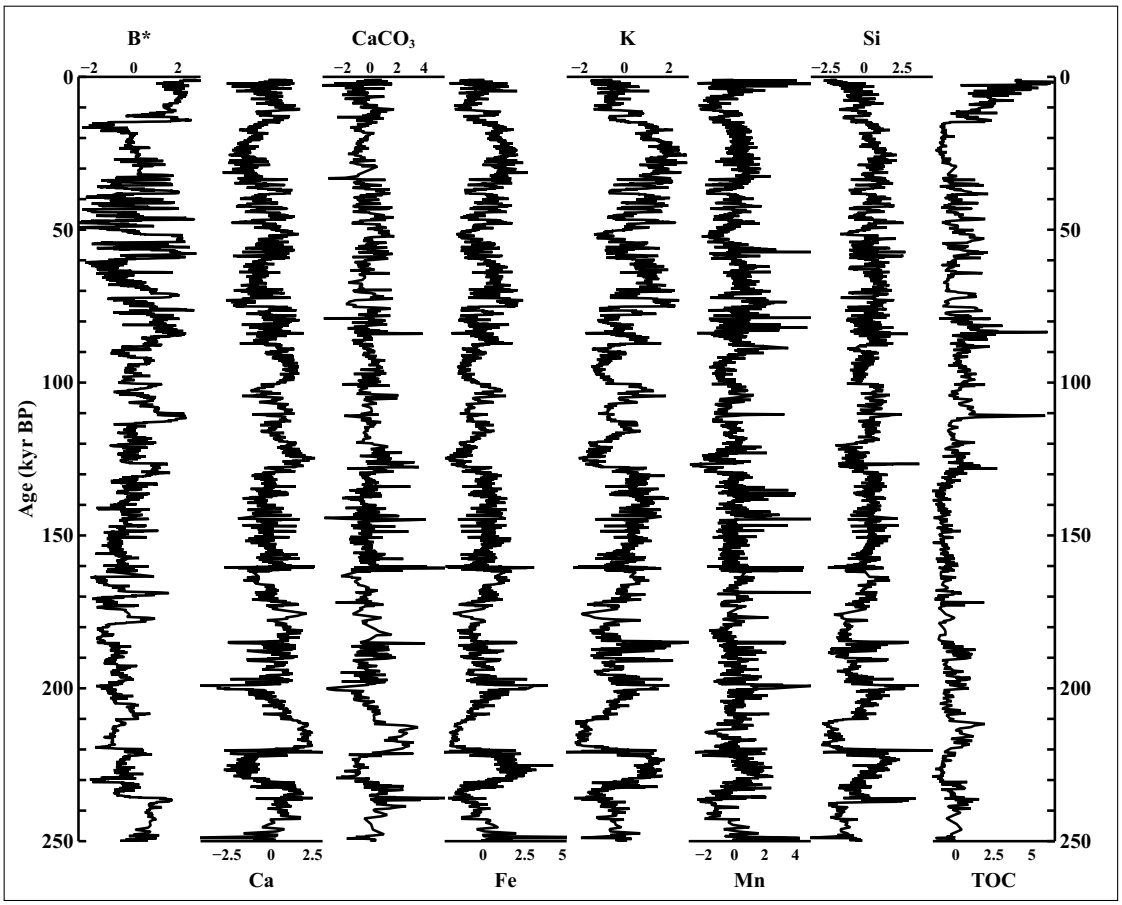

Figure 3.2 : Data processed in this study after interpolated to the age model of Fe and Mn, as described in Section 3.4.1. All the data in this study have been standardized by making each data zero mean and unit variance.

3.4.2 FastICA

FastICA is a numerical implementation of ICA that has been widely used during the last decade for problems as diverse as telecommunications theory, face recognition, image processing (see Part 4 in [61]), hydrology [76], climatology [24], and, recently, in paleoclimatology [6].

FastICA is one of the major blind signal separation methods with some critical assumptions. It has distinct advantages when compared to methods based on variance-covariance matrix, such as PCA or factor analysis. Its most important advantage is that it is not restricted to the second-order statistical constraints brought in by the quadratic nature of covariance. Secondly, extracted independent components have no hierarchy among themselves, unlike principal components which are based on the eigenvalue spectrum. However, not being subject to any hierarchy may be seen as a disadvantage because interpretation of the resulting components, at least for this study, depends on similarity methods, as set out below.

The FastICA model assumes that the matrix of observed variables $\mathbf{X}$ (in our case, the Lake Van AR record) is a linear transformation of the source matrix $\mathbf{S}$ (matrix of independent components) by the mixing matrix $\mathbf{A}$, which is;

$$\mathbf{X} = \mathbf{AS}. \tag{3.1}$$

Here, neither the mixing matrix $\mathbf{A}$, nor the source matrix $\mathbf{S}$ is known. Since, the sole object is to find the source matrix, the method tries to estimate $\mathbf{W}$, which is the inverse of $\mathbf{A}$, and finds $\mathbf{S}$ by;

$$\mathbf{S} = \mathbf{WX}. \tag{3.2}$$

In order to establish that this is mathematically possible, ICA approach assumes the following:

1. the source components that are being looked for should be statistically independent,

2. source components should have non-Gaussian distributions, and

3. mixing matrix $\mathbf{A}$ should be invertible.

The non-Gaussianity assumption here, through the central limit theorem, is the key to estimating the independent components [19].

FastICA searches for independent components through the well-defined, information theoretical concept of negentropy. The definition of negentropy of a random vector $\mathbf{y}$ is,

$$J(\mathbf{y}) = H(\mathbf{y}_{\mathbf{gauss}}) - H(\mathbf{y}), \tag{3.3}$$

where H is the Shannon's entropy and defined over the probability mass function P of $\mathbf{y}$ as:

$$H(\mathbf{y}) = -\sum_{y \in \mathbf{y}} P(y) \log P(y). \tag{3.4}$$

Intuitively speaking, negentropy defines a distance between the real distribution of a random variable and the normally distributed random variable with the same mean and variance.

Negentropy of a random vector defined by equation (3.3) is theoretically calculated by probability mass functions of random variables as given by equation (3.4). However, to describe the probability mass function of a random variable is a non-trivial problem. In order to estimate negentropy, FastICA uses a method based on maximum entropy principle with a selected contrast function [19, 63]. The contrast function is the nonlinear component of the analysis and for this study, we used:

$$G(u) = \log(\cosh(u)), \tag{3.5}$$

which [62] stated is suitable for general purposes such as this.

The FastICA scheme for estimating the first independent component is based on a selection of a random unit vector and execution of a fixed point iterative process until convergence is established, as described in [19]. The same algortihm used in estimating the first component is then used to estimate the rest of the components, by the deflation method. However, to prevent the convergence of components into the same directions outputs are decorrelated after every iteration through each estimation, as explained in [19].

Documented examples in [139] show that the *worst* outliers in the data may affect the results of FastICA. Here the term "worst outliers" (used by [139]) is taken to mean outliers that are not defined through classical spherical boundaries, whereas they

are defined by the term *medcouple* for skewed data and preserve the non-Gaussian nature and skewness of the data. We applied the adjusted outlyingness method [140] to eliminate the outliers for multivariate data by using the LIBRA library [141] in MATLAB, which is a generalization of the method described in [139]. The results from our case show that marking approximately 1.8% of all observations as outliers and deleting them before the FastICA operation is sufficient. Having deleted 89 data-rows, 4905 remain.

Before starting the FastICA algorithm, a random unit vector is selected. However, this selected random vector may slightly affect the results of FastICA, so [142] suggest to changing the initial vector several times using the Icasso package, which was originally developed for neuroimaging applications. After running the algorithm several times, the method projects the results onto a 2-D plane by curvilinear component analysis [143] and clusters the components gathered in each run via group average-link agglomeration, to check for the reliability of each component, prior to computing the distances of each candidate component from other candidates in the cluster and offering the component with the highest summed similarity value in each cluster. In order to validate the results of FastICA, we ran the algorithm 250 times by changing the randomly selected initial point with the contrast function described at equation (3.5), through the Icasso package. Unlike PCA, there is no need to standardize the data to apply FastICA (however, they need to be centered and whitened by transforming to orthogonal unit vectors, which is an essential preliminary step to remove the second-order dependency on the data). In each way the results will be the same, however, we chose to standardize the data before the analysis.

One peculiarity of ICA in our context is that, unlike other well-known dimension reduction methods (such as PCA or FA), neither the variances nor the order of the components are known [19]. Therefore, a strategy should be chosen by which to select appropriate components. For example, in a similar study, [6] decided the contextually appropriate components by looking at distance correlation coefficients [65] between the extracted components and well-known climate proxies. This distance correlation approach may fail to satisfy equitability [70, 144] meaning that, among different type of relationships with same amount of noise, the statistic should give a similar score. Alternatively, we can use another quantity called mutual information for this purpose,

since the data have enough elements to almost define probability mass functions by using histograms. Mutual information is a measure which finds the amount of information shared between two systems by using the Shannon's entropy idea in information theory [145] and it is theoretically equitable [144]. Mutual information between $\mathbf{x}$ and $\mathbf{y}$ is defined as:

$$I(\mathbf{x},\mathbf{y}) = \sum_{x\in\mathbf{x}}\sum_{y\in\mathbf{y}} p(x,y)\log\frac{p(x,y)}{p(x)p(y)} \tag{3.6}$$

where $p(x)$, $p(y)$ are the marginal probability mass functions and $p(x,y)$ is the joint probability mass function of the random variables $\mathbf{x}$ and $\mathbf{y}$. Notice that $I(\mathbf{x},\mathbf{y}) = 0$ if and only if $\mathbf{x}$ and $\mathbf{y}$ are statistically independent. Without loss of generality, we used e as the base of the logarithm through computations of mutual information.

Polar ice core δ^{18}O data provide reliable and almost continuous sources for past climate change and they are good reflectors of paleo-temperature change in particular [68]. In order to select the appropriate components, as a preliminary approach we computed the mutual information between each resulting independent component and each proxy record used through FastICA and also NGRIP δ^{18}O data [66]. Note that the NGRIP δ^{18}O data is padded with synthetic Greenland data [136], and have been linearly interpolated to the AR age model. While computing the mutual information, we described the marginal and joint probability functions by constructing histograms with 50 fixed width bins between the minimum and maximum value of the data. Mutual information does not give comparable results like the results of Pearson's correlation coefficient between $[-1,1]$. However, [146] proposes a transformation method of mutual information results as

$$I^*(\mathbf{x},\mathbf{y}) = \sqrt{1-\exp(-2I(\mathbf{x},\mathbf{y}))}. \tag{3.7}$$

By doing so, mutual information results are transformed between 0 and 1 (Table 3.1).

3.5 Results and Discussion

Using the methodology described by [142] (see Figures B.2 to B.5 for plots of different methods used to select the appropriate number of independent components), there are eight statistically valid clusters, i.e. it is proper to say that there are eight independent processes governing the eight dimensional data-set and correspondingly eight independent components (see Figure B.6). Since the aim is to select

Table 3.1 : Transformed mutual information results between the independent components of the AR record and NGRIP $\delta^{18}O$ combined with synthetic Greenland record and the AR data. Mutual information is measured in nats.

I^*	Van-IC1	Van-IC2	Van-IC3	Van-IC4	Van-IC5	Van-IC6	Van-IC7	Van-IC8
NGRIP-$\delta^{18}O$	0.33	0.39	0.36	0.41	0.37	0.48	0.51	0.54
B*	0.45	0.44	0.44	0.42	0.35	0.56	0.72	0.49
Ca	0.26	0.45	0.29	0.34	0.38	0.42	0.50	0.74
$CaCO_3$	0.32	0.76	0.37	0.36	0.30	0.29	0.42	0.48
Fe	0.30	0.45	0.32	0.35	0.48	0.42	0.51	0.73
K	0.26	0.44	0.29	0.34	0.34	0.43	0.57	0.80
Mn	0.33	0.37	0.37	0.62	0.35	0.35	0.44	0.46
Si	0.34	0.48	0.30	0.40	0.35	0.38	0.48	0.78
TOC	0.60	0.54	0.42	0.36	0.03	0.50	0.36	0.39

climate-related components, we followed a preliminary strategy of selecting candidates by calculating a statistical similarity measure (mutual information in our case) of the independent components with the Greenland (NGRIP) stable oxygen isotope record [66] combined with the synthetic Greenland isotope record [136].

Transformed mutual information results indicate that (Table 3.1), Van-IC8 give the highest similarity with the Greenland data. Furthermore, Van-IC8 shows visual similarity with the Greenland record (Figure 3.3) and with PC1 constructed by [37] (principal component which has the highest variance, see Fig.5 therein), where PC1 was interpreted as hydroclimatic variability through the sole assumption of B*, Si, K, TOC and Ca being sensitive to hydroclimate variations. The interpretation of [37] associating the hydroclimatic variability to the first principal component may seem reasonable, since maximal variance in sediment records of a lake should be mainly driven by precipitation, evaporation and surface/groundwater runoff components. However, in the AR record, linear correlation between Ca, K and Si are exceptionally high (see Figure B.7) and this can be seen in Fig.S1 in [37]. Therefore, PC1 of [37] is mainly governed by the variances in K, Ca and Si (represented by the loadings of PCA, see Fig.S3 in [37]) constituting a significant bias in their analysis. The bias stems from the fact that their principal components are constructed using only five different time series and three of them are highly correlated. Similar results can be obtained if PCA is applied to the extended data used in this study (see Figure B.9), since four of the eight profiles are highly correlated (see Figure B.7). We therefore reject the interpretation of PC1 in [138] and elaborate on this below. On the other hand, [108] constructed a

curve based on alkenone Uk37 index (Figure 3.3) and claim that it reflects changes in temperature and haptophyte species composition. Visual similarity between Van-IC8 and low resolution Uk37 index is high, and the reader should note that the age model used by [108] is based on an older chronology that is different from the most recent one up to 10 kyr during some intervals of MIS 6 (cf. [138] and [37]). Van-IC8 also resembles changes in sea surface temperature of the western Mediterranean [147] and Black Sea [120]. The similarity of Van-IC8 to Greenland isotope data, Uk37 index of Lake Van, and sea surface temperature data (Figure 3.3 and Figure 3.4) allows us to state that it reflects the paleo-temperature variability for the region. Using the Greenland δ^{18}O record as a paleothermometer is a subject of debate (see [148], [149] and references therein). However, it remains the only commonly used high resolution hemispheric paleo-temperature proxy. At this point, the relation between Van-IC8 and the data used in ICA can be queried but the high linear correlation between Ca, Fe, K and Si (Figures B.7 and B.8) make it difficult to compare and discuss Van-IC8 with the proxy data. Therefore, our interpretation of the Van-IC8 as a temperature proxy stands only on its overall similarity to the NGRIP δ^{18}O, Uk37 index and sea surface temperatures from the wider region. According to this temperature variability, the region's temperature approximately followed the hemispheric temperature curve, i.e. cold during glacials/stadials and warm during interglacials/interstadials.

The second highest similarity with the Greenland isotope data is established by Van-IC7 (Table 3.1). The Van-IC7 curve very closely resembles the Greenland curve (Figure 3.3), especially for abrupt events. However, trends and/or levels are not the same as in the case for the claimed temperature proxy, Van-IC8. The most striking differences are seen during times of maximal glaciation (the end of Late Pleistocene and MIS 6) and during interglacials, especially through MIS 1, MIS 5e and MIS 5c.

Lake Van sediments are laminated and these laminations are described as varves by [154]. Annual lamina couplets consist of dark and light alternations [131, 132]. According to [131], light layers represent the effects of spring runoff, summer organic productivity and mixing and runoff in fall. While autochthonous biological productivity partly depends on the temperature, its quantity is largely determined by runoff through the transfer of organic matter, dissolved nutrients and mineral particles [155]. Unstratified water column in Lake Van results in dark colored layers

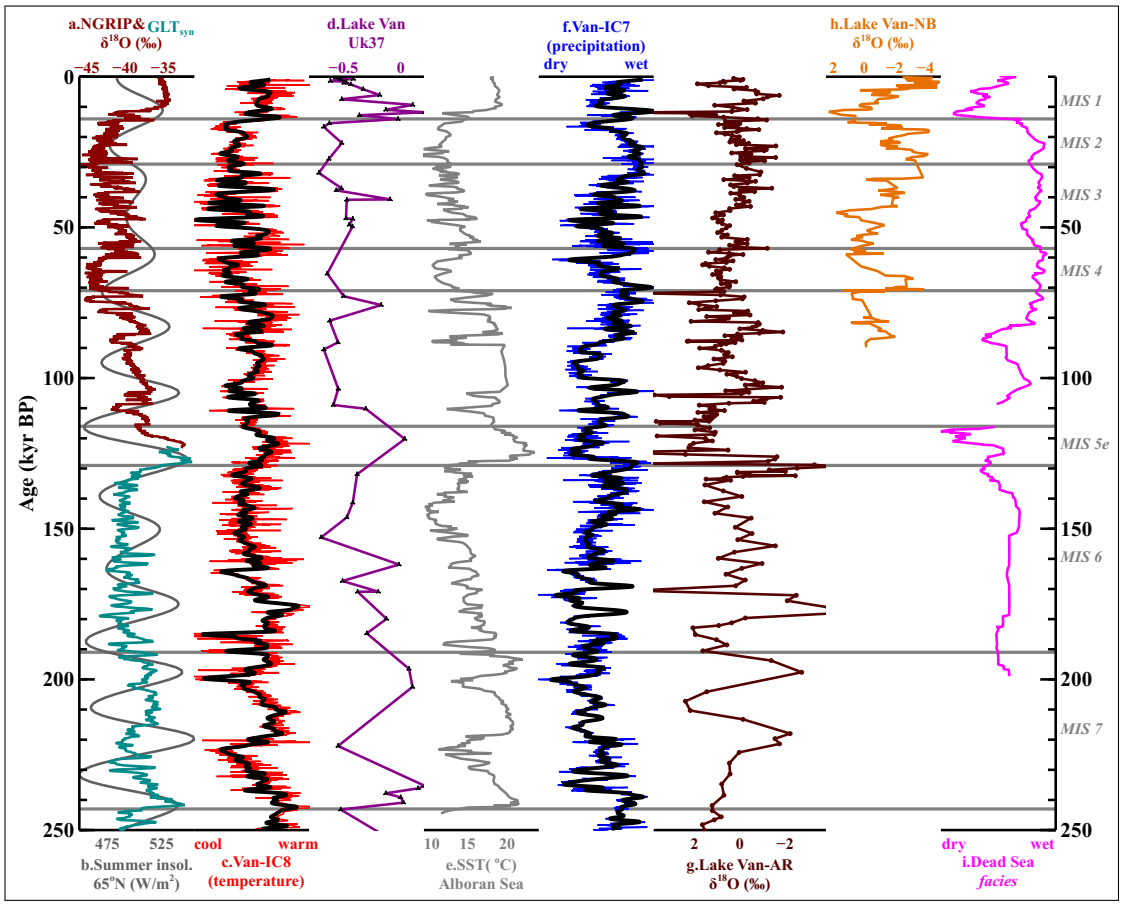

Figure 3.3 : Comparison of selected independent components with global and regional records. a. NGRIP δ^{18}O data [66] combined with synthetic Greenland record [136]. b. Summer insolation for 65°N [82]. c. Temperature proxy of Lake Van Van-IC8, proposed in this study. d. Lake Van Uk37 index, as a proxy for temperature [108]. e. Alboran Sea, surface temperature [147] f. Precipitation proxy of Lake Van Van-IC7, proposed in this study. g. Lake Van AR δ^{18}O data [104]. h. Lake Van NB δ^{18}O data [79]. i. Reconstruction of the hydroclimate of Levant by aragonite-detritus laminae [150]. Black curves over Van-IC7 and Van-IC8 are Butterworth lowpass filter designed with 1.5 kyr cutoff period applied to IC's interpolated to 50 years evenly spaced data. The horizontal lines are the MIS boundaries defined in [151].

during winter. However, it must be noted that changes in precipitation variability may also affect the thickness of dark layers [131]. Therefore, it can be seen that annual meteorological conditions, but mainly precipitation, are reflected in laminated sediments which in turn mainly define the changes in color profile of the sediment data. In a region where seasonality of precipitation is high (see Section 3.3 and Figure B.1), the color of sediments mainly reflects precipitation variability [156]. According to mutual information results, Van-IC7 has the highest similarity with normalized B* data (Table 3.1), which shows the highest information transferred to Van-IC7 through the

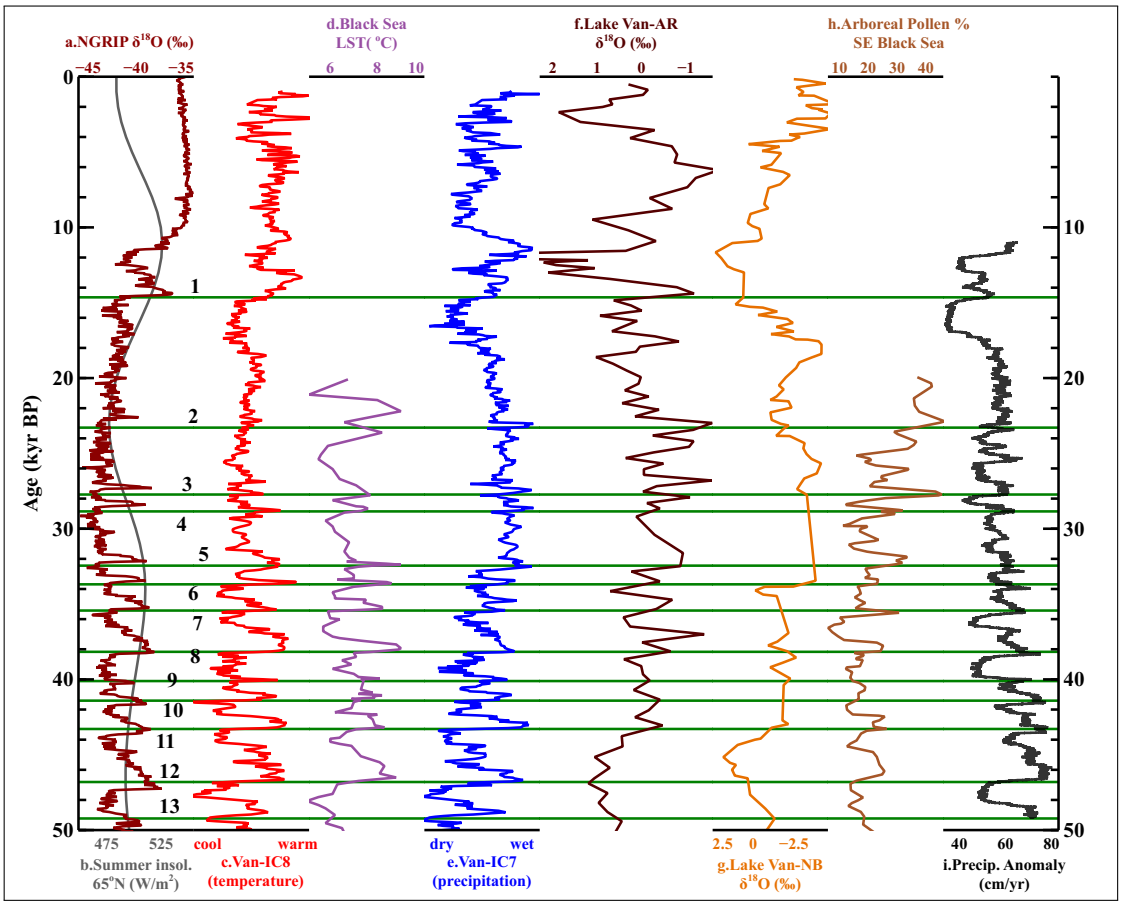

Figure 3.4 : Comparison of selected independent components with global and regional records for the last 50 kyr. a. NGRIP $\delta^{18}O$ data [66]. b. Summer insolation for 65°N [82]. c. Temperature proxy of Lake Van Van-IC8, proposed in this study. d. Black Sea, lake surface temperature [120]. e. Precipitation proxy of Lake Van Van-IC7, proposed in this study. f. Lake Van AR $\delta^{18}O$ data [104]. g. Lake Van NB $\delta^{18}O$ data [79]. h. Arboreal pollen percentage from core 25-GC1 [152], south Black Sea. i. LOVECLIM model precipitation anomaly data [153] for Lake Van region presented in [37]. Green lines indicate the start of the Greenland interstadials [134].

analyzed data. In light of the above discussions, we claim that Van-IC7 is a precipitation variability proxy for the region. Although the precipitation model presented here does not agree with the hydroclimate variability and lake level reconstruction presented in [37], Van-IC7 does show good correlation with lake level curve of the last 90 kyr BP (Figure 3.5) constructed by [79].

Further supporting evidence for our interpretation of Van-IC7 comes from the $\delta^{18}O_{bulk}$ data (Figure 3.3) retrieved from two different Lake Van composite profiles - AR [104] and NB [79]. The isotopic composition of carbonates in Mediterranean lakes is dependent on a number of different factors [11]. However, [130] and [11] explicitly

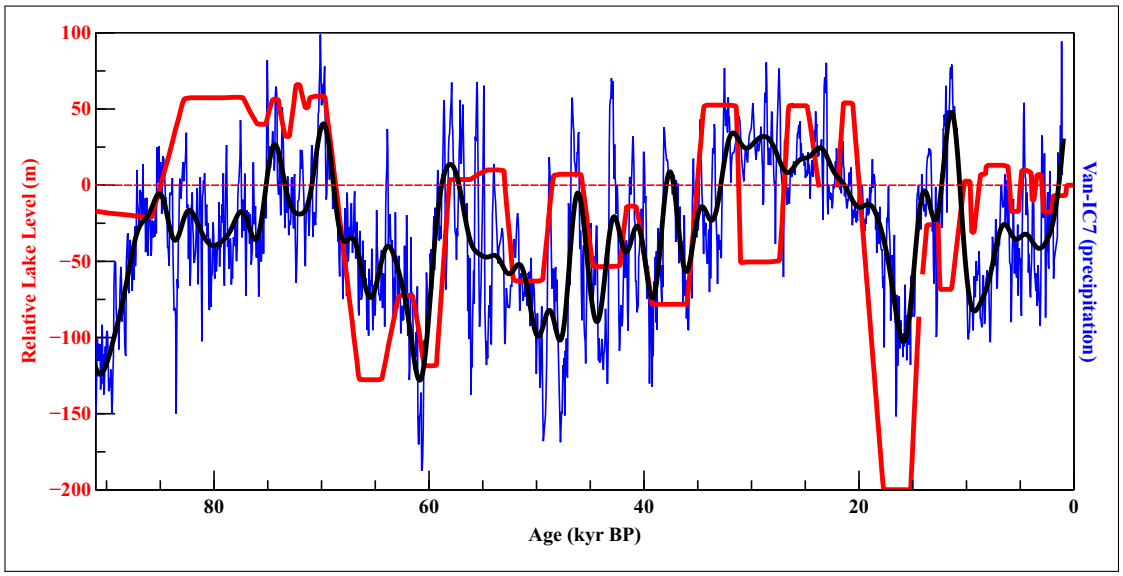

Figure 3.5 : Lake level changes constructed by [79] are plotted in red and Van-IC7 in blue and Butterworth lowpass filter of Van-IC7 with cutoff period 2.5 kyr in black. Note that, lake level reconstruction of [79] depends on lake terraces, seismic stratigraphy and lithology of a different composite record (NB) drilled from Lake Van.

state that the primary controlling factor of isotope fractionation in Lake Van is evaporation/precipitation balance. [104] (similarly [79]), after an extensive discussion reach a *tentative interpretation* (the original authors' term) about the $\delta^{18}O$ variability of Lake Van carbonates. They claim that $\delta^{18}O$ is a proxy of temperature and isotopic condition of the epilimnion subject to the precipitation type/season in the region. This conclusion was reached by rejecting the proposition that relative humidity was the main controlling factor of $\delta^{18}O$ and by assuming that glacial periods should be drier than interglacials. By assuming that relative humidity is the main controlling agent for $\delta^{18}O$ fractionation, the isotope profiles follow the trend of Van-IC7 during each marine isotope stage (readers should also note that the age model of $\delta^{18}O$ profiles depend on the chronology constructed by [138]). Correlation between the isotope profiles and Van-IC7 is not perfect, which is probably a result of dependence of $\delta^{18}O$ on other factors as stated by [11]. There are also differences between the NB and AR isotope profiles but general trends in each marine isotope stage do resemble one another and the difference between them may be a result of site difference, different age models and/or different laboratory measurements.

As already stated in Section 3.2, earlier continuous records from Lake Van are not long enough to test the results presented in this study. However, these studies suggest that the

LGM should be conisdered to have been wet, judging by the terraces around the lake, where the highest ones are 80 m above today's level [106]. On the other hand, neither the hydroclimate model (namely, PC1) nor the lake level reconstruction based on a low resolution climate model [157] presented by [37] capture a wet period during the LGM. According to the lake level reconstruction (where it has been expressed as an idealized low resolution experiment by the authors), [37] suggest it should have been somewhere around 200 m below today's level during the LGM. This means that existing proposed models fail to demonstrate an almost 280 m lake level rise. However, while most high resolution paleoproxies of Lake Van published by [104] and [37] correctly recover abrupt changes in the North Atlantic, such as Dansgaard–Oeschger events, PC1 fails to show a geologically established lake level rise of nearly 280 m. Furthermore, there is also a higher resolution hindcast climate simulation with a more realistic precipitation pattern [153] for the period between 50 kyr and 11 kyr BP which is presented in [37] but not used in lake level modeling, also it does not show low rates of precipitation during the LGM (Figure 3.4). Hence, the arguments of [37] about the lake level, clearly contradict the results of terrace studies.

Other than Lake Van, there are lakes with high-stand water levels throughout the LGM not only in Anatolia [95, 158] but also in the Middle East [159], southern Europe, and north Africa [93, 160, 161]. There are two schools of thought about the reasons for these high lake levels in the eastern Mediterranean during the LGM [162]. The first maintains that, during the LGM, very cold winters and cool cloudy summers caused a decrease in evaporation [92]. However, according to the water-balance model of past lake level changes and paleovegation cover in Lake Ioannina, this hypothesis does not hold up, yet it should be a wet period [160]. Moreover, sequences of thick aragonite-detritus deposits around the Dead Sea appear to imply that evaporation rates were in fact *higher* than they are today, at least in the Dead Sea basin [159]. Despite higher evaporation, the Dead Sea lake level was significantly higher than the present day [159]. Furthermore, [150] claim that the end of MIS 6 should have been wet and the end of MIS 5e should have been dry according to the Dead Sea *facies* record (see [150] due to the particular way in which they define the term *facies*). Within the age uncertainties in both records, Van-IC7 appears to follow the pattern of the Dead Sea *facies* curve (Figure 3.3), supporting a climate-induced high-stand for Lake Van during

the LGM. On the other hand, while pollen data from Lake Van do not reflect any increase in precipitation during LGM [163], there are other pollen records from across the Anatolian peninsula that so show evidence for high precipitation rates. Low percentage rate of arboreal pollen in the Lake Van profile during the LGM may be a result of severe colds and/or day-night diurnal difference across the region which is typical of high altitude geographies. Pollen profiles from the Marmara Sea [87] and Black Sea ([152], Figure 3.4), regions that are not affected by the continentality that Lake Van experiences, reveal low temperatures associated with moderate precipitation. Furthermore, glacier advances in south/southwest Anatolia during the LGM have been explained by high precipitation rates by one-dimensional ice flow models in two studies [90, 91], both of which claim that for the observed glacial advances to have formed in south Anatolia during the LGM, precipitation should be almost twice its current rate.

High precipitation around the end of MIS 6 and the LGM is likely to be the result of the expansion of the Northern Hemisphere ice sheet [159, 161]. The strengthening of the polar anticyclone may have forced the extratropical low pressure and subtropical high pressure systems to migrate southward and cause the Van region to be wet at this time, although a climatic link between the North Atlantic and eastern Anatolia is more direct during Greenland interstadials, which have been shown to be relatively warm and wet at the region (Figure 3.4).

3.6 Conclusions

How to obtaining pure climate signals from paleo-proxies remains a matter of open debate. In this study, we offer the results of independent component analysis of the Lake Van AR data as possible reflection of temperature and precipitation variability of eastern Anatolia during the last 250 kyr.

Our methodology was to first removing outliers in the data using an adjusted outlyingness method and then applying FastICA by changing the initial random vector several times and clustering the results. Preliminary selection of the climate related variables depend on common information between the resulting components and NGRIP δ^{18}O data. Consequently, we suggest that two of the independent components can be understood to reflect temperature (Van-IC8) and precipitation (Van-IC7) variability of the region. Our suggestions about these selected components

are supported by data from Lake Van and other regional records that also claimed to reflect temperature/precipitation variability.

According to our results, the Lake Van temperature record maps onto the NGRIP $\delta^{18}O$ record, whereby interglacials and interstadials are relatively warm and stadials are relatively cold. However, precipitation follows a different pattern, visually resembling the Dead Sea records and Lake Van level changes. During times when glaciation is at its maximum (the end of MIS 6 and LGM), precipitation increased. During interstadials (MIS 5e/c and Holocene) a wet early stage was followed by a dry period.

4. BAYESIAN TEST FOR THE 4.2 KA BP ABRUPT CLIMATIC CHANGE EVENT FOR THE EASTERN MEDITERRANEAN AND ARABIAN PENINSULA PALEOCLIMATE DATA USING STRUCTURAL TIME SERIES[1]

4.1 Abstract

It has been proposed that an abrupt climatic change around 4.2 ka BP contributed to the collapse of the Akkadian Empire. Since then, many published geological studies reached conclusions that supported this hypothesis. Even though numerous other studies contradict the idea of this abrupt climate change, the 4.2 ka BP time point has nevertheless been accepted as the stratigraphic boundary of Middle and Upper Holocene transition. However, time series plots of paleoclimate studies that claim to support the abrupt climate change theory show different temporal and geometric patterns. In this study, we use the Bayesian structural time series (BSTS) approach through Causal Impact package, which is designed by Google Inc. analysts, to test the data that are claimed to have a climatic anomaly around 4.2 ka BP in the eastern Mediterranean and Arabian peninsula. To do this, each "affected" time series is reconstructed using "unaffected" ones in a fully Bayesian framework by the BSTS method and then a Bayesian hypothesis test is applied on each result. While our results confirm that some studies that have previously been cited in support of the 4.2 ka BP event hypothesis hold true, we also demonstrate that in a number of other studies there is no statistically significant abrupt effect.

4.2 Introduction

There were numerous rapid climate change (RCC) events in the high latitudes of the Northern Hemisphere during the Late Pleistocene [164]. There have also been attempts to define RCC events similar to those seen in the Pleistocene for the Holocene, using

[1]This chapter is based on the paper: Ön, Z.B., Özeren, M.S., Greaves, A.M. and Akçer-Ön, S. Bayesian test for the 4.2 ka BP abrupt climatic change event for the eastern Mediterranean and Arabian peninsula paleoclimate data using structural time series, *submitted to Progress in Physical Geography*.

available proxy data [165, 166]. The possibility of RCC events in the Holocene is especially interesting because they would have taken place during a period of human history typified by complex cultures and civilizations and can serve as models for understanding the interaction between the natural environment and human society within the context of a constantly changing climate. One of the most controversial of the proposed RCC events is the so-called 4.2 ka BP event, first proposed by [8]. In their study [8] claim that, a major short-term climatic change between 4.2 and 3.9 ka BP contributed to the collapse of the Akkadian Empire.

Following [8], further studies were published that appeared to confirm their hypothesis (see [167] and [168] and references therein). In their initial article [8] used eolian deposits from archaeological contexts as well as excavated evidence and archaeological survey data to propose that increased regional aridity in the Habur Plains of Syria led to a decline in human settlement activity. Having begun as a drought phenomenon for the Upper Mesopotamia, mounting evidence from subsequent studies in other regions gradually led to controversial acceptance of 4.2 ka BP event as the geological stratigraphic boundary between Middle and Upper Holocene [169]. There are, however, still problems with some of the evidence that are most widely cited in support of the 4.2 ka BP event through discussions of the theory [167,170,171]. For example, different proxy data measurements are taken from the same sample, as in [130] where there is a disagreement between the time series from quartz (which is claimed as a proxy for eolian activity and is one of the most widely used form of evidence for the 4.2 ka BP event, by researchers other than the original authors) and any other time series in the same article (notably, relative humidity reconstruction). Furthermore, different laboratory measurements were taken from the same sample by [110] and [130] but their articles disagree on the time series of quartz which is one of the most widely used forms of evidence in the 4.2 ka BP event debate. The data published by [110] do not show any abrupt change at or around 4.2 ka BP but that published by [130] using the same core are claimed to show. Asynchrony is also present for the same proxies in samples taken from adjacent sites. For example, precipitation reconstruction of [172] at Tel Akko shows a dry period around 4.2 ka BP, whereas precipitation reconstruction during the same period from Dead Sea sediments reveals almost the wettest period of the last 10 ka [173], while it should also be noted that, being an

archaeological site, the pollen data from Tel Akko is subject to anthropomorphic factors that do not affect any of the other series in our study (cf. [174]). Furthermore, while the timing of the event was originally hypothesized by [8] as between 4.2 and 3.9 ka BP, some proxy data show a climatic event with different start and end dates. For example, precipitation reconstruction from Tel Akko [172] reveals a dry period starting at $\sim$4.4 ka BP and the Soreq Cave geochemistry data [175] show a drying trend starting at $\sim$4.7 ka BP [176]. It has therefore subsequently been claimed that this event may be a result of superimposed events starting around 4.7 ka BP [177]. Yet, on the other hand, there are also numerous examples of proxy data that do not show any abrupt change around 4.2 ka BP [6, 128, 176, 178].

Testing the presence of this abrupt event through individual datasets probabilistically is impractical and poses a number of problems. If one considers each time series individually conducting a frequentist approach, estimation or assumption of the probability distribution of the data is a must, while Bayesian approach would be a better alternative for the case which it is unknown. A Bayesian approach, if done on an individual basis, is not especially useful either, because it would prevent us from exploiting certain common stochastic trends shared across the whole or subsets of the whole ensemble of time series. This is because the climate is a non-linear dynamical system that is capable of producing certain self-organized criticalities at wide spatial and temporal scales, such as the millennial climate change events through the Late Pleistocene. Combining multiple time series and applying a Bayesian stochastic reconstruction within a large spatial scale and over spatially sparse datasets with age uncertainties is a challenging process. Although new paleoclimate studies with high resolution data and robust age models will always be welcome, there are already enough spatial/temporal data on which to begin building probabilistic models.

Our strategy in this study has been to reconstruct each paleo-proxy time series from the eastern Mediterranean and southwest Asia (Figure 4.1) which claimed to show an abrupt change around 4.2 ka BP, through time series that do not show any abrupt change during the period of interest (Table 4.1). Reconstruction during the period prior to the supposed RCC event is handled by the Bayesian structural time series (BSTS) method [179] and reconstructed time series are extrapolated over time accordingly. During the temporal interval of interest Bayesian hypothesis testing is applied to the difference between the

original and reconstructed data to ascertain the statistical significance of the impact on the proxy data using the causal impact method [9]. Within the scope of this study, the term *impact* signifies only a change in the nature of the time series. The physical cause of that impact may be external or an extreme climate state created as a result of nonlinear interactions within the dynamical climate system itself without any external triggering. In order not to bias the stochastic forecast by assuming a particular temporal impact shape (impulsive, exponential dissipation etc.), the prior distribution model was not informed by such processes.

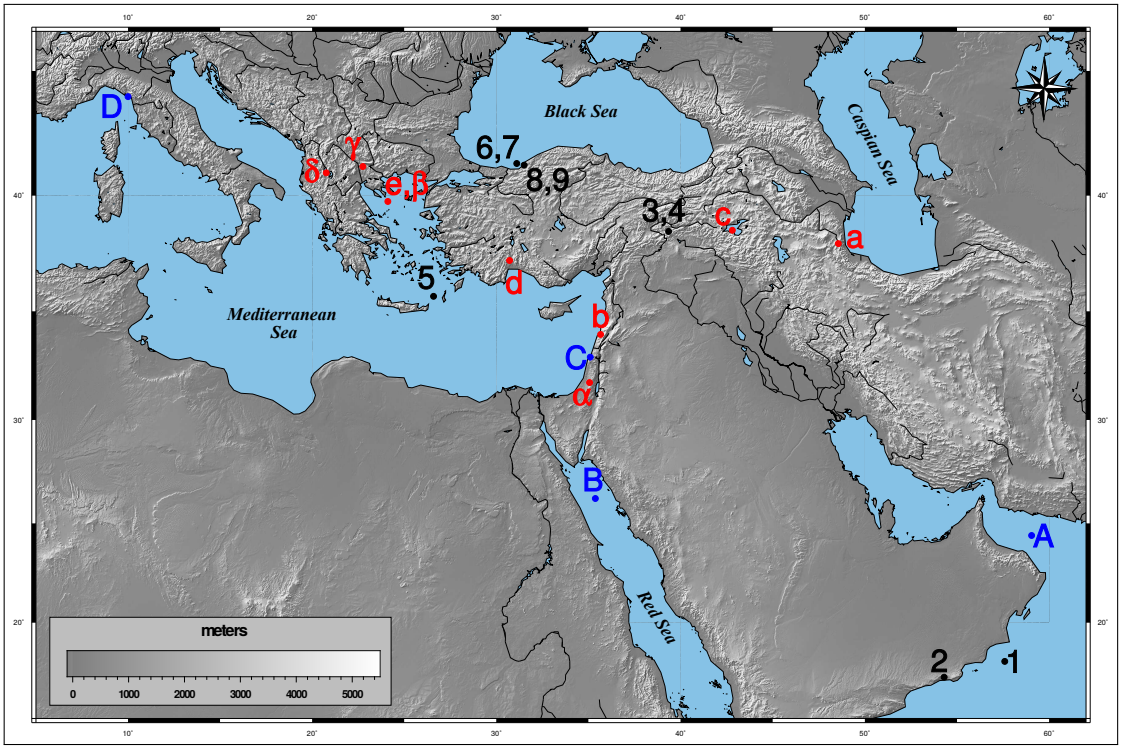

Figure 4.1 : Map of the wider region discussed in this study. Locations with numbers show the control set, and the locations shown with letters show the response variables. Black letters indicate the data confirming the hypothesis, whereas red letters indicate the locations which do not or partly confirm the hypothesis (for details, see Section 4.4). For the references of the whole data and differences between the letter characters of response variables, see Table 4.1. In this map, the locations of Grotte de Piste and NGRIP data are not shown for visual reasons. This map is prepared using GMT, version 5.2.1 [42] and ETOPO1 relief model [180].

The underlying idea of the causal impact method [9] depends on a fully Bayesian synthetic reconstruction of a time series (response variable, in this study each of the red and blue letters in Figure 4.1) which has been affected by an impact at a "known" point in time. The control set, (in this study the set of numbers in Figure 4.1, and they

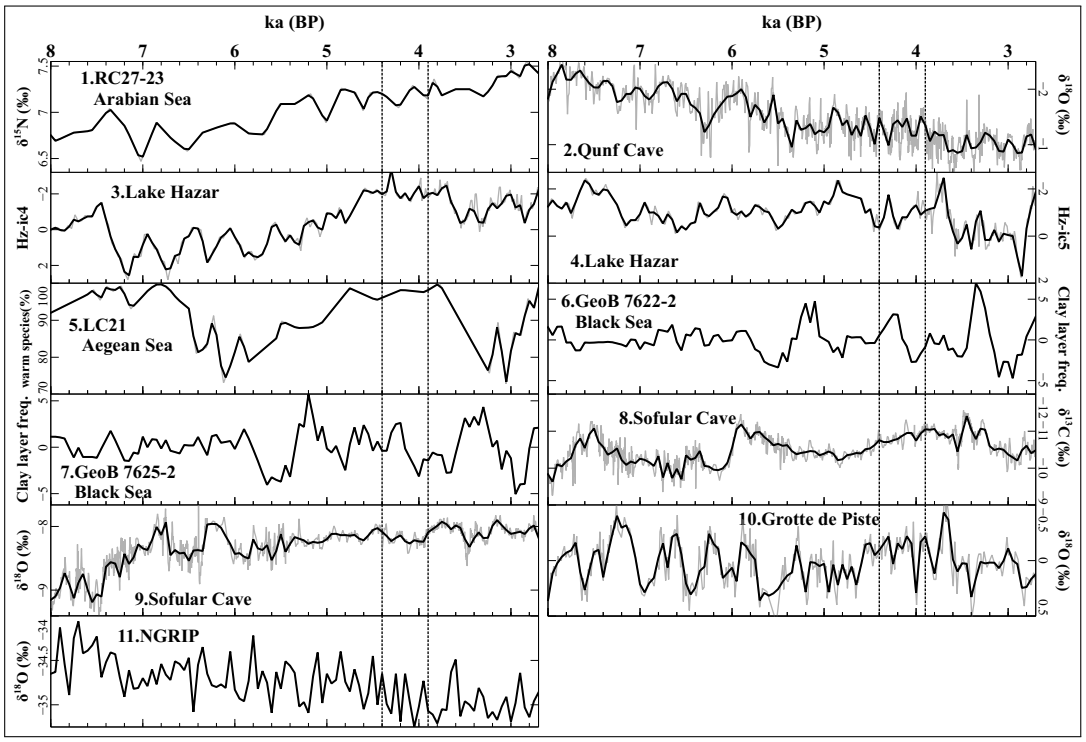

Figure 4.2 : Plots of the control set given in Table 4.1. Black lines show the original time series, interpolated to 50 years resolution and gray plots at the background show the raw data (see Section 4.3.1). Dashed vertical lines mark the interval between 4.4 and 3.9 ka BP. All the graphs are plotted to represent a drought/cooling effect in the negative direction. For the references of each data see Table 4.1.

are plotted in Figure 4.2) consists of other time series that are assumed to describe the same dynamic process but must themselves not be affected by the impact, neither in a positive nor a negative way. Furthermore, it is also assumed that the underlying relation between the control set and the response variable, except for the impact itself, also exists after the impact. Therefore, synthetically reconstructed response variable should not show any significant sign of impact, and consequently the comparison of the real variable with the reconstructed one at the period of impact gives a statistical result about the significance of that impact on the studied time series. Within this framework, the aim of this study is to generate synthetic time series of regional paleoclimate proxy data, which are claimed to include an abrupt climate change around 4.2 ka BP and test the statistical significance of that presumed abrupt change upon each of them.

4.3 Methods

4.3.1 Data

Reconstruction of targeted time series (response variable) through BSTS will be more robust if a longer data sequence is used and its application is only possible if the control set does not contain any missing values. It should therefore be noted that there is another controversial climate event similar to the 4.2 ka BP event at around 8.2 ka BP. We therefore selected elements for the control set from the wider region according to two criteria: that they have to span the period between 8 and 2.7 ka BP and that they should have a resolution of at least 50 years, approximately. The end member of our chosen interval, i.e. 2.7 ka BP, was selected because it marks the end of the almost continuous Qunf Cave record. It would also have been possible to select 3.9 ka BP as the end member but defining a longer period allows us to show the forecasting capability of the method. We therefore used the interval from 4.4 ka BP to 2.7 ka BP, a total forecasting period of 1700 years. The selection of 4.4 ka BP as the start of the impact is to avoid the possible creation of bias from the age models and to be able to show the the clear impact in the data coming from [177] (see Section 4.4 for the discussion).

While the BSTS method (Section 4.3.2.1) does not require evenly spaced data time points of control set and response variable must be contemporaneous. Since almost none of the time series data used in this study (Table 4.1) are synchronous, all of them are linearly interpolated to 50 years resolution to the NGRIP δ^{18}O 50 year resolution timescale converted from b2k to BP. Where some data sets had a higher temporal resolution, this was handled by filtering the data using a first order Savitzky-Golay filter [59] with a window spanning approximately 50 years of data. Filtering the Sofular Cave δ^{18}O and δ^{13}C data resulted in a window of 19 data points;five data points for the Jeita Cave δ^{18}O data; nine data points for the Qunf Cave δ^{18}O data; three data points for the Grotte de Piste δ^{18}O data; 23 data points for the Kocain Cave δ^{13}C data; and 17 data points for the Neor Lake XRF-Ti data.

Table 4.1 : Data used in this study. The data given in the upper panel are the response variables that it is claimed show an abrupt change during the period of interest, in the context of causal impact method. The letters are given according to the results gathered in this study: upper case Latin letters confirm the abrupt change hypothesis; lower case Greek letters indicate a change at the period of interest with a level shift; lower case Latin letters give no statistically valid change (for details, see Section 4.4). The letter k is the multiplier used through defining the gamma distribution of the prior distributions of the standard deviations of local linear trend term errors defined at Equation (4.1). The lower panel shows the control set in the context of causal impact method, which do not show a change during the period of interest. Site type abbreviations are as follows: M=Marine, AS= Archaeological Site, S= Speleothem, L= Lake, I= Ice Core.

Location	Site type	Proxy	Proxy Interpretation	Reference	k
A. Gulf of Oman (M5-422)	M	$CaCO_3$	Eolian deposition	[181]	0.1
B. Red Sea (GeoB 5836-2)	M	$\delta^{18}O$	Sea surface salinity	[182]	0.05
C. Tel Akko (Akko core)	AS	pollen	Precipitation	[172]	0.02
D. Buca della Renella (RL4)	S	$\delta^{18}O$	Precipitation	[177]	0.1
α. Soreq Cave (2-N)	S	$\delta^{18}O$	Precipitation	[175]	0.05
β. Aegean Sea (GeoTü SL148)	M	$\delta^{13}C_{Um}$	Productivity	[183]	0.1
γ. Lake Dojran (Co1260)	L	$CaCO_3$	Productivity	[184]	0.01
δ. Lake Ohrid (Lz1120)	L	$CaCO_3$	Productivity	[185]	0.1
a. Neor Lake	L	XRF-Ti	Eolian deposition	[186]	0.025
b. Jeita Cave (J-1)	S	$\delta^{18}O$	Precipitation	[187]	0.01
c. Lake Van (Van 90-10)	L	Quartz	Eolian deposition	[130]	0.02
d. Kocain Cave (Ko-1)	S	$\delta^{13}C$	Winter temperature	[188]	0.01
e. Aegean Sea (GeoTü SL148)	M	Smectite/Illite	Drought	[189]	0.05
1. Arabian Sea (RC27-23)	M	$\delta^{15}N$	Denitrification	[190]	
2. Qunf Cave (Q5)	S	$\delta^{18}O$	Precipitation	[191]	
3. Lake Hazar (Hz11-P03)	L	Hz-ic4	Precipitation	[6]	
4. Lake Hazar (Hz11-P03)	L	Hz-ic5	Temperature	[6]	
5. Aegean Sea (LC21)	M	warm species (%)	SST	[84]	
6. Black Sea (GeoB 7622-2)	M	clay layer freq.	Precipitation	[192]	
7. Black Sea (GeoB 7625-2)	M	clay layer freq.	Precipitation	[192]	
8. Sofular Cave (So-1)	S	$\delta^{13}C$	Effective moisture	[128]	
9. Sofular Cave (So-1)	S	$\delta^{18}O$	Moisture source	[128]	
10. Grotte de Piste	S	$\delta^{18}O$	Precipitation	[193]	
11. NGRIP	I	$\delta^{18}O$	Temperature	[66]	

4.3.2 Statistical methodology

4.3.2.1 Causal impact

Reconstruction of each response variable via control set depends on BSTS [179]. Structural time series models are powerful representations of time series in which regression, trend, seasonality and other desired components can be explicitly and

modularly defined. Basic structural time series model, which includes regression, local linear trend and seasonality, is defined through the following set of equations

$$\begin{aligned} y_{t+1} &= \mu_{t+1} + \gamma_{t+1} + \beta^T \mathbf{x_{t+1}} + \varepsilon_{t+1}, \\ \mu_{t+1} &= \mu_t + \delta_t + \xi_t, \\ \delta_{t+1} &= \delta_t + \zeta_t, \\ \gamma_{t+1} &= -\sum_{s=0}^{S-2} \gamma_{t-s} + \omega_t. \end{aligned} \tag{4.1}$$

In Equation (2.1), y_t is the observed data (in this study, any of the time series at the upper panel of Table 4.1, at time t), which in our case is claimed to show an abrupt change around 4.2 ka BP. Here y_t is defined with local linear trend μ_t, with dynamic slope δ_t defined as a random walk, and seasonal component γ_t, such that it sums up to zero in expectation over a full season. $\mathbf{x_t}$ is the vector of contemporaneous covariates (in this study, vector of data points at time t for the control set shown at the lower panel of Table 4.1), data which are not affected by the impact, and β is the regression coefficients vector associated with the control set. In the equations ε_t, ξ_t, ζ_t and ω_t are normally distributed Gaussian random noise error terms with zero mean and they are independent of each other. The parameters of the model, which priors should be defined for, are the variances of the error terms and β, the regression coefficients. As there is no seasonality component to the data used in this study, for simplicity we omit the seasonality term from now on.

Basic structural time series can easily be described as a state-space model

$$\begin{aligned} y_t &= Z_t \alpha_t + \varepsilon_t, \\ \alpha_{t+1} &= T_t \alpha_t + R_t \eta_t, \end{aligned} \tag{4.2}$$

where $\varepsilon_t \sim N(0, \sigma_t^2)$, $\eta_t \sim N(0, Q_t)$ and

$$\begin{aligned} \alpha_t^T &= \begin{bmatrix} \mu_t & \delta_t \end{bmatrix}, \quad Z_t = \begin{bmatrix} 1 & 0 \end{bmatrix}, \\ T_t &= \begin{bmatrix} 1 & 1 \\ 0 & 1 \end{bmatrix}, \quad R_t = \begin{bmatrix} 1 & 0 \\ 0 & 1 \end{bmatrix}, \\ \eta_t^T &= \begin{bmatrix} \xi_t & \zeta_t \end{bmatrix}, \quad Q_t = \begin{bmatrix} \sigma_\xi^2 & 0 \\ 0 & \sigma_\zeta^2 \end{bmatrix}. \end{aligned} \tag{4.3}$$

State-space model representation has the advantage of estimating parameters via Kalman filter and simulation smoothers [194]. Kalman filters are effective tools when variables of interest can be measured indirectly and give the model the

capacity of parameter selection through Bayesian inference. Kalman filter recursively computes $p(\alpha_{t+1} \mid y_{1:t})$ by combining the predictive distribution of the previous step, $p(\alpha_t \mid y_{1:t-1})$, with the emerged observation, y_t. At each step, simulation smoother [195] updates the mean and variance according to the previous predictive distributions [9, 179].

The inclusion of control set elements to the regression as Bayesian model averages is decided upon by placing spike and slab prior [196] to the regression coefficients and σ_ε, with conjugate normal-inverse gamma distribution priors [179]. Spike and slab variable selection technique is useful when the number of predictors is inconveniently large, or contains a mix of helpful and irrelevant variables. In the latter case one of its main advantages is that it correctly accounts for model selection uncertainty.

Inference of the parameters is established through repeating the following three step algorithm many times [179].

1. Latent state, $\boldsymbol{\alpha}$, is simulated through $p(\boldsymbol{\alpha} \mid \mathbf{y}, \theta, \beta, \sigma_\varepsilon^2)$, where $\theta = \{\sigma_\xi^2, \sigma_\zeta^2\}$ and $\mathbf{y}$ is the observed data vector, i.e. response variable until the start of the impact,
2. θ is simulated through $p(\theta \mid \mathbf{y}, \boldsymbol{\alpha}, \beta, \sigma_\varepsilon^2)$,
3. β and σ_ε^2 are simulated through a Markov chain stationary distribution $p(\beta, \sigma_\varepsilon^2 \mid \mathbf{y}, \boldsymbol{\alpha}, \theta)$.

The posterior predictive distribution of the model is defined through 100,000 Markov Chain Monte Carlo iterations using Gibbs sampler via

$$p(\tilde{\mathbf{y}}_{n+1:m} \mid \mathbf{y}_{1:n}, \mathbf{x}_{1:m}) \tag{4.4}$$

where, $\tilde{y}_{n+1}, \ldots, \tilde{y}_m$ is the set of the counterfactual values to forecast and $\mathbf{x}_{1:m}$ is the control set. The first 10% of the iterations are used as burn-in steps. The results are given as the mean of the posterior state and %95 credible interval for the post-impact period.

In order to control the incremental errors, prior distributions of σ_ξ^2 and σ_ζ^2 are assumed to be gamma distributions, where $1/\sigma_* \sim \Gamma(10^{-2}, k s_y^2)$. Here s_y^2 is the sample variance of the response variable and k is the multiplier, i.e. the prior standard deviation of the Gaussian random walk is expressed in terms of data standard deviation. In each

model, k as a hyperparameter describes the attribution of the random walk over the noise fluctuations. The larger its value, the fit before the impact may be more accurate. On the other hand, the forecast can be unrealistic and prediction bands would be wide. It is suggested by [9] to select k as being a number between 0.01 and 0.1. The value of k is selected through trials of numbers between 0.01 and 0.1 and visual control, by which a good fit with reasonable prediction intervals can be obtained. The selected value of k for each response variable is given in Table 4.1.

The significance of the impact is decided by finding the running average of the differences between the response variable and synthetic time series for the defined period and then Bayesian one-sided hypothesis testing is applied.

All the computations explained in this section are made through the open source CausalImpact package [9] in the freeware statistical software package, R [54].

4.3.2.2 Structural change

Whenever a regression model is constructed on time series, it is assumed that the regression coefficients remain temporally constant. However, if there is an abrupt shift in the time series, then a level shift that would cause regression coefficients to change, would be expected. Structural change method [197–199] finds the time points on a given series to minimize the residual sum of squares for different number of breaks. Here, by breaks, we mean oversimplifying the time series using a discontinuous function composed of a number of staircase-like steps. Our search focused on regression segments for at least 300 years and the optimal number of breaks were decided upon through the Bayesian Information Criterion.

All the computations explained in this section are made through the open source strucchange package [199] in the freeware statistical software package, R [54].

4.4 Results and Discussion

We performed BSTS stochastic fit to each of the data for which it had been claimed that they show an abrupt event around 4.2 ka BP. Our control set (Table 4.1) is composed of time series from the same wider region, but they *do not* show any abrupt change (in neither a positive nor negative manner) during the 4.2 ka BP period. All these data come from different studies, which may include certain biases both in terms of their

own age models, laboratory measurements and in terms of the nature of different proxy data. However, the use of multiple time series with Bayesian stochastic averaging, depending on the state of information, is believed to be one of the most robust, holistic and state-of-the-art approaches in the presence of such uncertainties [200, 201].

Selection of the control set elements mainly depends on the assumption of dynamic atmospheric connection through the extended region and therefore it is assumed that a relation between the proxy variables should exist. This connection can *somehow* be verified through the Late Pleistocene millennial scale catastrophic events in the region [67, 79, 159]. In some of the studies, even chronologies are constructed via this assumption [37, 202]. Also today, it is assumed that most of the variance in climate parameters of the region is mainly affected by the pressure gradient over North Atlantic with a phase contrast between east and west Mediterranean [203–205]. The direct connection of the North Atlantic to the region allows us to use NGRIP δ^{18}O dataset in the control set, since it is almost well defined with robust chronology. While Greenland ice core isotope data have problems for the Holocene [149], all the Greenland ice core data reveal, for example, the 8.2 ka BP abrupt event. We therefore selected NGRIP data for the sake of oscillations contained in. Furthermore, in order to implement the east-west connection of the Mediterranean region and increase the number of time series in the control set we add the Grotte de Piste speleothem δ^{18}O record from Morocco [193]. On the other hand, spike and slab prior variable selection technique is assumed to select the data from the control set which are statistically interrelated to the response variable.

According to the hypothesis proposed by [8], there was an abrupt climate change between 4.2 and 3.9 ka BP. Other studies enlarged the length of this interval, such as [177] who suggested that it took place between 4.4 and 3.8 ka BP. Since causal impact method applies a test on the differences between the response variable and the synthetically reconstructed time series during the period of interest, it may have given misleading results if we had restricted the onset of the event as 4.2 ka BP. Therefore, for all the time series in this study, we assumed that the onset of the climatic impact was 4.4 ka BP and it ends at 3.9 ka BP.

The hypothesis tests, based on our Bayesian stochastic fits to the time series, show that the putative abrupt change is not statistically significant in all thirteen of the time

series that we took into consideration. However, hypothesis test results of causal impact analysis presented here only take into account the period of interest and this may give misleading results in the scope of this study. Since the hypothesis testing procedure only takes into account the moving averages of the differences between the response variable and the synthetically constructed time series in the period of interest, if there is a level shift at the time of impact but it persists beyond the specified impact period, then causal impact will not give us any discriminatory measure after the specified impact interval. However, the approach still gives us a confident measure about the presence of *the onset* of that impact. In order to give a rough mathematical analysis for this condition, we used the results of structural change methodology (see, Section 4.3.2.2).

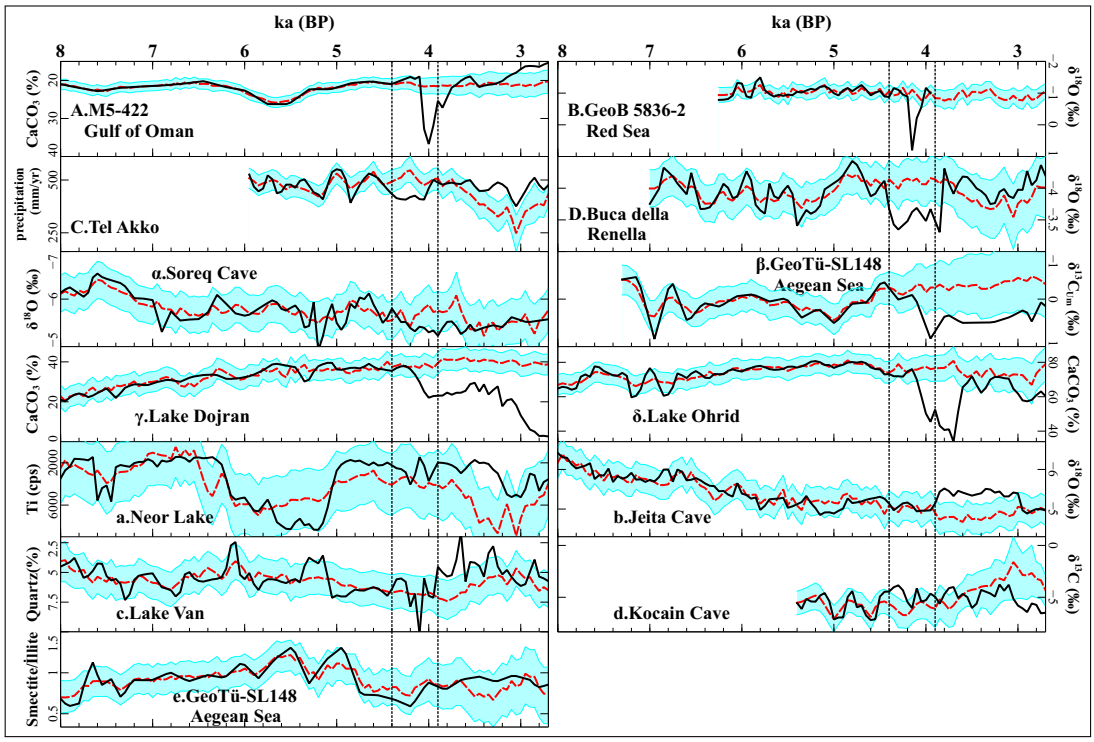

Figure 4.3 : Causal impact analyses for the response variables given in Table 4.1. Black lines show the original time series, interpolated to 50 years resolution, as explained in Section 4.3.1. Red dashed lines show the reconstructed times series, and the blue clouds in each plot indicate the 95% credible intervals. Dashed vertical lines mark the interval between 4.4 and 3.9 ka BP, where the hypothesis tests are applied. The intervals after 4.4 ka BP are the forecast periods. All the graphs are plotted to represent the effect in the negative direction.

For some of the time series analyzed the onset of the impact is clearly visible, however the *shapes* of the impact during the proposed drought period differ from case to case (Figure 4.3). The presumed impact has different influences on different time

series. In some of them, the general trend of the time series returns to its pre-impact levels after the cessation of the impact interval [172, 177, 181, 182], while in the other cases [175, 183–185] we don't observe any such resilience and the signals experience an enduring level shift (often negative) that lasts longer than the hypothesized impact interval. This is true even for records where the same proxy data is used and/or the sampling sites are close to one another (i.e. $CaCO_3$ proxy in [185] and [184]). This may be due to a *permanent* effect on the environment from which the proxies are sampled caused by the impact. For example, an extended drought may have imposed a significant change in the oceanic convective overturning regime that, in turn, permanently change the residence time of $\delta^{13}C$ [183] leading to a level shift in the time series after the cessation of the impact period. This may be a good example of a shift from one stable system to another stable state which can be described by multiple equilibria in the dynamical climate system (for example, see [206]).

The results suggest three different types of behavior in the time series following the presumed onset of the impact. The first group [172, 177, 181, 182] confirms the hypothesis of [8], namely, they not only confirm the onset date but also give approximately the same duration of the impact as proposed by [8]. The second proxy group [175, 183–185] shows that there is an impact in the time series but with an enduring level shift after cessation of the presumed impact period (Figure 4.4). The elements of the third group [130, 186–189], according to our methodology, do not indicate any abrupt change in the period of interest, i.e. the time series continue oscillating within the stochastic credible intervals.

A general consideration of the results show that the places where the proposed impact was detected do not form any coherent geographical/regional cluster. In fact, they are spatially diffuse across the study region. For example, we detected the impact in Buca della Renella in Italy [177] and the Gulf of Oman [181], but these are at diametrically opposed locations within the study region. Hence, if the impact did indeed exist, it was not necessarily localized to a specific region. According to our results, the hypothesis of a climatic change around 4.2 ka BP may not be completely false, but that the interpretations of the proxy data may not be appropriate due to the location from where the proxy is retrieved or the proxy's ability to represent hydroclimatic changes at the time scales we are interested in. Furthermore, we think that, without proper

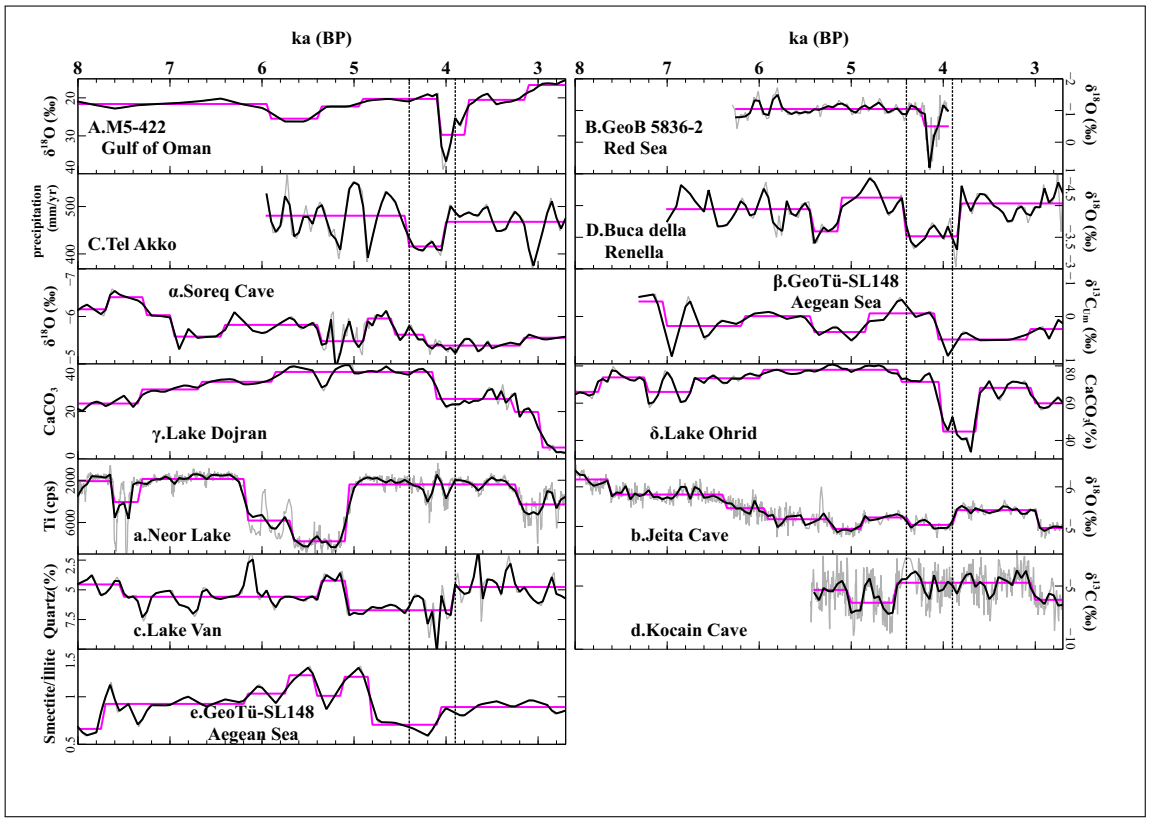

Figure 4.4 : Results of structural break method for the data who claim to show an abrupt change during the period of interest. Black lines show the original time series, interpolated to 50 years resolution and gray plots at the background show the raw data (see Section 4.3.1). Purple plots on each graph show the results of structural change method obtained by selecting minimal segment size as 300 years. Dashed vertical lines mark the interval between 4.4 and 3.9 ka BP. All the graphs are plotted to represent the effect in the negative direction.

discussion of a level shift in a proxy data after the climatic deterioration period, it should not be counted as a confirmation of the hypothesis. As stated by [3], "It is easy to obtain confirmations, or verifications, for nearly every theory-if we look for confirmations" (p. 47).

On the other hand, most impressive examples (spiky time series) of the 4.2 ka BP event, can be found around the Indian Ocean. These data are from the Red Sea [182], Gulf of Oman [181], northeast India [207], the Tibetan Plateau [208] and Mount Kilimanjaro [209]. Therefore, the drought which has been observed in upper Mesopotamia may be a reflection of an event in or around the Indian Ocean, which should be investigated at future studies.

4.5 Conclusions

Our study reconstructs paleoclimate proxy time series for which it has been claimed that they show the 4.2 ka BP abrupt climatic event through other ones around the same eastern Mediterranean and Arabian peninsula region using the BSTS method and then test the event's significance in the proxy record through the CausalImpact package. Three structural groups can be identified through the results of our analysis:

1. Data that show the claimed impact from the Gulf of Oman [181], the Red Sea [182], Buca della Renella [177] and Tel Akko [172] .

2. Data that show an impact at the period of interest but with an enduring level shift in the time series. This level shift may be due to the dynamical character of the proxy data which should be discussed in future studies. This is observed in data from the Soreq Cave [175], the Aegean Sea [183], Lake Ohrid [185] and Lake Dojran [184]

3. Finally, some proxy data do not show a sufficient change to describe it as an abrupt effect, including those from Lake Van [130], the Aegean Sea [189], Kocain Cave [188], Lake Neor [186] and Jeita Cave [187]. The oscillations of time series around the period of interest are acceptable within stochastic credible intervals.

5. CONCLUSIONS AND RECOMMENDATIONS

Our conclusions from the three studies can be summarized in three parts.

In Chapter 2, we present μ-XRF, $\delta^{18}O$ and $\delta^{13}C$ data of Lake Hazar. A Bayesian age model is fitted to the core and ICA is applied on μ-XRF data. Consequently, precipitation and a temperature models for the last 17.3 ka BP are offered for the region. According to the results, following outcomes can be summarized as conclusions:

i. The period before Bølling-Allerød was cold and wet, and Bølling-Allerød was warm and wet.

ii. According to the constructed age model, there is a hiatus during the Younger Dryas event, and this is an indicator of a dry period.

iii. Holocene temperatures were cooler at the start, however rise gradually to the "Holocene normals". Temperatures oscillate around Holocene normals, except the cold period between 3.5 ka BP and 2.8 ka BP

iv. Precipitation was high during the Holocene, except between 8 ka BP and 5 ka BP and 3.5 ka BP and 2.8 ka BP.

In Chapter 3, we apply ICA on Ca, Fe, K, Mn, Si intensities analysed by XRF core scanner, TOC and $CaCO_3$ content and B* (color reflectance) of the Ahlat Ridge sediment record spanning the last 250 ka BP and consequently a precipitation and a temperature model are constructed. Our results show that:

i. Temperature of the region almost mimics the NGRIP $\delta^{18}O$ record, i.e. warm during interglacials and interstadials but cold during glacials and stadials.

ii. On the other hand, precipitation model reveals somehow a different pattern than the recently proposed models. It is drier through cold periods, with an exception. The region seems relatively wet during the times of maximum glaciations, which at least is supported for the LGM by the terraces around the lake. The model also

shows that, during interstadials, the region is wetter than the stadials and during interglacials wet period is followed by a dry period.

In Chapter 4, we apply a test on the paleo-records from eastern Mediterranean and Arabian peninsula, which claim to support the abrupt climate change around 4.2 ka BP. This test is based on reconstruction of each record through other records of the region, which do not show any change at the time of interest, by the method of BSTS and consequently application of one sided Bayesian hypothesis testing. Our results indicate that, among the paleodata which have been tested, not all the records show a statistical significant change during the period of interest. The impacts claimed by the original authors of the studies seem to be stochastic oscillations within the boundaries of credible intervals.

REFERENCES

[1] **IPCC** (2013). *Climate Change 2013: The Physical Science Basis. Contribution of Working Group I to the Fifth Assessment Report of the Intergovernmental Panel on Climate Change*, Cambridge University Press, Cambridge, United Kingdom.

[2] **Bradley, R.S.** (2015). *Paleoclimatology*, Academic Press, San Diego, 3rd edition.

[3] **Popper, K.R.** (1963). *Conjectures and Refutations: The Growth of Scientific Knowledge*, Classics Series, Routledge, New York, 2002 reprint from the 3rd edition.

[4] **Mayewski, P.A.**, **Meeker, L.D.**, **Twickler, M.S.**, **Whitlow, S.**, **Yang, Q.**, **Lyons, W.B. and Prentice, M.** (1997). Major features and forcing of high-latitude northern hemisphere atmospheric circulation using a 110,000-year-long glaciochemical series, *Journal of Geophysical Research: Oceans*, *102*(C12), 26345–26366.

[5] **Danladi, I.B. and Akçer-Ön, S.** (2017). Solar forcing and climate variability during the past millennium as recorded in a high altitude lake: Lake Salda (SW Anatolia), *Quaternary International*, *486*, 185 – 198.

[6] **Ön, Z.B.**, **Akçer-Ön, S.**, **Özeren, M.S.**, **Eriş, K.K.**, **Greaves, A.M. and Çağatay, M.N.** (2017). Climate proxies for the last 17.3 ka from Lake Hazar (Eastern Anatolia), extracted by independent component analysis of μ-XRF data, *Quaternary International*, *486*, 17 – 28.

[7] **Ön, Z.B. and Özeren, M.S.** (submitted). Temperature and precipitation variability in eastern Anatolia: Results from independent component analysis of Lake Van sediment data spanning the last 250 kyr BP, *Manuscript submitted for publication to Quaternary International*.

[8] **Weiss, H.**, **Courty, M.A.**, **Wetterstrom, W.**, **Guichard, F.**, **Senior, L.**, **Meadow, R. and Curnow, A.** (1993). The Genesis and Collapse of Third Millennium North Mesopotamian Civilization, *Science*, *261*(5124), 995–1004.

[9] **Brodersen, K.H.**, **Gallusser, F.**, **Koehler, J.**, **Remy, N. and Scott, S.L.** (2015). Inferring causal impact using Bayesian structural time-series models, *Annals of Applied Statistics*, *9*(1), 247–274.

[10] **Ön, Z.B.**, **Özeren, M.S.**, **Greaves, A.M. and Akçer-Ön., S.** (submitted). Bayesian test for the 4.2 ka BP abrupt climatic change event for the eastern Mediterranean and Arabian peninsula paleoclimate data using structural time series, *Manuscript submitted for publication to Progress in Physical Geography*.

[11] **Roberts, N.**, **Jones, M.D.**, **Benkaddour, A.**, **Eastwood, W.J.**, **Filippi, M.L.**, **Frogley, M.R.**, **... Zanchetta, G.** (2008). Stable isotope records of Late Quaternary climate and hydrology from Mediterranean lakes: the ISOMED synthesis, *Quaternary Science Reviews*, *27*(25–26), 2426 – 2441.

[12] **Davies, J.S.**, **Lamb, F.H. and Roberts, J.S.**, (2015). Micro-XRF Core Scanning in Palaeolimnology: Recent Developments, W.I. Croudace and G.R. Rothwell, editors, Micro-XRF Studies of Sediment Cores: Applications of a non-destructive tool for the environmental sciences, Springer Netherlands, Dordrecht, pp.189–226.

[13] **Croudace, I.W. and Rothwell, R.G.** (2015). *Micro-XRF Studies of Sediment Cores: Applications of a non-destructive tool for the environmental sciences*, Developments in Paleoenvironmental Research, Springer Netherlands.

[14] **Aires, F.**, **Chédin, A. and Nadal, J.P.** (2000). Independent component analysis of multivariate time series: Application to the tropical SST variability, *Journal of Geophysical Research: Atmospheres*, *105*(D13), 17437–17455.

[15] **Perron, M. and Sura, P.** (2012). Climatology of Non-Gaussian Atmospheric Statistics, *Journal of Climate*, *26*(3), 1063–1083.

[16] **Sura, P. and Hannachi, A.** (2014). Perspectives of Non-Gaussianity in Atmospheric Synoptic and Low-Frequency Variability, *J. Climate*, *28*(13), 5091–5114.

[17] **Stone, J.V.** (2004). *Independent Component Analysis: A Tutorial Introduction*, A Bradford Book, MIT Press, London.

[18] **Comon, P.** (1994). Independent component analysis, A new concept?, *Signal Processing*, *36*(3), 287 – 314.

[19] **Hyvärinen, A. and Oja, E.** (2000). Independent component analysis: algorithms and applications, *Neural Networks*, *13*(4–5), 411 – 430.

[20] **Acharya, D.P. and Panda, G.** (2008). A Review of Independent Component Analysis Techniques and their Applications, *IETE Technical Review*, *25*(6), 320–332.

[21] **Naik, G.R. and Kumar, D.K.** (2011). An Overview of Independent Component Analysis and Its Applications, *Informatica*, *35*(1), 63–81.

[22] **Basak, J.**, **Sudarshan, A.**, **Trivedi, D. and Santhanam, M.S.** (2004). Weather Data Mining Using Independent Component Analysis, *Journal of Machine Learning Research*, *5*, 239–253.

[23] **Mori, A.**, **Kawasaki, N.**, **Yamazaki, K.**, **Honda, M. and Nakamura, H.** (2006). A Reexamination of the Northern Hemisphere Sea Level Pressure Variability by the Independent Component Analysis, *SOLA*, *2*, 5–8.

[24] **Hannachi, A.**, **Unkel, S.**, **Trendafilov, N.T. and Jolliffe, I.T.** (2009). Independent Component Analysis of Climate Data: A New Look at EOF Rotation, *Journal of Climate*, *22*(11), 2797–2812.

[25] **Tatlı, H.**, **Dalfes, N.H. and Menteş, Ş.S.** (2004). A statistical downscaling method for monthly total precipitation over Turkey, *International Journal of Climatology*, *24*(2), 161–180.

[26] **Tatlı, H.**, **Dalfes, N.H. and Menteş, Ş.S.** (2005). Surface air temperature variability over Turkey and its connection to large-scale upper air circulation via multivariate techniques, *International Journal of Climatology*, *25*(3), 331–350.

[27] **Choi, S.**, **Cichocki, A.**, **Park, H.M. and Lee, S.Y.** (2005). Blind Source Separation and Independent Component Analysis: A Review, *Neural Information Processing - Letters and Reviews*, *6*(1), 1–57.

[28] **Eriş, K.K.** (2013). Late Pleistocene—Holocene sedimentary records of climate and lake-level changes in Lake Hazar, eastern Anatolia, Turkey, *Quaternary International*, *302*, 123 – 134.

[29] **Eriş, K.K.**, **Ön, S.A.**, **Çağatay, M.N.**, **Ülgen, U.B.**, **Ön, Z.B.**, **Gürocak, Z.**, **... Öztekin-Okan, Ö** (2017). Late Pleistocene to Holocene paleoenvironmental evolution of Lake Hazar, Eastern Anatolia, Turkey, *Quaternary International*, *486*, 4 – 16.

[30] **Roberts, N.**, **Reed, J.M.**, **Leng, M.J.**, **Kuzucuoğlu, C.**, **Fontugne, M.**, **Bertaux, J.**, **... Karabıyıkoğlu, M.** (2001). The tempo of Holocene climatic change in the eastern Mediterranean region: new high-resolution crater-lake sediment data from central Turkey, *The Holocene*, *11*(6), 721–736.

[31] **Roberts, N.**, **Allcock, S.L.**, **Arnaud, F.**, **Dean, J.R.**, **Eastwood, W.J.**, **Jones, M.D.**, **... Yiğitbaşıoğlu, H.** (2016). A tale of two lakes: a multi-proxy comparison of Lateglacial and Holocene environmental change in Cappadocia, Turkey, *Journal of Quaternary Science*, *31*(4), 348–362.

[32] **Woldring, H. and Bottema, S.** (2003). The vegetation history of East-Central Anatolia in relation to archaeology: the Eski Acıgöl pollen evidence compared with the Near Eastern environment, *Palaeohistoria*, *43/44*, 1–34.

[33] **Jones, M.D.**, **Roberts, C.N.**, **Leng, M.J. and Türkeş, M.** (2006). A high-resolution late Holocene lake isotope record from Turkey and links to North Atlantic and monsoon climate, *Geology*, *34*(5), 361.

[34] **Turner, R.**, **Roberts, N. and Jones, M.D.** (2008). Climatic pacing of Mediterranean fire histories from lake sedimentary microcharcoal, *Global and Planetary Change*, *63*(4), 317 – 324.

[35] **Dean, J.R.**, **Jones, M.D.**, **Leng, M.J.**, **Noble, S.R.**, **Metcalfe, S.E.**, **Sloane, H.J.**, **... Roberts, C.N.** (2015). Eastern Mediterranean hydroclimate over the late glacial and Holocene, reconstructed from the sediments of Nar lake, central Turkey, using stable isotopes and carbonate mineralogy, *Quaternary Science Reviews*, *124*, 162 – 174.

[36] **Litt, T. and Anselmetti, F.S.** (2014). *Special Issue: Results from the PALEOVAN Drilling Project: a 600,000 year long continental archive in the Near East*, Quaternary Science Reviews 104.

[37] **Stockhecke, M.**, **Timmermann, A.**, **Kipfer, R.**, **Haug, G.H.**, **Kwiecien, O.**, **Friedrich, T.**, **... Anselmetti, F.S.** (2016). Millennial to orbital-scale variations of drought intensity in the Eastern Mediterranean, *Quaternary Science Reviews*, *133*, 77 – 95.

[38] **Hempton, M.R. and Dunne, L.A.** (1984). Sedimentation in Pull-Apart Basins: Active Examples in Eastern Turkey, *The Journal of Geology*, *92*(5), 513–530.

[39] **Garcia Moreno, D.**, **Hubert-Ferrari, A.**, **Moernaut, J.**, **Fraser, J.G.**, **Boes, X.**, **Van Daele, M.**, **... De Batist, M.** (2011). Structure and recent evolution of the Hazar Basin: a strike-slip basin on the East Anatolian Fault, Eastern Turkey, *Basin Research*, *23*(2), 191–207.

[40] **Çetin, H.**, **Güneyli, H. and Mayer, L.** (2003). Paleoseismology of the Palu—Lake Hazar segment of the East Anatolian Fault Zone, Turkey, *Tectonophysics*, *374*(3–4), 163 – 197.

[41] **Nicoll, K.** (2010). Landscape development within a young collision zone: implications for post-Tethyan evolution of the Upper Tigris River system in southeastern Turkey, *International Geology Review*, *52*(4-6), 404–422.

[42] **Wessel, P.**, **Smith, W.H.F.**, **Scharroo, R.**, **Luis, J. and Wobbe, F.** (2013). Generic Mapping Tools: Improved Version Released, *Eos, Transactions American Geophysical Union*, *94*(45), 409–410.

[43] **Conrad, O.**, **Bechtel, B.**, **Bock, M.**, **Dietrich, H.**, **Fischer, E.**, **Gerlitz, L.**, **... Böhner, J.** (2015). System for Automated Geoscientific Analyses (SAGA) v. 2.1.4, *Geoscientific Model Development*, *8*(7), 1991–2007.

[44] **Koçer, M.A.T. and Şen, B.** (2012). The seasonal succession of diatoms in phytoplankton of a soda lake (Lake Hazar, Turkey), *Turkish Journal of Botany*, *36*, 738–746.

[45] **Türkeş, M. and Tatlı, H.** (2011). Use of the spectral clustering to determine coherent precipitation regions in Turkey for the period 1929-2007, *International Journal of Climatology*, *31*(14), 2055–2067.

[46] **Erol, O.** (2011). *General Climatology (in Turkish)*, Çantay, İstanbul, 11th edition.

[47] **Lionello, P.**, **Bhend, J.**, **Buzzi, A.**, **Della-Marta, P.M.**, **Krichak, S.O.**, **Jansà, A.**, **... Trigo, R.**, (2006). Cyclones in the Mediterranean region: Climatology and effects on the environment, P. Lionello, Malanotte-Rizzoli, P and R. Boscolo, editors, Mediterranean Climate Variability, volume 4 of *Developments in Earth and Environmental Sciences*, Elsevier, pp.325 – 372.

[48] **Fernández, J.**, **Sáenz, J. and Zorita, E.** (2003). Analysis of wintertime atmospheric moisture transport and its variability over southern Europe in the NCEP Reanalyses , *Climate Research*, *23*, 195–215.

[49] **Lionello, P.**, **Malanotte-Rizzoli, P.**, **Boscolo, R.**, **Alpert, P.**, **Artale, V.**, **Li, L.**, **... Xoplaki, E.**, (2006). The Mediterranean climate: An overview of the main characteristics and issues, P. Lionello, Malanotte-Rizzoli, P and R. Boscolo, editors, Mediterranean Climate Variability, volume 4 of *Developments in Earth and Environmental Sciences*, Elsevier, pp.1 – 26.

[50] **Bozkurt, D.**, **Turunçoğlu, U.**, **Şen, Ö.L.**, **Önol, B. and Dalfes, H.N.** (2012). Downscaled simulations of the ECHAM5, CCSM3 and HadCM3 global models for the eastern Mediterranean–Black Sea region: evaluation of the reference period, *Climate Dynamics*, *39*(1), 207–225.

[51] **Sars, G.O.** (1887). Nye Bidrag til Kundskaben om Middelhavets Invertebratfauna 4: Ostracoda Mediterranea (Sydeuropaeiske Ostracoder), *Archiv for Mathematik og Naturvidenskab*, *12*, 173–324.

[52] **Reimer, P.**, **Bard, E.**, **Bayliss, A.**, **Beck, J.**, **Blackwell, P.**, **Ramsey, C.B.**, **... van der Plicht, J.** (2013). IntCal13 and Marine13 Radiocarbon Age Calibration Curves 0–50,000 Years cal BP, *Radiocarbon*, *55*(4).

[53] **Blaauw, M. and Christen, J.A.** (2011). Flexible paleoclimate age-depth models using an autoregressive gamma process, *Bayesian Anal.*, *6*(3), 457–474.

[54] **R Core Team**, (2018). R: A Language and Environment for Statistical Computing, R Foundation for Statistical Computing, Vienna, Austria, URL `https://www.R-project.org/`.

[55] **Bronk Ramsey, C.** (2008). Deposition models for chronological records, *Quaternary Science Reviews*, *27*(1–2), 42 – 60.

[56] **Parnell, A.C.**, **Haslett, J.**, **Allen, J.R.M.**, **Buck, C.E. and Huntley, B.** (2008). A flexible approach to assessing synchroneity of past events using Bayesian reconstructions of sedimentation history, *Quaternary Science Reviews*, *27*(19–20), 1872 – 1885.

[57] **Goring, S.**, **Williams, J.W.**, **Blois, J.L.**, **Jackson, S.T.**, **Paciorek, C.J.**, **Booth, R.K.**, **... Christen, J.A.** (2012). Deposition times in the northeastern United States during the Holocene: establishing valid priors for Bayesian age models, *Quaternary Science Reviews*, *48*, 54 – 60.

[58] **Masson-Delmotte, V.**, **Schulz, M.**, **Abe-Ouchi, A.**, **Beer, J.**, **Ganopolski, A.**, **González Rouco, J.F.**,**... Timmermann, A.**, (2013). Information from paleoclimate archives, T. Stocker, D. Qin, G.K. Plattner, M. Tignor, S.K. Allen, J. Boschung, ... P.M. Midgley, editors, Climate Change 2013: The Physical Science Basis. Contribution of Working Group I to the Fifth Assessment Report of the Intergovernmental Panel on Climate Change, Cambridge University Press, Cambridge, pp.383–464.

[59] **Savitzky, A. and Golay, M.J.E.** (1964). Smoothing and Differentiation of Data by Simplified Least Squares Procedures., *Analytical Chemistry*, *36*(8), 1627–1639.

[60] **Hyvärinen, A., Hurri, J. and Hoyer, P.O.**, (2009). Natural Image Statistics: A Probabilistic Approach to Early Computational Vision, chapterPrincipal Components and Whitening, Springer, London, pp.93–130.

[61] **Hyvärinen, A., Karhunen, J. and Oja, E.** (2004). *Independent Component Analysis*, Adaptive and Cognitive Dynamic Systems: Signal Processing, Learning, Communications and Control, Wiley.

[62] **Hyvärinen, A.** (1999). Fast and robust fixed-point algorithms for independent component analysis, *Neural Networks, IEEE Transactions on*, *10*(3), 626–634.

[63] **Hyvärinen, A.** (1998). New Approximations of Differential Entropy for Independent Component Analysis and Projection Pursuit, *Proceedings of the 1997 Conference on Advances in Neural Information Processing Systems 10*, NIPS '97, MIT Press, Cambridge, MA, USA, pp.273–279.

[64] **Hyvärinen, A., Särelä, J. and Vigário, R.** (1999). Spikes and Bumps: Artefacts Generated by Independent Component Analysis with Insufficient Sample Size (ICA '99), *Proc. Int. Workshop on Independent Component Analysis and Signal Seperation*, Aussois, France, pp.425–429.

[65] **Székely, G.J., Rizzo, M.L. and Bakirov, N.K.** (2007). Measuring and testing dependence by correlation of distances, *Ann. Statist.*, *35*(6), 2769–2794.

[66] **Andersen, K.K., Azuma, N., Barnola, J.M., Bigler, M., Biscaye, P., Caillon, N., ... White, J.W.C.** (2004). High-resolution record of Northern Hemisphere climate extending into the last interglacial period, *Nature*, *431*(7005), 147–151.

[67] **Fleitmann, D., Cheng, H., Badertscher, S., Edwards, R.L., Mudelsee, M., Göktürk, O.M., ... Tüysüz, O.** (2009). Timing and climatic impact of Greenland interstadials recorded in stalagmites from northern Turkey, *Geophysical Research Letters*, *36*(19).

[68] **Joussaume, S. and Jouzel, J.** (1993). Paleoclimatic tracers: An investigation using an atmospheric general circulation model under ice age conditions: 2. Water isotopes, *Journal of Geophysical Research: Atmospheres*, *98*(D2), 2807–2830.

[69] **Johnsen, S.J., Dahl-Jensen, D., Gundestrup, N., Steffensen, J.P., Clausen, H.B., Miller, H., ... White, J.** (2001). Oxygen isotope and palaeotemperature records from six Greenland ice-core stations: Camp Century, Dye-3, GRIP, GISP2, Renland and NorthGRIP, *Journal of Quaternary Science*, *16*(4), 299–307.

[70] **Kinney, J.B. and Atwal, G.S.** (2014). Equitability, mutual information, and the maximal information coefficient, *Proceedings of the National Academy of Sciences*, *111*(9), 3354–3359.

[71] **Martínez-Gómez, E., Richards, M.T. and Richards, D.S.P.** (2014). Distance Correlation Methods for Discovering Associations in Large Astrophysical Databases, *The Astrophysical Journal*, *781*(1), 39.

[72] **Richards, M.T.**, **Richards, D.S.P. and Martínez-Gómez, E.** (2014). Interpreting the Distance Correlation Results for the COMBO-17 Survey, *The Astrophysical Journal Letters*, *784*(2), L34.

[73] **Simon, N. and Tibshirani, R.** (2014). Comment on "Detecting Novel Associations In Large Data Sets" by Reshef et al, Science Dec 16, 2011, *ArXiv e-prints*, 1401.7645.

[74] **Andersen, K.K.**, **Bigler, M.**, **Buchardt, S.L.**, **Clausen, H.B.**, **Dahl-Jensen, D.**, **Davies, S.M.**, **... Vinther, B.M.**, (2007), Greenland Ice Core Chronology 2005 (GICC05) and 20 year means of oxygen isotope data from ice core NGRIP, http://doi.pangaea.de/10.1594/PANGAEA.586838.

[75] **Whitfield, P.H.**, **Clark, M.J. and Cannon, A.** (1999). Signals and noise in environmental data—Characterization of non-random uncertainty in environmental monitoring, *Environmental Modeling, Proceedings of the International Conference on Water, Environment, Ecology, Socioeconomics, and Health Engineering (WEESHE), Seoul, Korea*, pp.86–96.

[76] **Westra, S.**, **Brown, C.**, **Lall, U. and Sharma, A.** (2007). Modeling multivariable hydrological series: Principal component analysis or independent component analysis?, *Water Resources Research*, *43*(6).

[77] **MacLachlan, S.E.**, **Hunt, J.E. and Croudace, I.W.**, (2015). An Empirical Assessment of Variable Water Content and Grain-Size on X-Ray Fluorescence Core-Scanning Measurements of Deep Sea Sediments, I.W. Croudace and R.G. Rothwell, editors, Micro-XRF Studies of Sediment Cores: Applications of a non-destructive tool for the environmental sciences, Springer Netherlands, Dordrecht, pp.173–185.

[78] **Kelts, K. and Hsü, K.J.**, (1978). Freshwater Carbonate Sedimentation, A. Lerman, editor, Lakes: Chemistry, Geology, Physics, Springer New York, New York, NY, pp.295–323.

[79] **Çağatay, M.N.**, **Öğretmen, N.**, **Damcı, E.**, **Stockhecke, M.**, **Sancar, Ü.**, **Eriş, K.K. and Özeren, S.** (2014). Lake level and climate records of the last 90 ka from the Northern Basin of Lake Van, eastern Turkey, *Quaternary Science Reviews*, *104*, 97 – 116.

[80] **Cohen, A.S.** (2003). *Paleolimnology: The History and Evolution of Lake Systems*, Oxford University Press, USA.

[81] **Gaillardet, J.**, **Viers, J. and Dupré, B.**, (2014). Trace Elements in River Waters, K.K. Turekian and D.H. Heinrich, editors, Treatise on Geochemistry, Elsevier, Oxford, 2nd edition, pp.195 – 235.

[82] **Berger, A. and Loutre, M.F.** (1991). Insolation values for the climate of the last 10 million years, *Quaternary Science Reviews*, *10*(4), 297 – 317.

[83] **Bond, G.**, **Kromer, B.**, **Beer, J.**, **Muscheler, R.**, **Evans, M.N.**, **Showers, W.**, **... Bonani, G.** (2001). Persistent Solar Influence on North Atlantic Climate During the Holocene, *Science*, *294*(5549), 2130–2136.

[84] **Rohling, E.**, **Mayewski, P.**, **Abu-Zied, R.**, **Casford, J. and Hayes, A.** (2002). Holocene atmosphere-ocean interactions: records from Greenland and the Aegean Sea, *Climate Dynamics*, *18*(7), 587–593.

[85] **Vannière, B.**, **Power, M.J.**, **Roberts, N.**, **Tinner, W.**, **Carrión, J.**, **Magny, M.**, **... Vescovi, E.** (2011). Circum-Mediterranean fire activity and climate changes during the mid-Holocene environmental transition (8500-2500 cal. BP), *The Holocene*, *21*(1), 53–73.

[86] **Prentice, I.C.**, **Guiot, J. and Harrison, S.P.** (1992). Mediterranean vegetation, lake levels and palaeoclimate at the Last Glacial Maximum, *Nature*, *360*, 658–660.

[87] **Mudie, P.J.**, **Rochon, A. and Aksu, A.E.** (2002). Pollen stratigraphy of Late Quaternary cores from Marmara Sea: land—sea correlation and paleoclimatic history, *Marine Geology*, *190*(1–2), 233 – 260.

[88] **Roberts, N. and Wright, H.E.**, (1993). Vegetational, Lake-Level, and Climatic History of the Near East and Southwest Asia, H.E. Wright, J.E. Kutzbach, T. Webb, W.F. Ruddiman, F.A. Street-Perrott and P.J. Bartlein, editors, Global Climates since the Last Glacial Maximum, University of Minnesota Press, pp.194–220.

[89] **Erol, O.**, (1997). Geomorphologic Arguments for Mid- to Late Holocene Environmental Change in Central Anatolian (Pluvial) Lake Basins, H.N. Dalfes, G. Kukla and H. Weiss, editors, Third Millennium BC Climate Change and Old World Collapse, Springer, Berlin, Heidelberg, pp.321–350.

[90] **Sarıkaya, M.A.**, **Zreda, M.**, **Çiner, A. and Zweck, C.** (2008). Cold and wet Last Glacial Maximum on Mount Sandıras, SW Turkey, inferred from cosmogenic dating and glacier modeling, *Quaternary Science Reviews*, *27*(7–8), 769 – 780.

[91] **Sarıkaya, M.A.**, **Çiner, A.**, **Haybat, H. and Zreda, M.** (2014). An early advance of glaciers on Mount Akdağ, SW Turkey, before the global Last Glacial Maximum; insights from cosmogenic nuclides and glacier modeling, *Quaternary Science Reviews*, *88*, 96 – 109.

[92] **COHMAP Members** (1988). Climatic Changes of the Last 18,000 Years: Observations and Model Simulations, *Science*, *241*(4869), 1043–1052.

[93] **Harrison, S.P.**, **Yu, G. and Tarasov, P.E.** (1996). Late Quaternary Lake-Level Record from Northern Eurasia, *Quaternary Research*, *45*(2), 138 – 159.

[94] **Bar-Matthews, M.**, **Ayalon, A.**, **Kaufman, A. and Wasserburg, G.J.** (1999). The Eastern Mediterranean paleoclimate as a reflection of regional events: Soreq cave, Israel, *Earth and Planetary Science Letters*, *166*(1–2), 85 – 95.

[95] **Fontugne, M.**, **Kuzucuoğlu, C.**, **Karabıyıkoğlu, M.**, **Hatté, C. and Pastre, J.F.** (1999). From Pleniglacial to Holocene: a ^{14}C chronostratigraphy of environmental changes in the Konya Plain, Turkey, *Quaternary Science Reviews*, *18*(4), 573 – 591.

[96] **Bar-Matthews, M.**, **Ayalon, A. and Kaufman, A.** (1997). Late Quaternary Paleoclimate in the Eastern Mediterranean Region from Stable Isotope Analysis of Speleothems at Soreq Cave, Israel, *Quaternary Research*, *47*(2), 155 – 168.

[97] **Arz, H.W.**, **Lamy, F.**, **Pätzold, J.**, **Müller, P.J. and Prins, M.** (2003). Mediterranean Moisture Source for an Early-Holocene Humid Period in the Northern Red Sea, *Science*, *300*(5616), 118–121.

[98] **deMenocal, P.**, **Ortiz, J.**, **Guilderson, T.**, **Adkins, J.**, **Sarnthein, M.**, **Baker, L. and Yarusinsky, M.** (2000). Abrupt onset and termination of the African Humid Period: rapid climate responses to gradual insolation forcing, *Quaternary Science Reviews*, *19*(1–5), 347 – 361.

[99] **Haug, G.H.**, **Hughen, K.A.**, **Sigman, D.M.**, **Peterson, L.C. and Röhl, U.** (2001). Southward Migration of the Intertropical Convergence Zone Through the Holocene, *Science*, *293*(5533), 1304–1308.

[100] **Arbuszewski, J.A.**, **deMenocal, P.B.**, **Cleroux, C.**, **Bradtmiller, L. and Mix, A.** (2013). Meridional shifts of the Atlantic intertropical convergence zone since the Last Glacial Maximum, *Nature Geoscience*, *6*(11), 959—-962.

[101] **Roth, R. and Joos, F.** (2013). A reconstruction of radiocarbon production and total solar irradiance from the Holocene ^{14}C and CO_2 records: implications of data and model uncertainties, *Climate of the Past*, *9*(4), 1879–1909.

[102] **Debret, M.**, **Bout-Roumazeilles, V.**, **Grousset, F.**, **Desmet, M.**, **McManus, J.F.**, **Massei, N.**, **... Trentesaux, A.** (2007). The origin of the 1500-year climate cycles in Holocene North-Atlantic records, *Climate of the Past*, *3*(4), 569–575.

[103] **Dalfes, H.N.**, **Kukla, G. and Weiss, H.** (1997). *Third Millennium BC Climate Change and Old World Collapse*, NATO ASI series, Springer.

[104] **Kwiecien, O.**, **Stockhecke, M.**, **Pickarski, N.**, **Heumann, G.**, **Litt, T.**, **Sturm, M.**, **... and Haug, G.H.** (2014). Dynamics of the last four glacial terminations recorded in Lake Van, Turkey, *Quaternary Science Reviews*, *104*, 42 – 52.

[105] **Stockhecke, M.**, **Sturm, M.**, **Brunner, I.**, **Schmincke, H.U.**, **Sumita, M.**, **Kipfer, R.**, **... Anselmetti, F.S.** (2014). Sedimentary evolution and environmental history of Lake Van (Turkey) over the past 600 000 years, *Sedimentology*, *61*(6), 1830–1861.

[106] **Kuzucuoğlu, C.**, **Christol, A.**, **Mouralis, D.**, **Doğu, A.F.**, **Akköprü, E.**, **Fort, M.**, **... Guillou, H.** (2010). Formation of the Upper Pleistocene terraces of Lake Van (Turkey), *Journal of Quaternary Science*, *25*(7), 1124–1137.

[107] **Litt, T.**, **Pickarski, N.**, **Heumann, G.**, **Stockhecke, M. and Tzedakis, P.C.** (2014). A 600,000 year long continental pollen record from Lake Van, eastern Anatolia (Turkey), *Quaternary Science Reviews*, *104*, 30 – 41.

[108] **Randlett, M.È.**, **Coolen, M.J.L.**, **Stockhecke, M.**, **Pickarski, N.**, **Litt, T.**, **Balkema, C.**, **... Schubert, C.J.** (2014). Alkenone distribution in Lake Van sediment over the last 270 ka: influence of temperature and haptophyte species composition, *Quaternary Science Reviews*, *104*, 53 – 62.

[109] **Ön, Z.B.**, **Özeren, M.S.**, **Akçer-Ön, S. and Çağatay, M.N.** (2017). Spectral Features of 250 kyr Long Lake Van Sediments: Milankovitch Cycles and Their Harmonics, *Geological Bulletin of Turkey*, *60*, 471 – 488.

[110] **Landmann, G.**, **Reimer, A. and Kempe, S.** (1996). Climatically induced lake level changes at Lake Van, Turkey, during the Pleistocene/Holocene Transition, *Global Biogeochemical Cycles*, *10*(4), 797–808.

[111] **Kempe, S.**, **Landmann, G. and Müller, G.** (2002). A floating varve chronology from the last glacial maximum terrace of Lake Van/Turkey, *Zeitschrift für Geomorphologie*, *126*, 97–114.

[112] **Wick, L.**, **Lemcke, G. and Sturm, M.** (2003). Evidence of Lateglacial and Holocene climatic change and human impact in eastern Anatolia: high-resolution pollen, charcoal, isotopic and geochemical records from the laminated sediments of Lake Van, Turkey, *The Holocene*, *13*(5), 665–675.

[113] **Valeton, I.**, (1978). A morphological and petrological study of the terraces around Lake Van, Turkey., E.T. Degens and F. Kurtman, editors, The Geology of Lake Van, MTA Press, Ankara, pp.64 – 80.

[114] **Tomonaga, Y.**, **Brennwald, M.S.**, **Livingstone, D.M.**, **Kwiecien, O.**, **Randlett, M.È.**, **Stockhecke, M.**, **... Kipfer, R.** (2017). Porewater salinity reveals past lake-level changes in Lake Van, the Earth's largest soda lake, *Scientific Reports*, *7*(1), 313.

[115] **Bloemsma, M.R.**, **Zabel, M.**, **Stuut, J.B.W.**, **Tjallingii, R.**, **Collins, J.A. and Weltje, G.J.** (2012). Modelling the joint variability of grain size and chemical composition in sediments, *Sedimentary Geology*, *280*, 135 – 148.

[116] **Krumsiek, J.**, **Suhre, K.**, **Illig, T.**, **Adamski, J. and Theis, F.J.** (2012). Bayesian Independent Component Analysis Recovers Pathway Signatures from Blood Metabolomics Data, *Journal of Proteome Research*, *11*(8), 4120–4131.

[117] **Yang, J. and Cheng, Q.** (2015). A comparative study of independent component analysis with principal component analysis in geological objects identification. Part II: A case study of Pinghe District, Fujian, China, *Journal of Geochemical Exploration*, *149*, 136 – 146.

[118] **Iwamori, H.**, **Yoshida, K.**, **Nakamura, H.**, **Kuwatani, T.**, **Hamada, M.**, **Haraguchi, S. and Ueki, K.** (2017). Classification of geochemical data

based on multivariate statistical analyses: Complementary roles of cluster, principal component, and independent component analyses, *Geochemistry, Geophysics, Geosystems*, *18*(3), 994–1012.

[119] **Middleton, M.A.**, **Whitfield, P.H. and Allen, D.M.** (2015). Independent component analysis of local scale temporal variability in sediment water interface temperature, *Water Resources Research*, *51*(12), 9679–9695.

[120] **Wegwerth, A.**, **Ganopolski, A.**, **Ménot, G.**, **Kaiser, J.**, **Dellwig, O.**, **Bard, E.**, **... Arz, H.W.** (2015). Black Sea temperature response to glacial millennial-scale climate variability, *Geophysical Research Letters*, *42*(19), 8147–8154.

[121] **Yılmaz, Y.**, **Güner, Y. and Şaroğlu, F.** (1998). Geology of the quaternary volcanic centres of the east Anatolia, *Journal of Volcanology and Geothermal Research*, *85*(1), 173 – 210.

[122] **Türkeş, M.** (1996). Spatial and temporal analysis of annual rainfall variations in Turkey, *International Journal of Climatology*, *16*(9), 1057–1076.

[123] **Ünal, Y.**, **Kındap, T. and Karaca, M.** (2003). Redefining the climate zones of Turkey using cluster analysis, *International Journal of Climatology*, *23*(9), 1045–1055.

[124] **van Zeist, W. and Bottema, S.**, (1982). Vegetational History of the Eastern Mediterranean and the Near East During the Last 20.000 Years, J.L. Bintliff and W. van Zeist, editors, Palaeoclimates, Palaeoenvironments and Human Communities in the Eastern Mediterranean Region in Later Prehistory, B.A.R. International Series, Oxford, pp.277–371.

[125] **Göktürk, O.M.**, (2005). North Sea – Caspian Pattern and Its Influence on the Hydrometeorological Parameters over Turkey, Master's thesis, İstanbul Teknik Üniversitesi, Avrasya Yer Bilimleri Enstitüsü.

[126] **Türkeş, M. and Erlat, E.** (2003). Precipitation changes and variability in Turkey linked to the North Atlantic oscillation during the period 1930–2000, *International Journal of Climatology*, *23*(14), 1771–1796.

[127] **Bozkurt, D. and Şen, Ö.L.** (2011). Precipitation in the Anatolian Peninsula: sensitivity to increased SSTs in the surrounding seas, *Climate Dynamics*, *36*(3), 711–726.

[128] **Göktürk, O.M.**, **Fleitmann, D.**, **Badertscher, S.**, **Cheng, H.**, **Edwards, R.L.**, **Leuenberger, M.**, **... Kramers, J.** (2011). Climate on the southern Black Sea coast during the Holocene: implications from the Sofular Cave record, *Quaternary Science Reviews*, *30*(19), 2433 – 2445.

[129] **Reimer, A.**, **Landmann, G. and Kempe, S.** (2009). Lake Van, Eastern Anatolia, Hydrochemistry and History, *Aquatic Geochemistry*, *15*(1), 195–222.

[130] **Lemcke, G. and Sturm, M.** (1997). δ^{18}O and Trace Element Measurements as Proxy for the Reconstruction of Climate Changes at Lake Van (Turkey): Preliminary Results, H.N. Dalfes, G. Kukla and H. Weiss, editors, Third

Millennium BC Climate Change and Old World Collapse, Springer Berlin Heidelberg, Berlin, Heidelberg, pp.653–678.

[131] **Stockhecke, M.**, **Anselmetti, F.S.**, **Meydan, A.F.**, **Odermatt, D. and Sturm, M.** (2012). The annual particle cycle in Lake Van (Turkey), *Palaeogeography, Palaeoclimatology, Palaeoecology*, *333*, 148 – 159.

[132] **Landmann, G.**, **Reimer, A.**, **Lemcke, G. and Kempe, S.** (1996). Dating Late Glacial abrupt climate changes in the 14,570 yr long continuous varve record of Lake Van, Turkey, *Palaeogeography, Palaeoclimatology, Palaeoecology*, *122*(1), 107 – 118.

[133] **Steffensen, J.P.**, **Andersen, K.K.**, **Bigler, M.**, **Clausen, H.B.**, **Dahl-Jensen, D.**, **Fischer, H.**, **... White, J.W.C.** (2008). High-Resolution Greenland Ice Core Data Show Abrupt Climate Change Happens in Few Years, *Science*, *321*(5889), 680–684.

[134] **Svensson, A.**, **Andersen, K.K.**, **Bigler, M.**, **Clausen, H.B.**, **Dahl-Jensen, D.**, **Davies, S.M.**, **... Vinther, B.M.** (2008). A 60,000 year Greenland stratigraphic ice core chronology, *Climate of the Past*, *4*(1), 47–57.

[135] **Wolff, E.W.**, **Chappellaz, J.**, **Blunier, T.**, **Rasmussen, S.O. and Svensson, A.** (2010). Millennial-scale variability during the last glacial: The ice core record, *Quaternary Science Reviews*, *29*(21), 2828 – 2838.

[136] **Barker, S.**, **Knorr, G.**, **Edwards, R.L.**, **Parrenin, F.**, **Putnam, A.E.**, **Skinner, L.C.**, **... Ziegler, M.** (2011). 800,000 Years of Abrupt Climate Variability, *Science*, *334*(6054), 347–351.

[137] **Veres, D.**, **Bazin, L.**, **Landais, A.**, **Toyé Mahamadou Kele, H.**, **Lemieux-Dudon, B.**, **Parrenin, F.**, **... Wolff, E.W.** (2013). The Antarctic ice core chronology (AICC2012): an optimized multi-parameter and multi-site dating approach for the last 120 thousand years, *Climate of the Past*, *9*(4), 1733–1748.

[138] **Stockhecke, M.**, **Kwiecien, O.**, **Vigliotti, L.**, **Anselmetti, F.S.**, **Beer, J.**, **Çağatay, M.N.**, **... Sturm, M.** (2014). Chronostratigraphy of the 600,000 year old continental record of Lake Van (Turkey), *Quaternary Science Reviews*, *104*, 8 – 17.

[139] **Brys, G.**, **Hubert, M. and Rousseeuw, P.J.** (2005). A robustification of independent component analysis, *Journal of Chemometrics*, *19*(5-7), 364–375.

[140] **Hubert, M. and Van der Veeken, S.** (2008). Outlier detection for skewed data, *Journal of Chemometrics*, *22*(3-4), 235–246.

[141] **Verboven, S. and Hubert, M.** (2010). MATLAB library LIBRA, *Wiley Interdisciplinary Reviews: Computational Statistics*, *2*(4), 509–515.

[142] **Himberg, J.**, **Hyvärinen, A. and Esposito, F.** (2004). Validating the independent components of neuroimaging time series via clustering and visualization, *NeuroImage*, *22*(3), 1214 – 1222.

[143] **Demartines, P. and Herault, J.** (1997). Curvilinear component analysis: a self–organizing neural network for nonlinear mapping of data sets, *IEEE Transactions on Neural Networks*, *8*(1), 148–154.

[144] **Reshef, D.N.**, **Reshef, Y.A.**, **Finucane, H.K.**, **Grossman, S.R.**, **McVean, G.**, **Turnbaugh, P.J.**, **... Sabeti, P.C.** (2011). Detecting Novel Associations in Large Data Sets, *Science*, *334*(6062), 1518–1524.

[145] **Cover, T.M. and Thomas, J.A.** (2006). *Elements of Information Theory*, A Wiley-Interscience publication, Wiley, New Jersey, 2nd edition.

[146] **Joe, H.** (1989). Relative Entropy Measures of Multivariate Dependence, *Journal of the American Statistical Association*, *84*(405), 157–164.

[147] **Martrat, B.**, **Grimalt, J.O.**, **Lopez-Martinez, C.**, **Cacho, I.**, **Sierro, F.J.**, **Flores, J.A.**, **... Hodell, D.A.** (2004). Abrupt Temperature Changes in the Western Mediterranean over the Past 250,000 Years, *Science*, *306*(5702), 1762–1765.

[148] **Brook, E.**, (2013). Antarctic Stable Isotopes, S.A. Elias and C.J. Mock, editors, Encyclopedia of Quaternary Science, Elsevier, Amsterdam, 2nd edition, pp.395 – 402.

[149] **Vinther, B. and Johnsen, S.**, (2013). Greenland Stable Isotopes, S.A. Elias and C.J. Mock, editors, Encyclopedia of Quaternary Science, Elsevier, Amsterdam, 2nd edition, pp.403 – 409.

[150] **Torfstein, A.**, **Goldstein, S.L.**, **Kushnir, Y.**, **Enzel, Y.**, **Haug, G. and Stein, M.** (2015). Dead Sea drawdown and monsoonal impacts in the Levant during the last interglacial, *Earth and Planetary Science Letters*, *412*(Supplement C), 235 – 244.

[151] **Lisiecki, L.E. and Raymo, M.E.** (2005). A Pliocene-Pleistocene stack of 57 globally distributed benthic δ^{18}O records, *Paleoceanography*, *20*(1).

[152] **Shumilovskikh, L.S.**, **Fleitmann, D.**, **Nowaczyk, N.R.**, **Behling, H.**, **Marret, F.**, **Wegwerth, A. and Arz, H.W.** (2014). Orbital- and millennial-scale environmental changes between 64 and 20 ka BP recorded in Black Sea sediments, *Climate of the Past*, *10*(3), 939–954.

[153] **Menviel, L.**, **Timmermann, A.**, **Friedrich, T. and England, M.H.** (2014). Hindcasting the continuum of Dansgaard-Oeschger variability: Mechanisms, patterns and timing, *Climate of the Past*, *10*(1), 63–77.

[154] **Kempe, S. and Degens, E.T.**, (1978). Lake Van varve record: the past 10,420 years, E.T. Degens and F. Kurtman, editors, The Geology of Lake Van, MTA Press, Ankara, pp.56 – 63.

[155] **Zolitschka, B.**, **Francus, P.**, **Ojala, A.E.K. and Schimmelmann, A.** (2015). Varves in lake sediments – a review, *Quaternary Science Reviews*, *117*, 1 – 41.

[156] **Putnam, A.E. and Broecker, W.S.** (2017). Human-induced changes in the distribution of rainfall, *Science Advances*, *3*(5).

[157] **Timmermann, A.**, **Friedrich, T.**, **Timm, O.E.**, **Chikamoto, M.O.**, **Abe-Ouchi, A. and Ganopolski, A.** (2014). Modeling Obliquity and CO_2 Effects on Southern Hemisphere Climate during the Past 408 ka, *Journal of Climate*, *27*(5), 1863–1875.

[158] **Kuzucuoğlu, C.**, **Bertaux, J.**, **Black, S.**, **Denefle, M.**, **Fontugne, M.**, **Karabıyıkoğlu, M.**, **... Orth, P.** (1999). Reconstruction of climatic changes during the Late Pleistocene, based on sediment records from the Konya Basin (Central Anatolia, Turkey), *Geological Journal*, *34*(1-2), 175–198.

[159] **Torfstein, A.**, **Goldstein, S.L.**, **Stein, M. and Enzel, Y.** (2013). Impacts of abrupt climate changes in the Levant from Last Glacial Dead Sea levels, *Quaternary Science Reviews*, *69*(Supplement C), 1 – 7.

[160] **Prentice, I.C.**, **Guiot, J. and Harrison, S.P.** (1992). Mediterranean vegetation, lake levels and palaeoclimate at the Last Glacial Maximum, *Nature*, *360*(6405), 658–660.

[161] **Harrison, S.P. and Digerfeldt, G.** (1993). European lakes as palaeohydrological and palaeoclimatic indicators, *Quaternary Science Reviews*, *12*(4), 233 – 248.

[162] **Tzedakis, P.C.** (2007). Seven ambiguities in the Mediterranean palaeoenvironmental narrative, *Quaternary Science Reviews*, *26*(17–18), 2042 – 2066.

[163] **Pickarski, N.**, **Kwiecien, O.**, **Langgut, D. and Litt, T.** (2015). Abrupt climate and vegetation variability of eastern Anatolia during the last glacial, *Climate of the Past*, *11*(11), 1491–1505.

[164] **Rasmussen, S.O.**, **Bigler, M.**, **Blockley, S.P.**, **Blunier, T.**, **Buchardt, S.L.**, **Clausen, H.B.**, **... Winstrup, M.** (2014). A stratigraphic framework for abrupt climatic changes during the Last Glacial period based on three synchronized Greenland ice-core records: refining and extending the INTIMATE event stratigraphy, *Quaternary Science Reviews*, *106*, 14 – 28.

[165] **Mayewski, P.A.**, **Rohling, E.E.**, **Stager, J.C.**, **Karlén, W.**, **Maasch, K.A.**, **Meeker, L.D.**, **... Steig, E.J.** (2004). Holocene climate variability, *Quaternary Research*, *62*(3), 243 – 255.

[166] **Wanner, H.**, **Beer, J.**, **Bütikofer, J.**, **Crowley, T.J.**, **Cubasch, U.**, **Flückiger, J.**, **... Widmann, M.** (2008). Mid- to Late Holocene climate change: an overview, *Quaternary Science Reviews*, *27*(19), 1791 – 1828.

[167] **Weiss, H.**, (2017). Seventeen Kings Who Lived in Tents, F. Höflmayer, editor, The late third millennium in the Ancient Near East: Chronology, C14, and climate change, University of Chicago, USA, pp.131 – 162.

[168] **Railsback, L.B.**, **Liang, F.**, **Brook, G.**, **Voarintsoa, N.R.G.**, **Sletten, H.R.**, **Marais, E.**, **... Edwards, R.L.** (2018). The timing, two-pulsed nature, and variable climatic expression of the 4.2 ka event: A review and new high-resolution stalagmite data from Namibia, *Quaternary Science Reviews*, *186*, 78 – 90.

[169] **Voosen, P.** (2018). New geological age comes under fire, *Science*, *361*(6402), 537–538.

[170] **Walker, M.J.C.**, **Berkelhammer, M.**, **Björck, S.**, **Cwynar, L.C.**, **Fisher, D.A.**, **Long, A.J.**, **... Weiss, H.** (2012). Formal subdivision of the Holocene Series/Epoch: a Discussion Paper by a Working Group of INTIMATE (Integration of ice-core, marine and terrestrial records) and the Subcommission on Quaternary Stratigraphy (International Commission on Stratigraphy), *Journal of Quaternary Science*, *27*(7), 649–659.

[171] **Weiss, H.**, (2015). Megadrought, collapse, and resilience in late 3rd millennium BC Mesopotamia, H. Meller, H.W. Arz, R. Jung and R. Risch, editors, 2200 BC: a climatic breakdown as a cause for the collapse of the old world? : 7th Archaeological Conference of Central Germany, October 23-26, 2014 in Halle (Saale), Landesamt für Denkmalpflege und Archäologie Sachsen-Anhalt, Landesmuseum für Vorgeschichte, pp.35 – 52.

[172] **Kaniewski, D.**, **Van Campo, E.**, **Morhange, C.**, **Guiot, J.**, **Zviely, D.**, **Shaked, I.**, **... Artzy, M.** (2013). Early urban impact on Mediterranean coastal environments, *Scientific reports*, *3*, 3540.

[173] **Litt, T.**, **Ohlwein, C.**, **Neumann, F.H.**, **Hense, A. and Stein, M.** (2012). Holocene climate variability in the Levant from the Dead Sea pollen record, *Quaternary Science Reviews*, *49*, 95 – 105.

[174] **Li, J.**, **Zhao, Y.**, **Xu, Q.**, **Zheng, Z.**, **Lu, H.**, **Luo, Y.**, **... Seppä, H.** (2014). Human influence as a potential source of bias in pollen-based quantitative climate reconstructions, *Quaternary Science Reviews*, *99*, 112 – 121.

[175] **Bar-Matthews, M.**, **Ayalon, A.**, **Gilmour, M.**, **Matthews, A. and Hawkesworth, C.J.** (2003). Sea–land oxygen isotopic relationships from planktonic foraminifera and speleothems in the Eastern Mediterranean region and their implication for paleorainfall during interglacial intervals, *Geochimica et Cosmochimica Acta*, *67*(17), 3181 – 3199.

[176] **Arz, H.W.**, **Kaiser, J. and Fleitmann, D.**, (2015). Paleoceanographic and paleoclimatic changes around 2200 BC recorded in sediment cores from the northern Red Sea, H. Meller, H.W. Arz, R. Jung and R. Risch, editors, 2200 BC: A climatic breakdown as a cause for the collapse of the old world? 7th Archaeological Conference of Central Germany, October 23-26, 2014 in Halle (Saale), Landesamt für Denkmalpflege und Archäologie Sachsen-Anhalt, Landesmuseum für Vorgeschichte, pp.53 – 60.

[177] **Drysdale, R.**, **Zanchetta, G.**, **Hellstrom, J.**, **Maas, R.**, **Fallick, A.**, **Pickett, M.**, **... Piccini, L.** (2006). Late Holocene drought responsible for the collapse of

Old World civilizations is recorded in an Italian cave flowstone, *Geology*, *34*(2), 101.

[178] **Jones, S.**, **Fleitmann, D. and Black, S.** (2016). A critical evaluation of the 4.2 ka BP event using new high resolution evidence from stalagmites in the Middle East, *EGU General Assembly Conference Abstracts*, volume 18, pp.EPSC2016–582.

[179] **Scott, S.L. and Varian, H.R.** (2014). Predicting the present with Bayesian structural time series, *International Journal of Mathematical Modelling and Numerical Optimisation*, *5*(1-2), 4–23.

[180] **Amante, C. and Eakins, B.W.** (2009). ETOPO1 1 Arc-Minute Global Relief Model: Procedures, Data Sources and Analysis, **Technical Memorandum NESDIS NGDC-24**, NOAA.

[181] **Cullen, H.M.**, **deMenocal, P.B.**, **Hemming, S.**, **Hemming, G.**, **Brown, F.H.**, **Guilderson, T. and Sirocko, F.** (2000). Climate change and the collapse of the Akkadian empire: Evidence from the deep sea, *Geology*, *28*(4), 379.

[182] **Arz, H.W.**, **Lamy, F. and Pätzold, J.** (2006). A pronounced dry event recorded around 4.2 ka in brine sediments from the northern Red Sea, *Quaternary Research*, *66*(3), 432 – 441.

[183] **Kuhnt, T.**, **Schmiedl, G.**, **Ehrmann, W.**, **Hamann, Y. and Andersen, N.** (2008). Stable isotopic composition of Holocene benthic foraminifers from the Eastern Mediterranean Sea: Past changes in productivity and deep water oxygenation, *Palaeogeography, Palaeoclimatology, Palaeoecology*, *268*(1), 106 – 115.

[184] **Francke, A.**, **Wagner, B.**, **Leng, M.J. and Rethemeyer, J.** (2013). A Late Glacial to Holocene record of environmental change from Lake Dojran (Macedonia, Greece), *Climate of the Past*, *9*(1), 481–498.

[185] **Wagner, B.**, **Lotter, A.F.**, **Nowaczyk, N.**, **Reed, J.M.**, **Schwalb, A.**, **Sulpizio, R.**, **... Zanchetta, G.** (2009). A 40,000-year record of environmental change from ancient Lake Ohrid (Albania and Macedonia), *Journal of Paleolimnology*, *41*(3), 407–430.

[186] **Sharifi, A.**, **Pourmand, A.**, **Canuel, E.A.**, **Ferer-Tyler, E.**, **Peterson, L.C.**, **Aichner, B.**, **... Swart, P.K.** (2015). Abrupt climate variability since the last deglaciation based on a high-resolution, multi-proxy peat record from NW Iran: The hand that rocked the Cradle of Civilization?, *Quaternary Science Reviews*, *123*, 215 – 230.

[187] **Cheng, H.**, **Sinha, A.**, **Verheyden, S.**, **Nader, F.H.**, **Li, X.L.**, **Zhang, P.Z.**, **... Edwards, R.L.** (2015). The climate variability in northern Levant over the past 20,000 years, *Geophysical Research Letters*, *42*(20), 8641–8650.

[188] **Göktürk, O.M.** (2011). Climate in the Eastern Mediterranean through the Holocene inferred from Turkish stalagmites, Phd thesis, University of Bern.

[189] **Ehrmann, W.**, **Schmiedl, G.**, **Hamann, Y.**, **Kuhnt, T.**, **Hemleben, C. and Siebel, W.** (2007). Clay minerals in late glacial and Holocene sediments of the northern and southern Aegean Sea, *Palaeogeography, Palaeoclimatology, Palaeoecology*, *249*(1), 36 – 57.

[190] **Altabet, M.A.**, **Higginson, M.J. and Murray, D.W.** (2002). The effect of millennial-scale changes in Arabian Sea denitrification on atmospheric CO_2, *Nature*, *415*, 159.

[191] **Fleitmann, D.**, **Burns, S.J.**, **Mangini, A.**, **Mudelsee, M.**, **Kramers, J.**, **Villa, I.**, **... Matter, A.** (2007). Holocene ITCZ and Indian monsoon dynamics recorded in stalagmites from Oman and Yemen (Socotra), *Quaternary Science Reviews*, *26*(1), 170 – 188.

[192] **Lamy, F.**, **Arz, H.W.**, **Bond, G.C.**, **Bahr, A. and Pätzold, J.** (2006). Multicentennial-scale hydrological changes in the Black Sea and northern Red Sea during the Holocene and the Arctic/North Atlantic Oscillation, *Paleoceanography*, *21*(1).

[193] **Wassenburg, J.A.**, **Dietrich, S.**, **Fietzke, J.**, **Fohlmeister, J.**, **Jochum, K.P.**, **Scholz, D.**, **... Immenhauser, A.** (2016). Reorganization of the North Atlantic Oscillation during early Holocene deglaciation, *Nature Geoscience*, *9*, 602.

[194] **Durbin, J. and Koopman, S.J.** (2012). *Time series analysis by state space methods*, volume 38 of *Oxford Statistical Science Series*, OUP Oxford, Oxford, 2nd edition.

[195] **Durbin, J. and Koopman, S.J.** (2002). A simple and efficient simulation smoother for state space time series analysis, *Biometrika*, *89*(3), 603–616.

[196] **George, E.I. and McCulloch, R.E.** (1997). Approaches for Bayesian variable selection, *Statistica Sinica*, *7*(2), 339–373.

[197] **Bai, J. and Perron, P.** (1998). Estimating and testing linear models with multiple structural changes, *Econometrica*, 47–78.

[198] **Bai, J. and Perron, P.** (2002). Computation and analysis of multiple structural change models, *Journal of Applied Econometrics*, *18*(1), 1–22.

[199] **Zeileis, A.**, **Kleiber, C.**, **Krämer, W. and Hornik, K.** (2003). Testing and dating of structural changes in practice, *Computational Statistics & Data Analysis*, *44*(1), 109 – 123.

[200] **Scott, S.L. and Varian, H.R.**, (2015). Bayesian variable selection for nowcasting economic time series, A. Goldfarb, S.M. Greenstein and C.E. Tucker, editors, Economic analysis of the digital economy, University of Chicago Press, pp.119–135.

[201] **Sweeney, J.**, **Salter-Townshend, M.**, **Edwards, T.**, **Buck, C.E. and Parnell, A.C.** (2018). Statistical challenges in estimating past climate changes, *Wiley Interdisciplinary Reviews: Computational Statistics*.

[202] **Zanchetta, G.**, **Regattieri, E.**, **Giaccio, B.**, **Wagner, B.**, **Sulpizio, R.**, **Francke, A.**, **... Leicher, N.** (2016). Aligning and synchronization of MIS5 proxy records from Lake Ohrid (FYROM) with independently dated Mediterranean archives: implications for DEEP core chronology, *Biogeosciences*, *13*(9), 2757–2768.

[203] **Cullen, H.M. and deMenocal, P.B.** (2000). North Atlantic influence on Tigris-–Euphrates streamflow, *International Journal of Climatology*, *20*(8), 853–863.

[204] **Ulbrich, U.**, **Lionello, P.**, **Belušić, D.**, **Jacobeit, J.**, **Knippertz, P.**, **Kuglitsch, F.G.**, **... Ziv, B.**, (2012). Climate of the Mediterranean: Synoptic Patterns, Temperature, Precipitation, Winds, and Their Extremes, P. Lionello, editor, The Climate of the Mediterranean Region, Elsevier, Oxford, pp.301 – 346.

[205] **Roberts, N.**, **Moreno, A.**, **Valero-Garcés, B.L.**, **Corella, J.P.**, **Jones, M.**, **Allcock, S.**, **... Türkeş, M.** (2012). Palaeolimnological evidence for an east-west climate see-saw in the Mediterranean since AD 900, *Global and Planetary Change*, *84-85*, 23 – 34.

[206] **Ferreira, D.**, **Marshall, J. and Rose, B.** (2011). Climate Determinism Revisited: Multiple Equilibria in a Complex Climate Model, *Journal of Climate*, *24*(4), 992–1012.

[207] **Berkelhammer, M.**, **Sinha, A.**, **Stott, L.**, **Cheng, H.**, **Pausata, F.S.R. and K., Y.**, (2013). An Abrupt Shift in the Indian Monsoon 4000 Years Ago, L. Giosan, D.Q. Fuller, K. Nicoll, R.K. Flad and P.D. Clift, editors, Climates, Landscapes, and Civilizations, American Geophysical Union, pp.75–88.

[208] **Hong, Y.T.**, **Hong, B.**, **Lin, Q.H.**, **Zhu, Y.X.**, **Shibata, Y.**, **Hirota, M.**, **... Yi, L.** (2003). Correlation between Indian Ocean summer monsoon and North Atlantic climate during the Holocene, *Earth and Planetary Science Letters*, *211*(3), 371 – 380.

[209] **Thompson, L.G.**, **Mosley-Thompson, E.**, **Davis, M.E.**, **Henderson, K.A.**, **Brecher, H.H.**, **Zagorodnov, V.S.**, **... Beer, J.** (2002). Kilimanjaro Ice Core Records: Evidence of Holocene Climate Change in Tropical Africa, *Science*, *298*(5593), 589–593.

APPENDICES

APPENDIX A : Supplementary figures for "Climate proxies for the last 17.3 ka from Lake Hazar (Eastern Anatolia), extracted by independent component analysis of μ-XRF data"

APPENDIX B : Supplementary figures for "Temperature and precipitation variability in Eastern Anatolia: Results from independent component analysis of Lake Van sediment data spanning the last 250 kyr BP"

APPENDIX C : Supplementary figures for "Bayesian test for the 4.2 ka BP abrupt climatic change event for the eastern Mediterranean and Arabian peninsula paleoclimate data using structural time series"

APPENDIX A

This supporting information provides supplementary figures for Chapter 2.

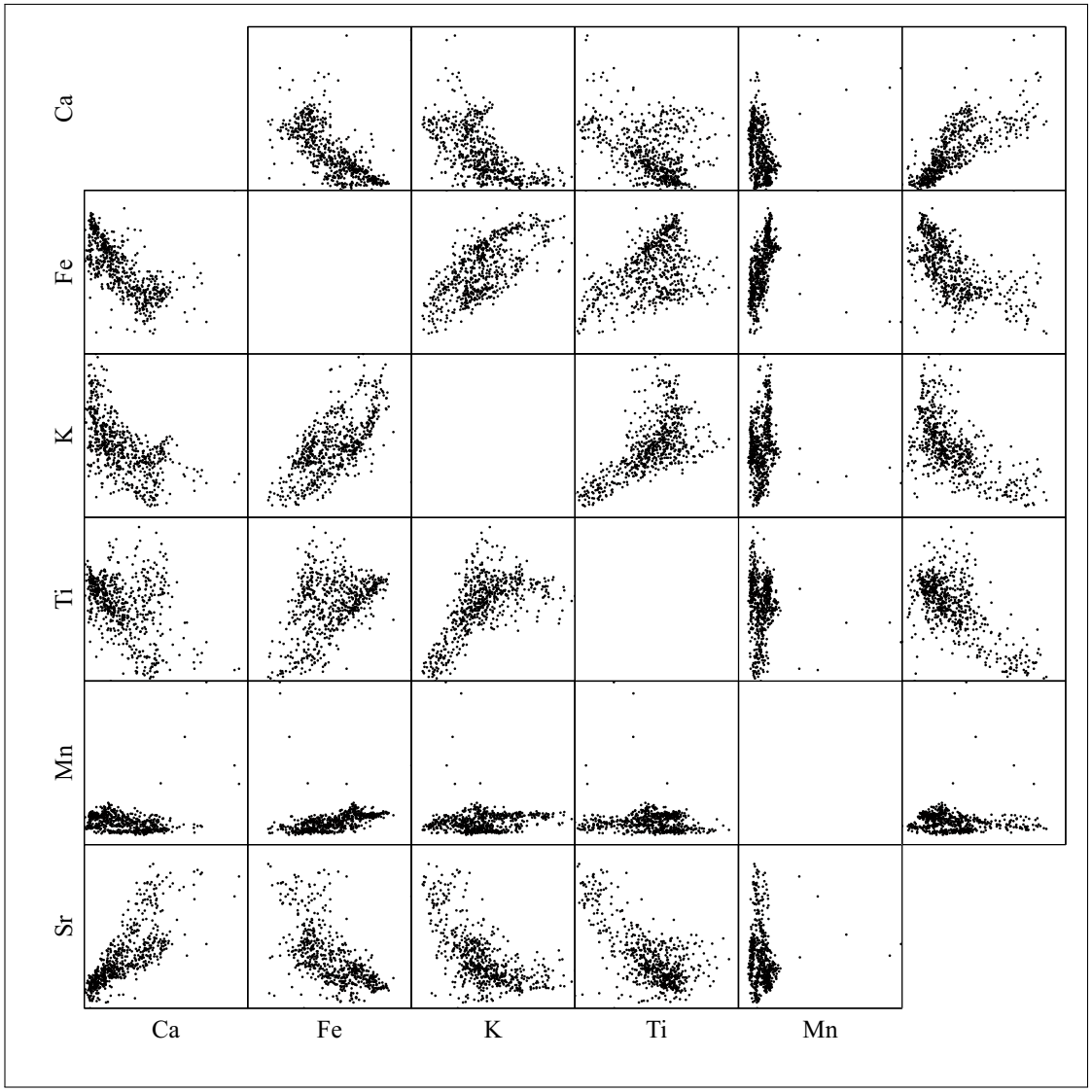

Figure A.1 : Scatter plots of the data used in this study.

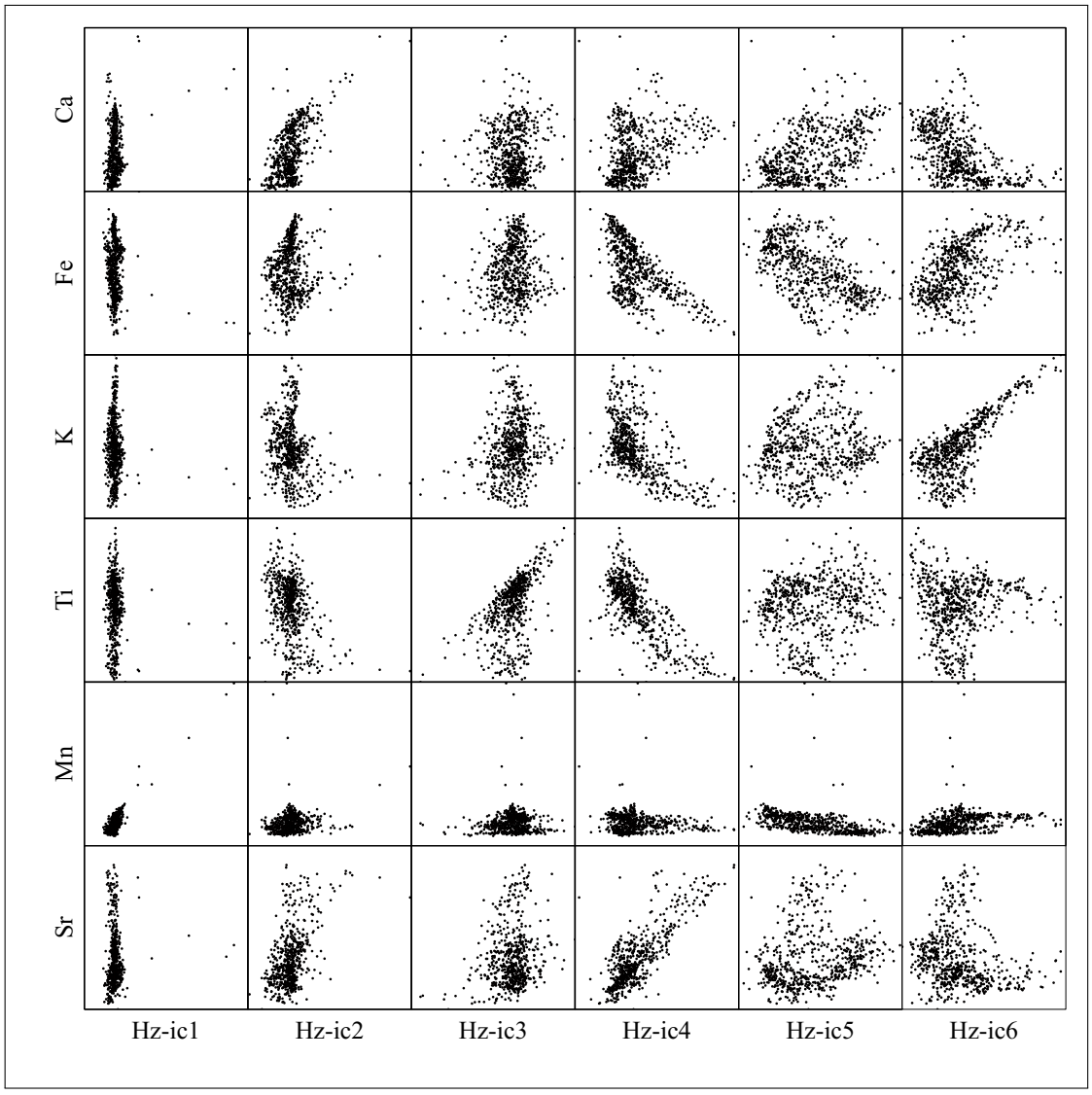

Figure A.2 : Scatter plots of independent components versus the data used in this study.

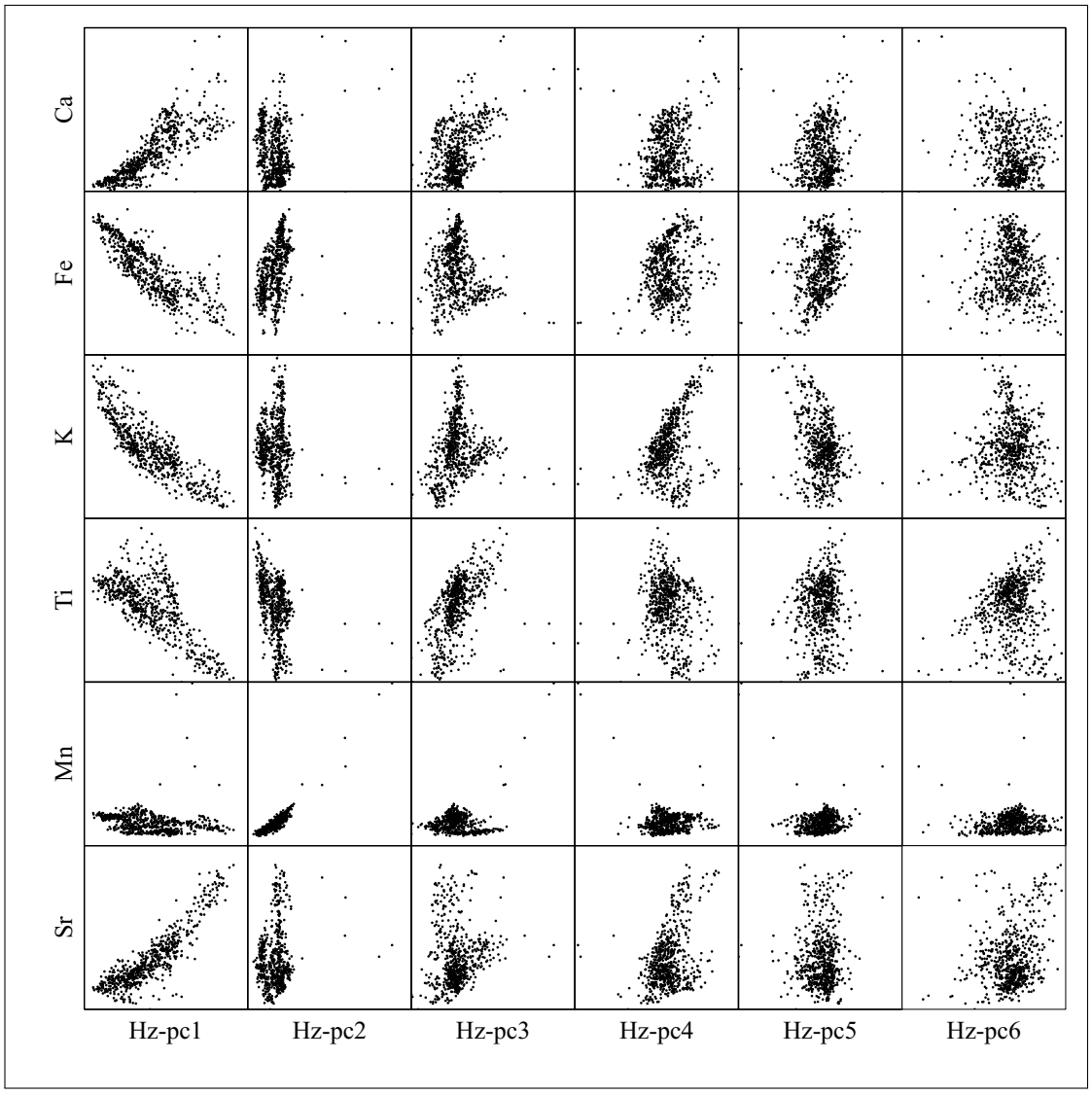

Figure A.3 : Scatter plots of principal components versus the data used in this study. PCA is applied on the same data used through FastICA in this study.

APPENDIX B

This supporting information provides the figures mentioned in Chapter 3, but not available in text.

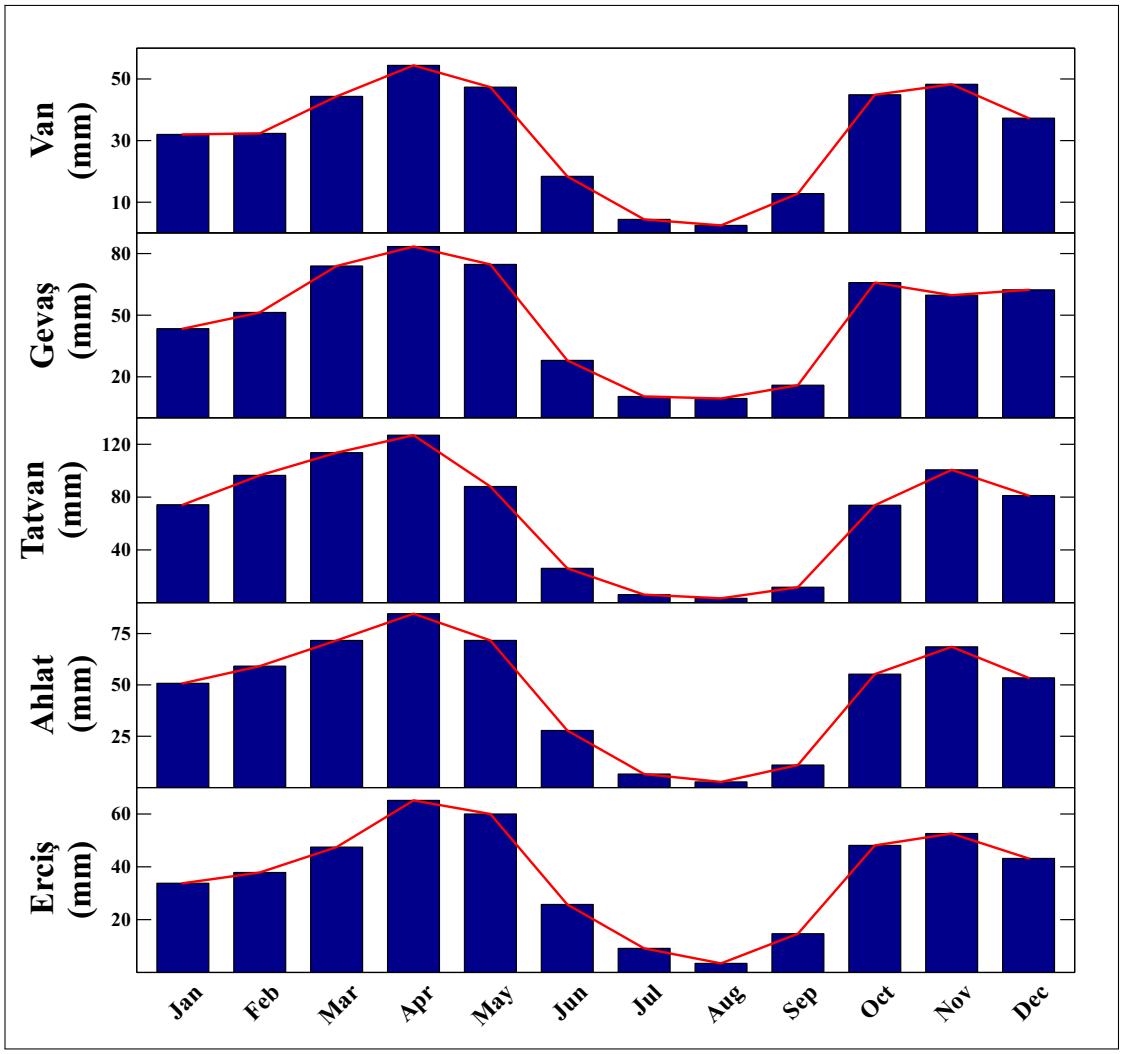

Figure B.1 : Monthly average precipitation through 1948-2004 for different stations around the lake. Years with missing monthly data are not taken into account. Meteorology station data has been collected and organized by [125].

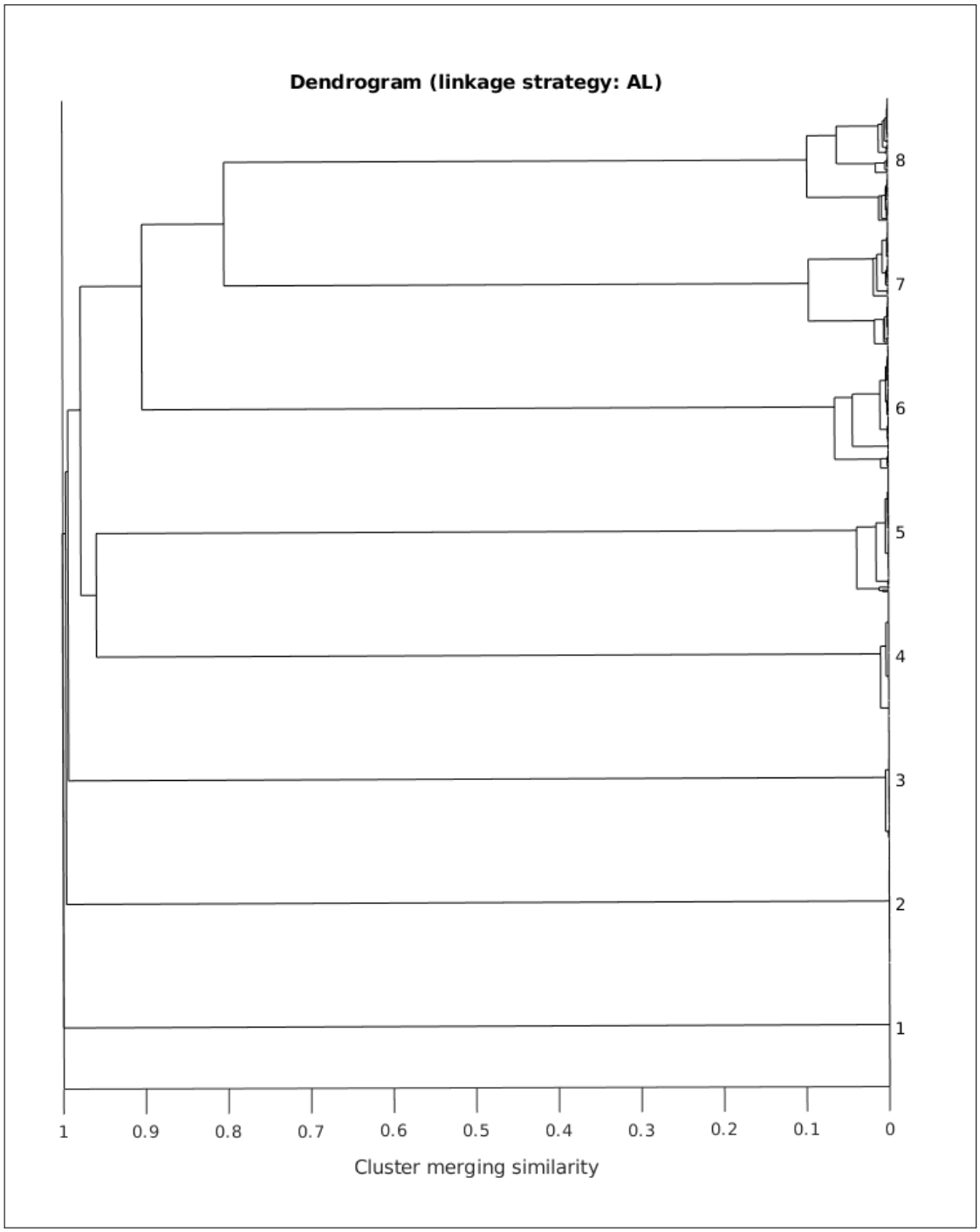

Figure B.2 : Dendrogram of the average-link agglomeration, x-axis represents the dissimilarity scale, which is equal to similarity values subtracted from one. Similarity measure is calculated by absolute value of the mutual correlation coefficient described in [142]. Dissimilarity oven 0.1 gives 8 different possible clusters.

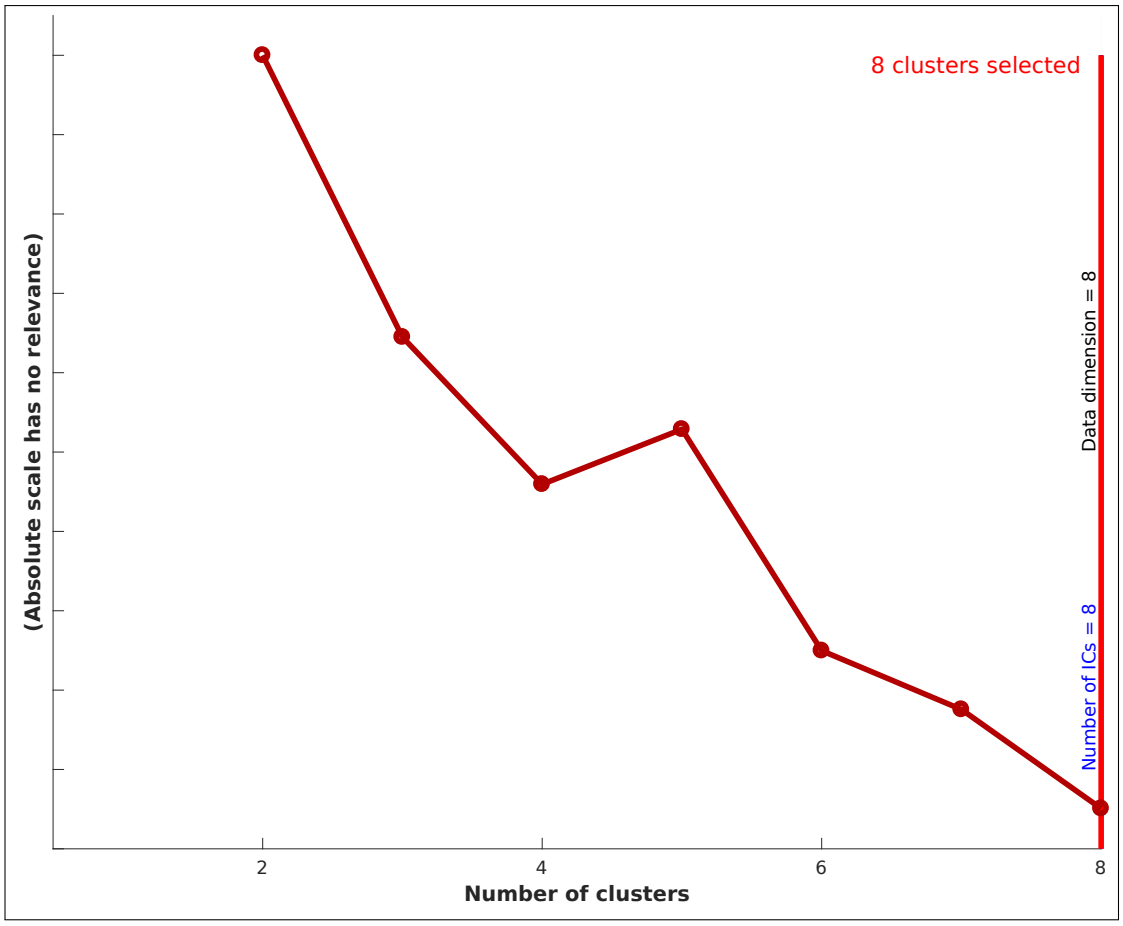

Figure B.3 : Possible clusters and R-index of the selected clusters via group average-link agglomeration (Eq.4 in [142]). According to this exploratory method, possible number of independent components is equal to the data dimension.

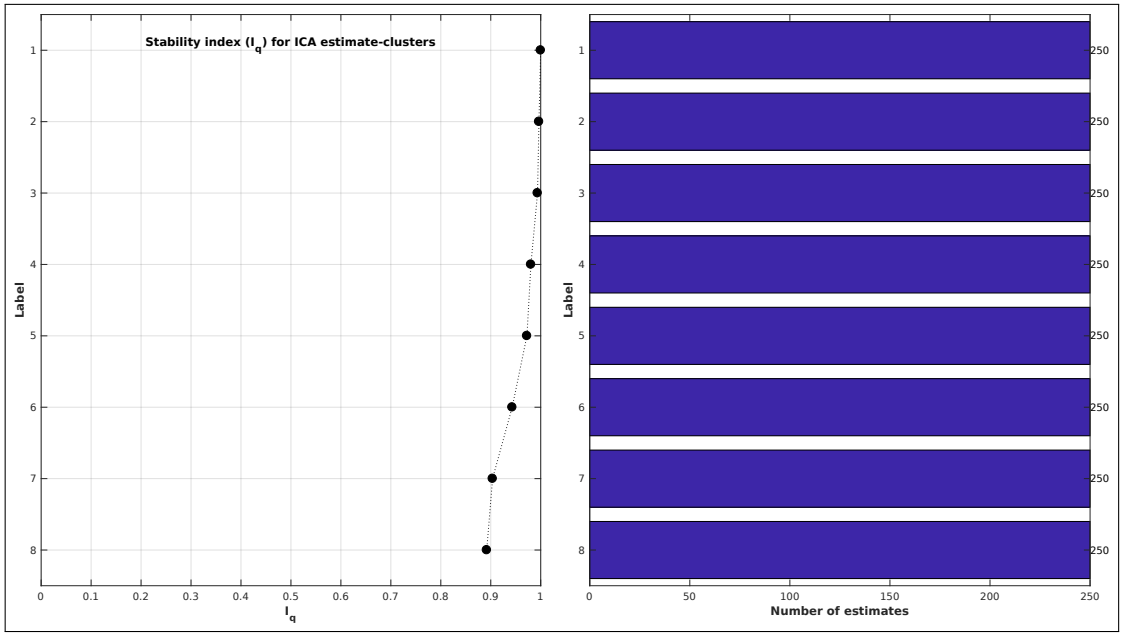

Figure B.4 : Cluster quality (stability) index, as given by Eq.3 in [142], which is another exploratory method for the number of independent components. Quality indices of all the components are satisfactory.

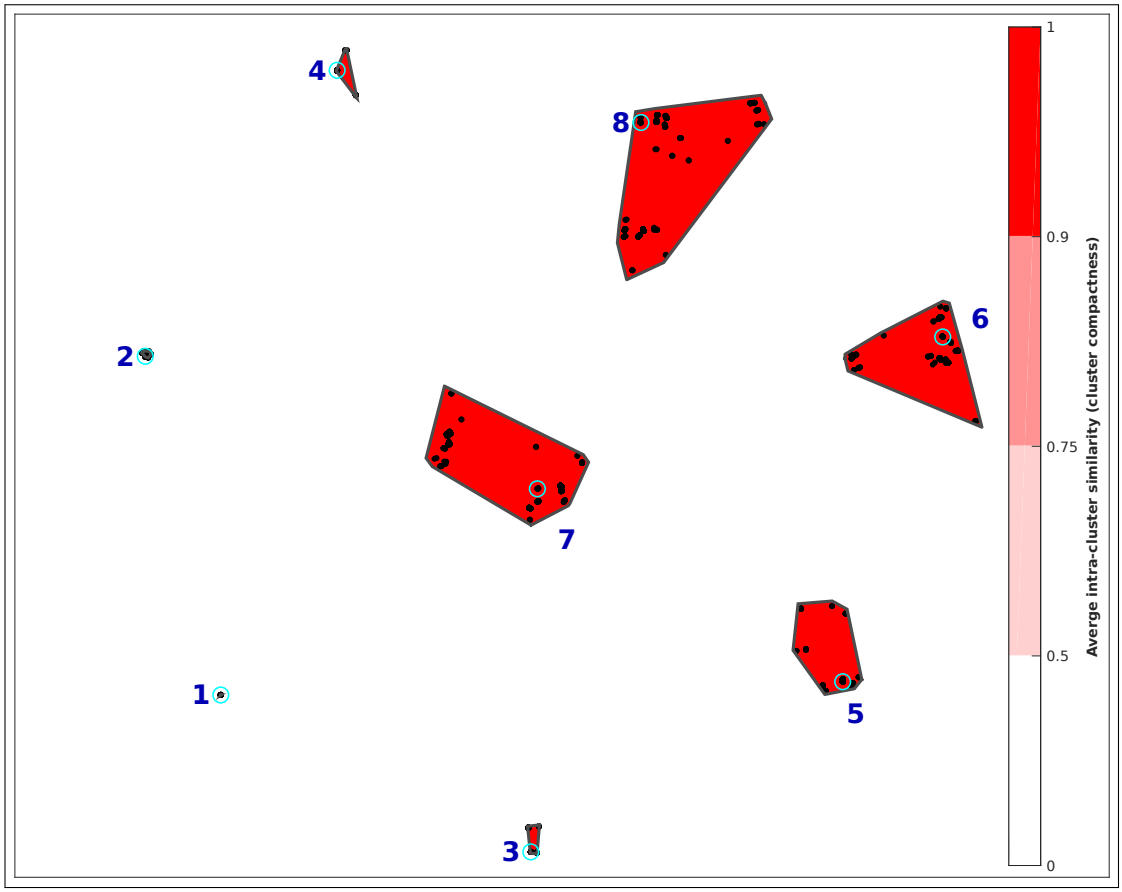

Figure B.5 : 2-dimensional projection of the clusters generated via curvilinear component analysis [143]. Black dots indicate different results of different runs of FastICA with different random inital points. Red convex hulls represent the each intra-cluster similarity (Eq.2 in [142]) above 0.90. Blue circles indicate the centrotypes of each cluster, which has the maximum sum of similarity to other points within the cluster.

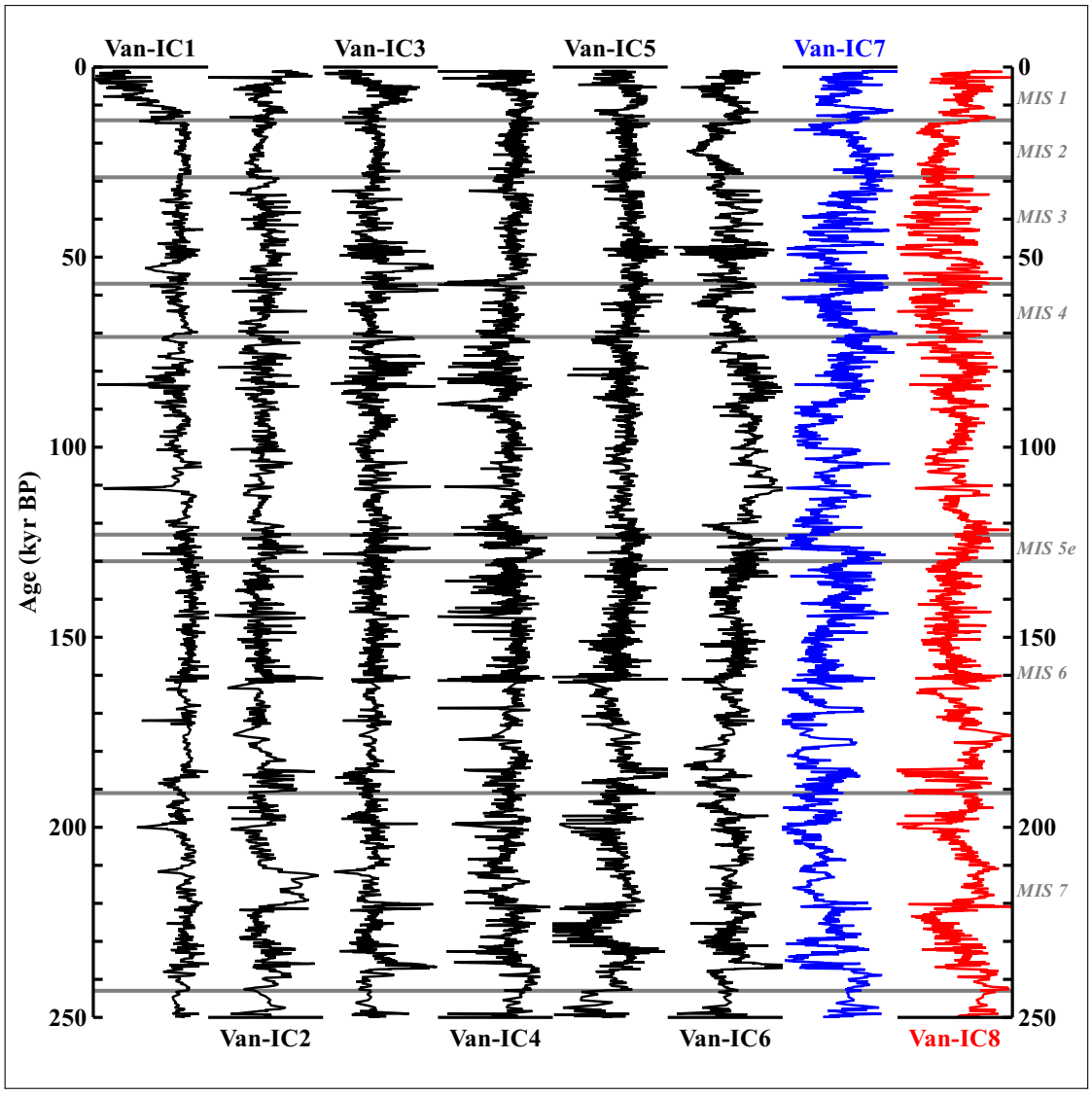

Figure B.6 : Independent components gathered via FastICA algorithm after running the procedure 250 times. Each independent component is the centrotype of each cluster, as explained under B.5. Van-IC7 and Van-IC8 are selected, as explained in the Section 2 of main text, and they represent proxies of precipitation and temperature of the region, respectively.

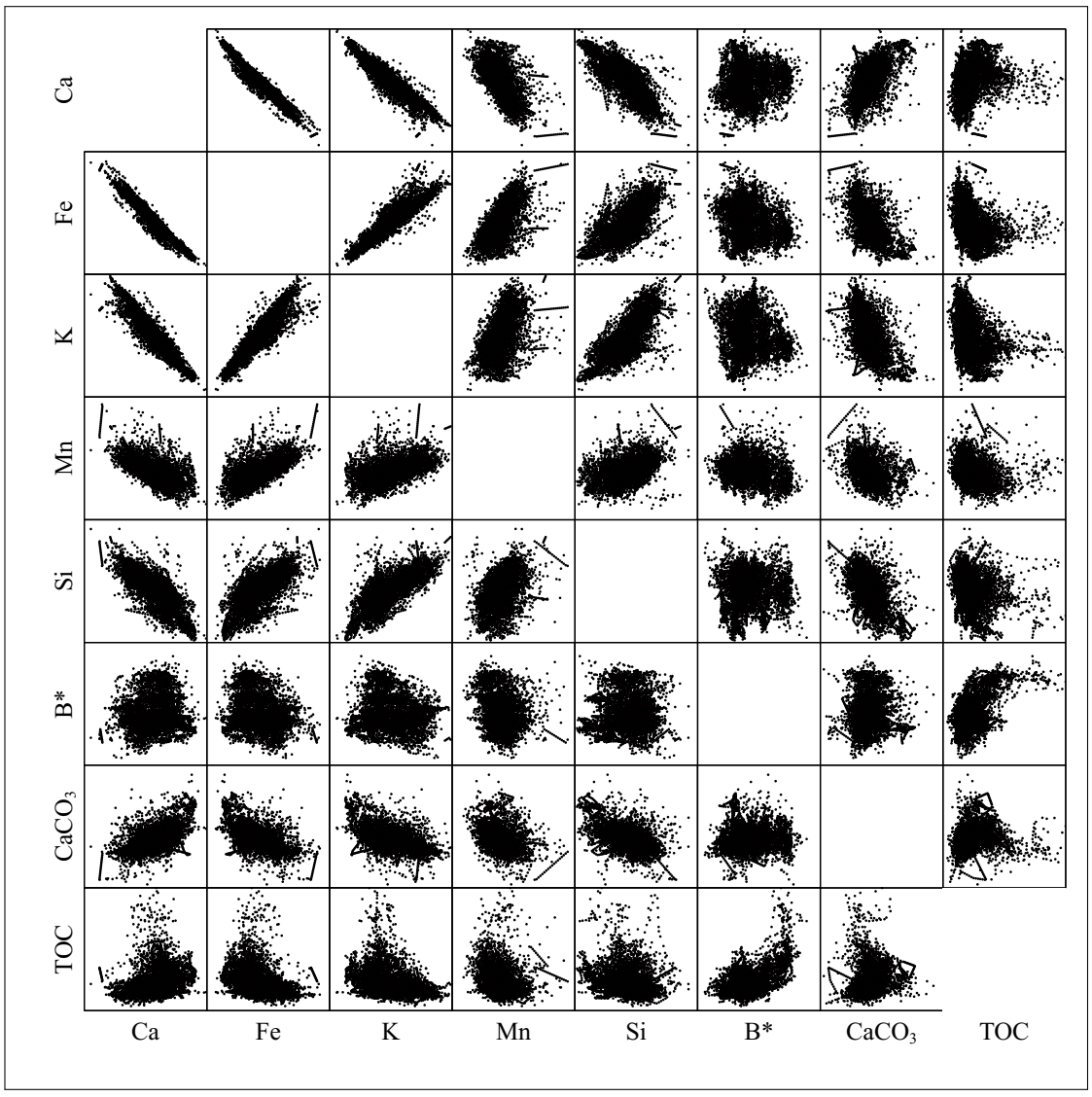

Figure B.7 : Scatter plots of the data used in this study.

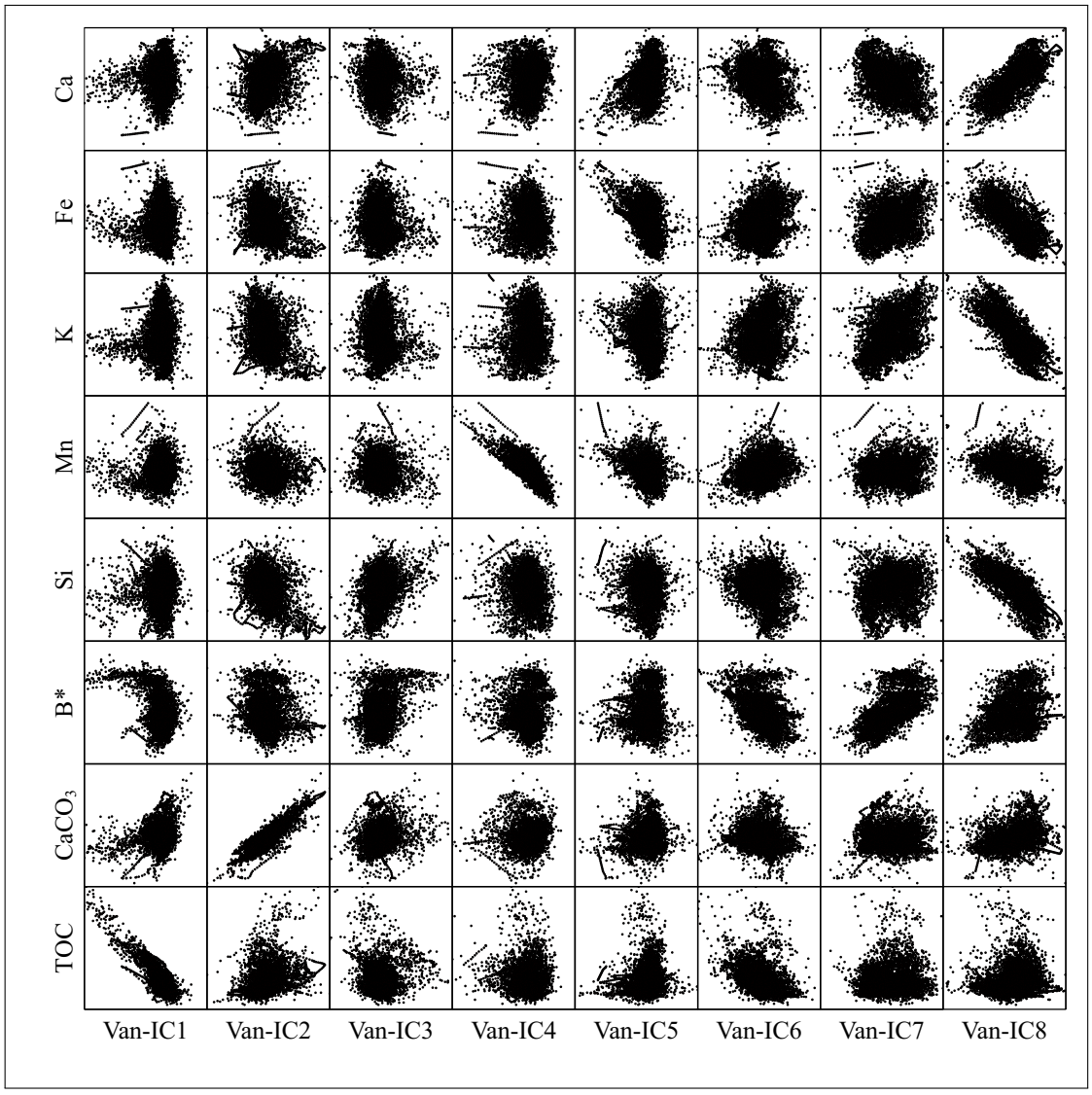

Figure B.8 : Scatter plots of independent components versus the data used in this study.

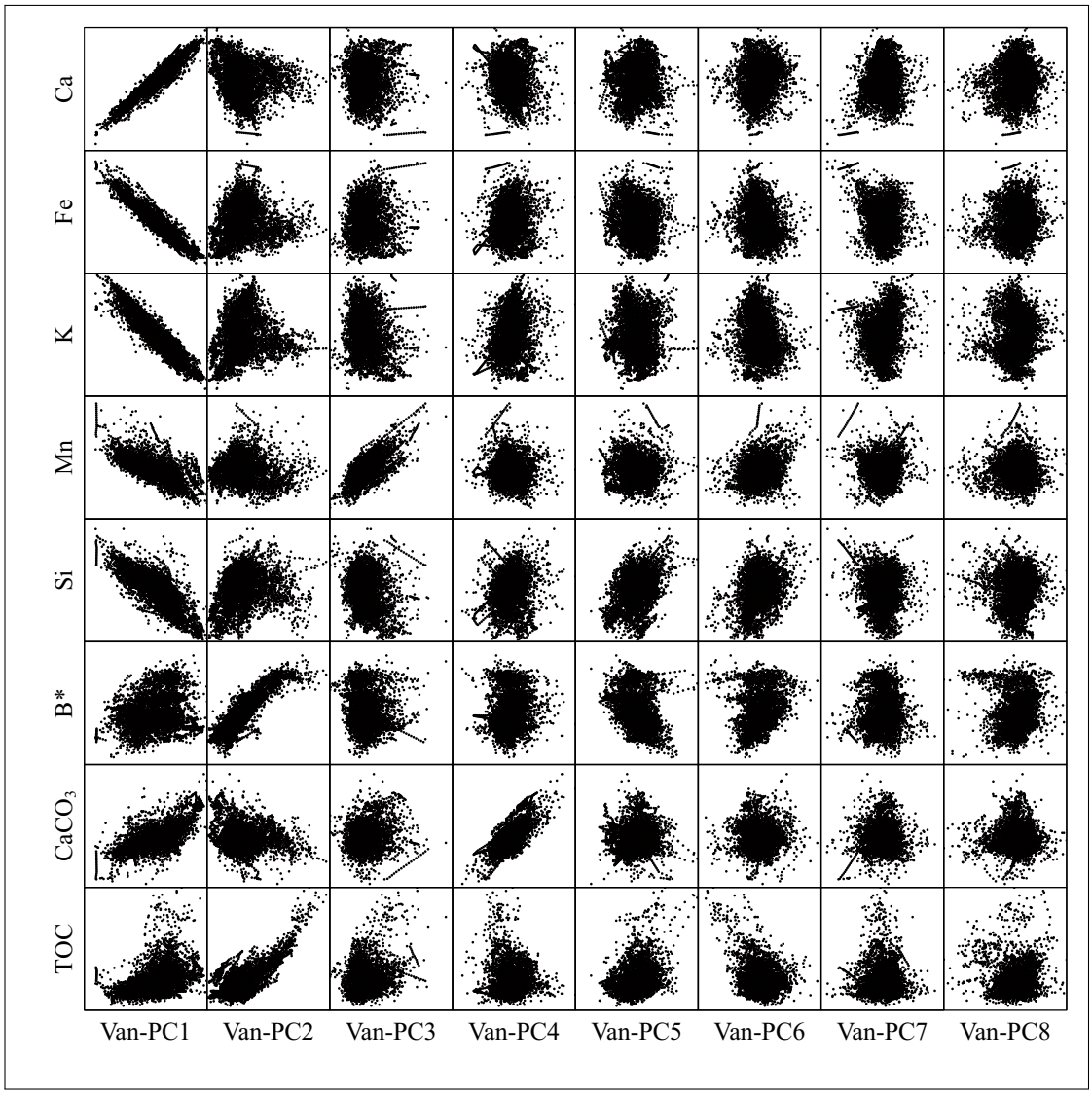

Figure B.9 : Scatter plots of principal components versus the data used in this study. PCA is applied on the same data used through FastICA in this study.

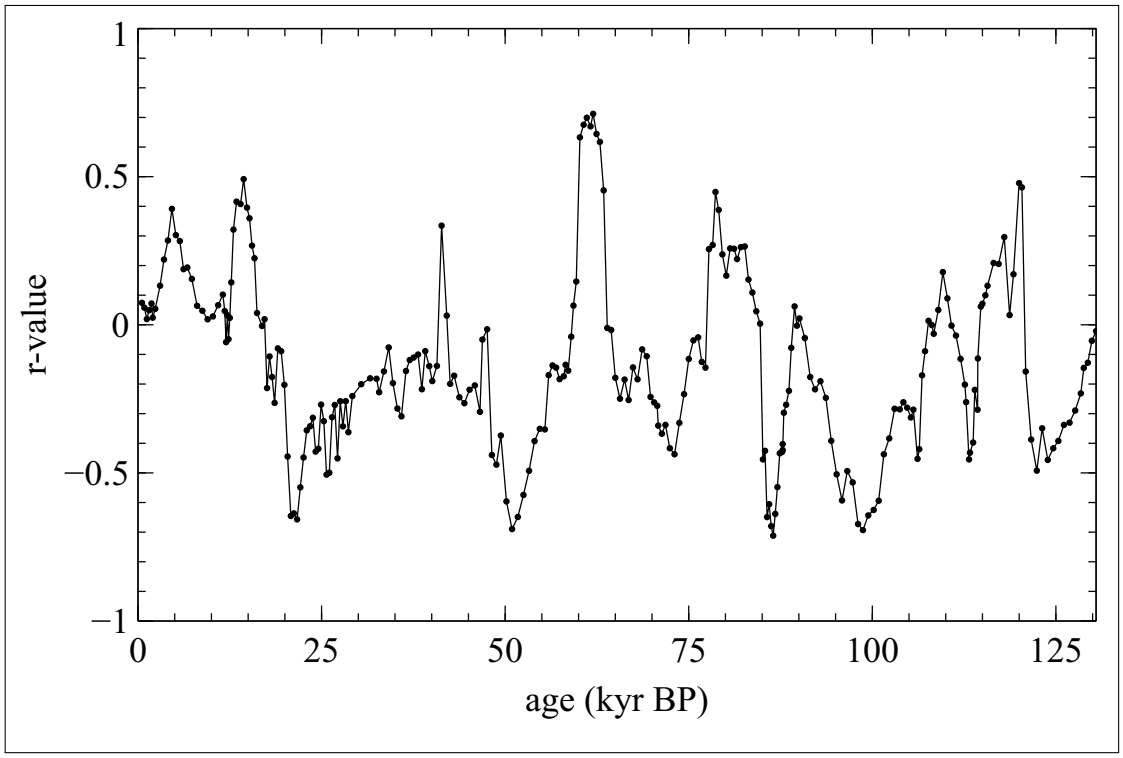

Figure B.10 : Moving 15 point Pearson r-coefficient of Van-IC7 and AR δ^{18}O data for the last 130 kyr BP. Savitzky-Golay filter with an 11 window length has been applied on Van-IC7 and then linearly interpolated to age model δ^{18}O data.

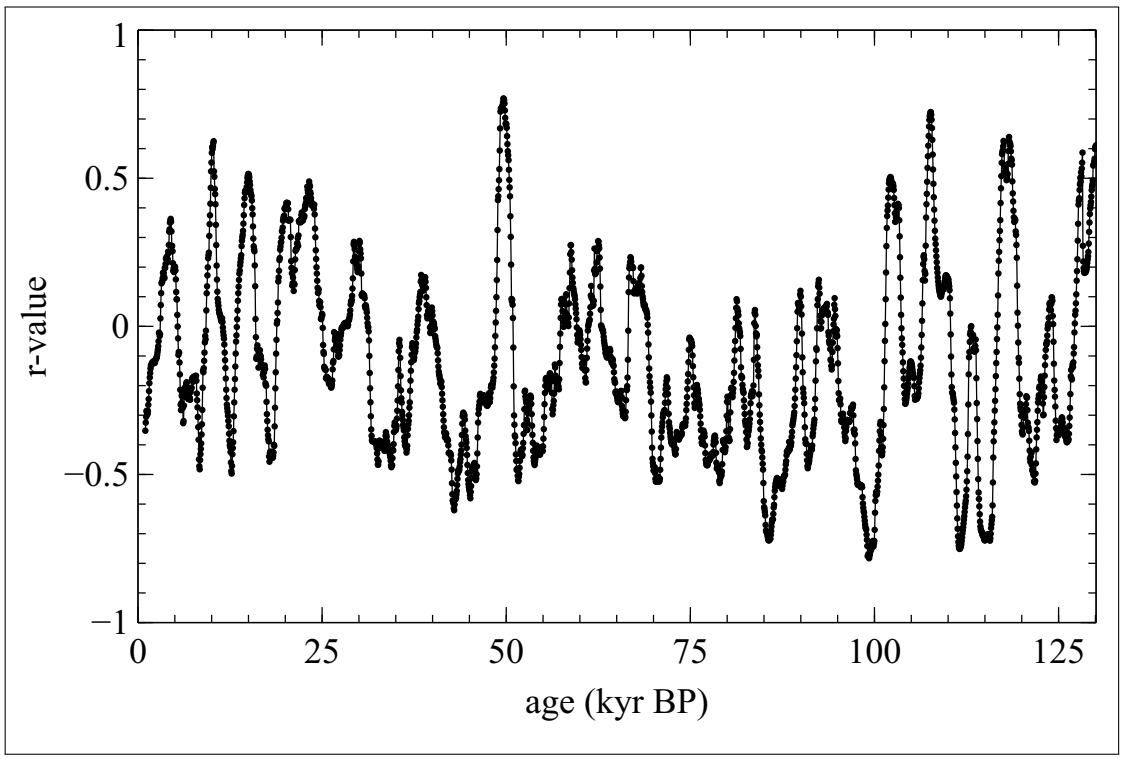

Figure B.11 : Moving 75 point Pearson r-coefficient of Van-IC8 and NGRIP δ^{18}O data for the last 130 kyr BP.

APPENDIX C

This supporting information provides the supplementary figure for Chapter 4.

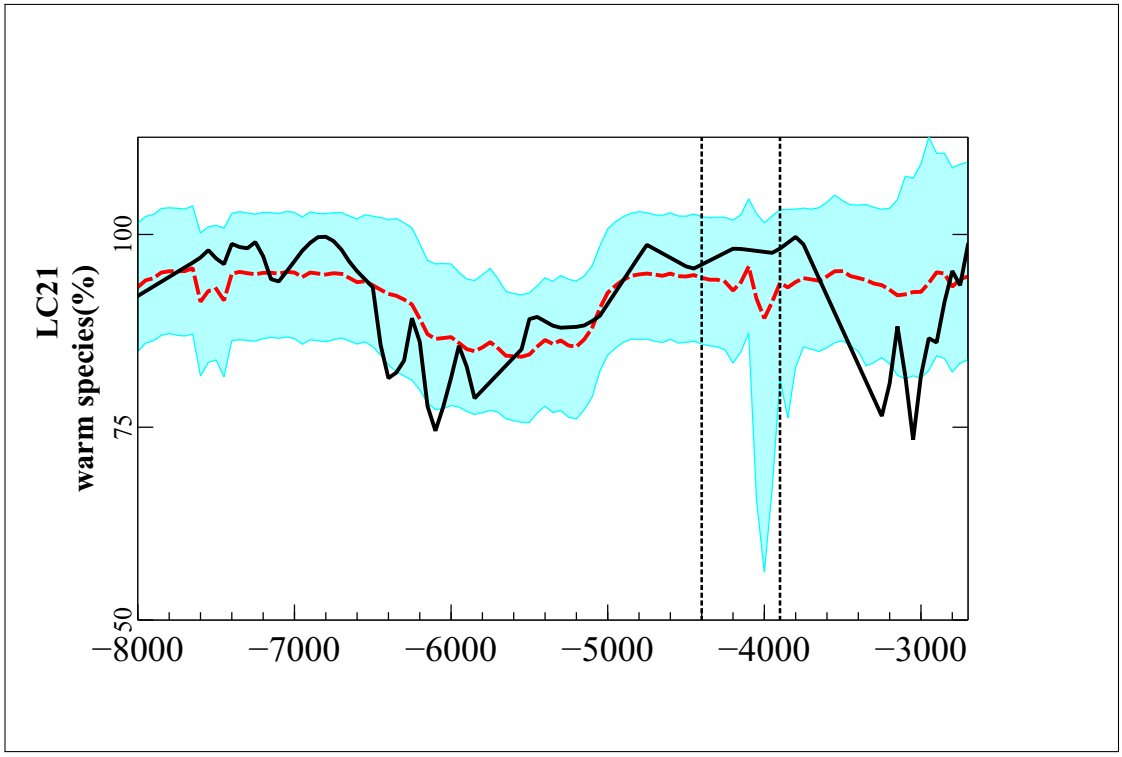

Figure C.1 : An example of causal impact used on randomly selected data from the control set and response variable from the main text. Data used for control set are: $\mathbf{4}, \mathbf{6}, \mathbf{9}, \boldsymbol{A}, \boldsymbol{a}, \boldsymbol{b}, \boldsymbol{e}, \alpha, \delta, \gamma$ as indicated in the maintext. Response variable is selected as **5** [84] and according to this contradictory trial data, while **5** is not showing a specific event at the period of interest, the analysis shows a statistically significant impact. This is a good example of the wrong usage of the methodology described in Chapter 4.

CURRICULUM VITAE

Name Surname: Zeki Bora ÖN

Place and Date of Birth: 1979 - İstanbul

E-Mail: boraon@mu.edu.tr

EDUCATION:

- **B.Sc.:** 2009, Boğaziçi University, Arts and Sciences Faculty, Mathematics Department
- **M.Sc.:** 2013, Muğla University, Graduate School of Natural and Applied Sciences, Geological Engineering Programme

PROFESSIONAL EXPERIENCE AND REWARDS:

- 2012-... Muğla University, Engineering Faculty, Research Assistant

PUBLICATIONS ON THE THESIS:

- **Ön, Z.B.**, Akçer-Ön, S., Özeren, M.S., Eriş, K.K., Greaves, A.M., Çağatay, M.N. 2017. Climate proxies for the last 17.3 ka from Lake Hazar (Eastern Anatolia), extracted by independent component analysis of μ-XRF data, *Quaternary International* 486, 17–28. doi:10.1016/j.quaint.2017.08.066

PRESENTATIONS ON THE THESIS:

- Ön, **Z.B.**, Akçer-Ön, S., Özeren, M.S., Eriş, K.K. 2016. Independent component analysis of μ-XRF time-series data: an example from Lake Hazar. *National Congress, TURQUA*, May 8-11, İstanbul, Turkey.
- **Ön, Z.B.**, Akçer-Ön, S., Özeren, M.S., Eriş, K.K., Greaves, A.M., Çağatay, M.N. 2016. Extracting the precipitation and temperature proxies from Lake Hazar (SE Anatolia) μ-XRF core data, by using independent component analysis. *International Congress, MedCLIVAR*, September 26-30, Athens, Greece.
- **Ön, Z.B.**, Akçer-Ön, S., Özeren, M.S., Eriş, K.K., Greaves, A.M., Çağatay, M.N. 2017. Revealing the precipitation and temperature records of Lake Hazar (Eastern Anatolia) from μXRF data, for the last 17.8 ka via Independent Component Analysis. *International Congress, International Open Workshop-Socio-Environmental Dynamics over the Last 12,000 Years: The Creation of Landscapes V*, March 20-24, Kiel, Germany.

- **Ön, Z.B.**, Özeren, M.S. 2018. Cold and wet glacial maximum periods in eastern Mediterranean: Independent component analysis results of 250 kyr long continuous Lake Van sediments. *National Congress, TURQUA*, May 2-5, İstanbul, Turkey.

- **Ön, Z.B.**, Özeren, M.S., Akçer-ön, S., Greaves, A.M. 2018. The 4.2 ka BP event, was it really global? *National Congress, TURQUA*, May 2-5, İstanbul, Turkey.

OTHER PUBLICATIONS

- Kaiser, J., **Ön, B.**, Arz, H.W., Akçer-Ön, S. 2016. Sedimentary lipid biomarkers in the magnesium rich and highly alkaline Lake Salda (south-western Anatolia), *Journal of Limnology*, 75, 581–596. doi:10.4081/jlimnol.2016.1337

- **Ön, Z.B.**, Özeren, M.S., Akçer-Ön, S., Çağatay, M.N. 2017. Spectral Features of 250 kyr Long Lake Van Sediments: Milankovitch Cycles and Their Harmonics, *Geological Bulletin of Turkey* 60, 1–28. doi:10.25288/tjb.360604

- Eriş, K.K., Akçer-Ön, S., Çağatay, M.N., Ülgen, U.B., **Ön, Z.B.**, Gürocak, Z., Nagihan Arslan, T., Akkoca, D.B., Damcı, E., İnceöz, M., Okan, Ö.Ö. 2017. Late Pleistocene to Holocene paleoenvironmental evolution of Lake Hazar, Eastern Anatolia, Turkey, *Quaternary International* 486, 4–16. doi:10.1016/j.quaint.2017.09.027

OTHER PRESENTATIONS

- Akçer-Ön, S., Çağatay, M.N., Sakınç, M., **Ön, Z.B.**, Acar, D. 2013. Little Ice Age and Medieval Period in İstanbul: Correlation of Küçükçekmece Lagoon sedimentary records with historical data. *National Congress, 66th Geological Congress of Turkey*, April 1-5, Ankara, Turkey.

- **Ön, Z.B.**, Özeren, M.S., Çağatay, M.N., Akçer-Ön, S., Damcı, E., Sancar, Ü. 2013. Late Pleistocene-Holocene climatic cycles from Lake Van sediments. *National Congress, 66th Geological Congress of Turkey*, April 1-5, Ankara, Turkey.

- Ankut, Z., Ercan, S., Eroğlu, C., Akçer-Ön, S., Korkmaz, T., **Ön, Z.B.**, Acar, D. 2014. Determination of Late Holocene climatic changes at Lake KöyceğİZ sedimentary records: preliminary results. *National Congress, 67th Geological Congress of Turkey*, April 14-18, Ankara, Turkey.

- **Ön, Z.B.**, Özeren, M.S., Çağatay, M.N., Eriş, K.K. 2014. Late Pleistocene-Holocene climatic cycles from Eastern Turkey: Lake Van and Lake Hazar sediment records. *International Congress, MedCLIVAR*, June 22-25, Ankara, Turkey.

- Akçer-Ön, S., Eriş, K.K., Nagihan Arslan, T., **Ön, Z.B.**, Acar, D. 2014. Late Pleistocene-Holocene climate variability from Lake Hazar (SE Turkey) sedimentary records. *International Congress, MedCLIVAR*, June 22-25, Ankara, Turkey.

- Erel, T.L., Batir, B., **Ön, Z.B.** 2014. The Impact of the Changing Coastline on the Harbors in Bodrum and Datça Peninsulas, and the Examples of Bodrum (Halikarnassos), Aspat (Strobilos), Datça (Stadia), Tekirburnu (Knidos). *International Congress, 8th International Symposium on Eastern Mediterranean Geology*, October, 13-17, Muğla, Turkey.

- **Ön, Z.B.**, Özeren, M.S., Çağatay, M.N., Eriş, K.K., Akçer-Ön, S. 2014. Late Pleistocene-Holocene climatic cycles from Eastern Anatolia. *International Congress, 8th International Symposium on Eastern Mediterranean Geology*, October, 13-17, Muğla, Turkey.

- Akçer-Ön, S., Çağatay, N., Sakınç, M., **Ön, Z.B.**, Acar, D. 2014. Little Ice Age and Medieval Warm Period in Istanbul: Correlation of Küçükçekmece Lagoon sedimentary records with historical data. *International Congress, 8th International Symposium on Eastern Mediterranean Geology*, October, 13-17, Muğla, Turkey.

- Akçer-Ön, S., Greaves, A.M., Çağatay, M.N., Sakınç, M., **Ön, Z.B.**, Tunoğlu, C. 2015. When did Latmos Gulf close? Geology versus archaeology. *National Congress, 68th Geological Congress of Turkey*, April 6-10, Ankara, Turkey.

- Akçer-Ön, S., **Ön, Z.B.**, Acar, D., Danladi, I.B., Çağatay, M.N., Helvacı, C. 2016. High resolution climatic records of Western Anatolia for the last 700 ka: Acıgöl lake sediments. *National Congress, TURQUA*, May 8-11, İstanbul, Turkey.

- Eriş, K.K., Akçer-Ön, S., **Ön, Z.B.**, Çağatay, M.N. 2016. Lare Pleistocene to Holocene paleoenvironmental evolution of Lake Hazar, Eastern Anatolia, Turkey; Evidences from multi-proxy records. *National Congress, TURQUA*, May 8-11, İstanbul, Turkey.

- Akçer-Ön, S., **Ön, Z.B.**, Çağatay, M.N., Wulf, S., Salihoglu, R., Danladi, I.B., Eriş, K.K., Appelt, O., Acar, D. 2016. High resolution Middle-Late Holocene climatic records from Lake Salda (W. Anatolia) sediments. *National Congress, TURQUA*, May 8-11, İstanbul, Turkey.

- Akçer-Ön, S., **Ön, Z.B.**, Çağatay, M.N., Eriş, K.K., Sakınç, M., Wulf, S., Helvacı, C., Acar, D., Gündoğan, I., Akkiraz, M.S., Sancar, Ü., García-Veigas, J., Danladi, I.B., Salihoglu, R., Büyükmeriç, Y., Appelt, O., Şen, Ö.L., Özdoğan, M. 2016. High resolution Middle-Late Holocene climatic records from Lake Salda (W. Anatolia) sediments. *International Congress, MedCLIVAR*, September 26-30, Athens, Greece.

- Danladi, I.B., Salihoglu, R., **Ön, Z.B.**, Akçer-Ön, S. 2016. High-resolution multi proxy evidences of climate changes during the past 1400 years from Lake Salda sediment records (SW Turkey). *International Congress, MedCLIVAR*, September 26-30, Athens, Greece.

- Akçer-Ön, S., **Ön, Z.B.**, Çağatay, M.N., Sakınç, M., Helvacı, C., Gündoğan, I., Eriş, K.K., Acar, D., Akkiraz, M.S., Sancar, Ü., García-Veigas, J., Büyükmeriç, Y., Danladi, I.B., Salihoglu, R., Wulf, S., Appelt, O., Şen, Ö.L., Özdoğan, M. 2016. High resolution climatic records of Western Anatolia for the last 700 ka: Acıgöl Lake sediments. *International Congress, MedCLIVAR*, September 26-30, Athens, Greece.

- Akçer-Ön, S., Greaves, A.M., **Ön, Z.B.**, Sturt W. Manning, Çağatay, M.N., Sakınç, M., Tunoglu, C. 2017. When did Latmos Gulf close? Geology versus Archaeology. *International Congress, International Open Workshop-Socio-Environmental Dynamics over the Last 12,000 Years: The Creation of Landscapes V*, March 20-24, Kiel, Germany.

- Korkmaz, T., **Ön, Z.B.**, Akçer-Ön, S. 2018. Preliminary results on tephrochronological record of Lake Acıgöl. *National Congress, TURQUA*, May 2-5, İstanbul, Turkey.
- Eriş, K.K., Akçer-Ön, S., Çağatay, M.N., **Ön, Z.B.** 2018. Late Pleistocene-Holocene paleoclimate and water level changes in Lake Hazar, eastern Anatolia, Turkey. *National Congress, TURQUA*, May 2-5, İstanbul, Turkey.